University of New Orleans
ScholarWorks@UNO

University of New Orleans Theses and Dissertations | Dissertations and Theses

5-20-2005

Synthesis and Characterization of Miniaturized Fluorescence Sensors for Aqueous and Cellular Measurements

Aihui Ma
University of New Orleans

Follow this and additional works at: https://scholarworks.uno.edu/td

Recommended Citation

Ma, Aihui, "Synthesis and Characterization of Miniaturized Fluorescence Sensors for Aqueous and Cellular Measurements" (2005). *University of New Orleans Theses and Dissertations*. 266.
https://scholarworks.uno.edu/td/266

This Dissertation is protected by copyright and/or related rights. It has been brought to you by ScholarWorks@UNO with permission from the rights-holder(s). You are free to use this Dissertation in any way that is permitted by the copyright and related rights legislation that applies to your use. For other uses you need to obtain permission from the rights-holder(s) directly, unless additional rights are indicated by a Creative Commons license in the record and/or on the work itself.

This Dissertation has been accepted for inclusion in University of New Orleans Theses and Dissertations by an authorized administrator of ScholarWorks@UNO. For more information, please contact scholarworks@uno.edu.

SYNTHESIS AND CHARACTERIZATION OF MINIATURIZED FLUORESCENCE SENSORS FOR AQUEOUS AND CELLULAR MEASUREMENTS

A Dissertation

Submitted to the Graduate Faculty of the
University of New Orleans
in partial fulfillment of the
requirements for the degree of

Doctor of Philosophy
in
The Department of Chemistry

by

Aihui Ma

B.S., Liaocheng University, Shandong, P.R.China,1997
M.S., University of Science and Technology of China, Anhui, P.R.China, 2000

May 2005

Copyright 2005, Aihui Ma

ACKNOWLEDGEMENTS

This dissertation is dedicated to my wonderful husband who is my partner and my soulmate. With his full support, I have come to this end point of obtaining my Ph.D. I also dedicate this dissertation to my wise parents who gave me this freedom to pursue my higher education and my happy marriage life overseas.

I would like to thank my advisor, Professor Zeev Rosenzweig. His wisdom, invaluable advice, support, encouragement, humor, and fatherly love have always been and will be there for me through my whole life.

I also sincerely thank Professor Nitsa Rosenzweig for her patience to teach me the cell growth and maintenance, her student Abdul Hamide for his help in cell preparation; Professor Matthew Tarr, Professor Ron Evilia, Professor John Wiley, and Professor GuijunWang for their advice and fruitful discussions.

I would like to thank everyone in my group I have worked with in the past and present for their friendship. Especially, I'd like to thank Harry Rees, Thuvan Nguyen, Li Chen, Yanjie Jiang, Lifang Shi, and Ying Long for their friendship which has accompanied me through my graduate life.

Financial support for this work was obtained from the National Science Foundation through Grant CHE-013427.

TABLE OF CONTENTS

List of Tables……..……v
List of Figures……..……..…….vi
Abstract……...ix

CHAPTER I INTRODUCTION…….….1
1.1 Objectives and Aims……1
1.2 Significance and Impact…….……..1
1.3 Fluorescence Principle…….2
1.4 Fluorescence Sensors…….……..5
1.5 Particle Based Fluorescence Sensors…….……..5
1.6 Previous Work With Lipobead Based Sensors……..11
1.7 Reference…….……..12

CHAPTER II EXPERIMENTAL…….15
2.1 Experimental……..15
2.2 Optical Measurement Instrumentation…….…….16
2.3 Cell Culture of Hela and MCF7 Cells……27

CHAPTER III SUBMICROMETRIC LIPOBEAD-BASED FLUORESCENCE SENSORS FOR CHLORIDE ION MEASUREMENTS IN AQUEOUS SOLUTION……...29
3.1 Introduction……29
3.2 Experimental……..31
3.3 Results and Discussion……..33
3.4 Conclusions……50
3.5 References……..54

CHAPTER IV LIPOBEAD-BASED FLUORESCENCE BIOSENSOR FOR UREA.……..56
4.1 Introduction……56
4.2 Experimental……..58
4.3 Results and Discussion……..64
4.4 Conclusions……78
4.5 References……..……81

CHAPTER V DELIVERY OF PARTICLES INTO CELLS FOR INTRACELLULAR MEASUREMENTS……...83
5.1 Introduction……83
5.2 Experimental……..85
5.3 Results and Discussion……..87
5.4 Conclusions……..108
5.5 References……109

CHAPTER VI SUMMARY……111

VITA……116

LIST OF TABLES

Table 3.1. Properties of chloride indicators……..35

Table 5.1. 24 hour cell viability study……104

LIST OF FIGURES

Figure 1.1. Jabloński Diagram……3

Figure 2.1. Schematic of a Photomultiplier Tube……19

Figure 2.2. Diagram of the Spectramax Microplate reader……..……..21

Figure 2.3. Diagram of a typical digital fluorescence microscope…….……..22

Figure 2.4. Filter cube and its components…….……..23

Figure 2.5. Frame transfer CCD and Interline transfer CCD……26

Figure 3.1. Lucigenin structure……36

Figure 3.2. (a) Fluorescence spectra of lucigenin in phosphate buffer solutions at pH 7.4 with increasing chloride ion concentrations from 0 to 50 mM (λex=430 nm) (b) A Stern-Volmer plot describing the ratio between the initial fluorescence (F_0) intensity and the fluorescence intensity at a given chloride ion concentration (F) against chloride ion concentration. The Stern-Volmer constant, K_{sv}, was determined to be 225 M^{-1}……37

Scheme 3.1 A proposed mechanism for the incorporation of the ion-pair into the phospholipid membrane. The lucigenin molecules partition effectively into the phospholipid membrane due to the formation of ion pairs with hexadecanesulfonate……39

Figure 3.3. Absorption spectra (a) and fluorescence spectra (b) comparing the spectroscopic properties of free lucigenin in aqueous solution and the lucigenin- hexadecanesulfonate ion pair dissolved in chloroform. The ion pair formation had minimal effect on the spectroscopic properties of lucigenin……...40

Figure 3.4. Digital fluorescence images of (a) lipobeads containing free lucigenin, (b) lipobeads containing the lucigenin- hexadecanesulfonate ion pair. The signal to background ratio improves from 13 (image 4a) to about 100 (image 4b)……42

Figure 3.5. Mechanism of the phase transport of chloride ions from the aqueous phase, by the ionophore, into the lipobead membrane. $Iono^+$ is the ionophore, Cl^- the anion analyte, and $Iono^+Cl^-$ the ionophore:analyte complex. The ionophore transports the anion from the aqueous phase into the phospholipid membrane, thus allowing the chloride to quench the fluorescence of lucigenin……44

Figure 3.6. Structure of the chloride ionophore MC-3……46

Figure 3.7. The chloride response of MC-3 containing lipobeads (F_0/F_{50mM}) as a function of MC-3 concentration. F_0 is the fluorescence intensity of MC-3 containing lipobeads in a chloride free phosphate buffer solution at pH 7.2. F_{50mM} is the fluorescence intensity of the lipobeads solution

when the chloride ion concentration is raised to 50 mM. It can be seen that the optimal MC-3 concentration in the phospholipid solution used to prepare the lipobeads is 5 mM…….47

Figure 3.8. A Stern-Volmer plot describing the chloride ion response F_0/F with increasing chloride ion concentrations. F0 is the fluorescence intensity of the lipobeads in a chloride free phosphate buffer solution at pH 7.2. F is the fluorescence intensity of the lipobead solution at a given chloride ion concentration. Typical variations from linearity are observed at chloride ion concentrations lower than 2 mM and higher than 30 mM…….49

Figure 3.9. Characterization of the response time of the chloride ion sensing lipobeads- the fluorescence intensity of the lipobeads prior and following the injection of an aliquot of concentrated chloride solution is shown……51

Figure 4.1. Ionization form of fluoresceins……..61

Figure 4.2. Structure of Fluorescein-5-thiosemicarbazide…….……..62

Scheme 4.1. Synthesis of activated lipobeads…….……..66

Figure 4.3. A calibration curve of free urease fluorescence versus urease concentrations ranging from 0 to 0.1 mg/ml. The shape of the large concentration spanning curve is nonlinear. Insert - linear plot of urease fluorescence against. urease concentrations ranging from 0 to 0.02 mg/ml…….68

Figure 4.4 FTIR spectra monitoring different steps of the lipobeads synthesis: (a) bare silica beads, (b) silica lipobeads prior to acylation, and (c) silica lipobeads following acylation with sebacoyl chloride……...70

Figure 4.5. Scanning electron microscopy (SEM) image of (a) bare silica beads, (b) Silica lipobeads. Both images reveal that the particles are spherical, evenly dispersed, and average 1.7 ± 3% μM in diameter with narrow size distribution. (c) A digital fluorescence image of the lipobeads. The signal to noise ratio is about 50 ± 15%…….72

Figure 4.6. The pH dependent emission spectra of (a) 0.05 mM fluorescein-5-thiosemicarbazide in 0.2 mM EDTA solution and (b) lipobeads solution containing fluorescein-5-thiosemicarbazide between pH 6.0 and 8.0 in a 0.2 mM EDTA solution. The spectra were measured at a fixed excitation wavelength of 490 nm and the fluorescence intensity was measured at 520 nm……..74

Figure 4.7. pH reversibility study describing the fluorescence intensity of the urea sensing lipobeads versus time at different pH levels……..75

Figure 4.8. A Lineweaver-Burke plot of the invert of the initial reaction rate versus invert substrate concentration. K_m was calculated at 7.0 ± 1.8 mM for the urea sensing lipobeads……77

Figure 4.9. A semi-log plot describing the fluorescence intensity of the urea sensing lipobeads against increasing urea concentrations……..79

Figure 5.1. Flubida structure and esterase conversion to the fluorescent species (46).……89

Figure 5.2. (a) 2 uM flubida-biotin with and without KOH. (b) 6 uL 120 nm streptavidin microspheres with and without KOH……91

Figure 5.3. Digital images of particles with MCF 7 cells where (a) is the MCF 7 cells transmission image, and (b) is the digital fluorescence image of MCF 7 cells and particles……..92

Figure 5.4. Digital images of the control experiment to determine whether the particles are penetrating into the Hela cells. In Figure 4, (a) is the Hela cells transmission image, (b) is the transmission-fluorescence image of the Hela cells, and (c) is the digital fluorescence image…….…….93

Figure 5.5. Plot of the emission spectra comparing the particles in a suspension of Hela cells where (a) is the mixture of particles with the Hela cells representing a baseline measurement of the fluorescent emission, (b) is the fluorescent emission after 4 hours of incubation with cells, and (c) is the fluorescent emission after adjusting the pH to 10 with KOH……..96

Figure 5.6. Microplate reader results for cells treated with (a) 30 µL Dubelco's buffer, (b) 30 µL TAT peptide, (c) 30 µL particles with cells, (d) 20 µL flubida covalently bound particles incubated with the cells for four hours, and (e) flubida and TAT peptide covalently bound particles incubated with the cells for 4 hours……...100

Figure 5.7. Fluorescence intensity versus time for free flubida in (a) blank well, (b) 30 uL cell medium, (c) 30 µL Dulbecco's buffer, (d) 30 uL serum free medium, (e) 20 uL flubida biotin in cell growth medium, (f) 20 uL flubida biotin in Dulbecco's buffer, and (g) 20 uL flubida biotin in serum free medium……..103

Figure 5.8. Comparison of nanoparticles incubated with cells in (a) control blank, (b) serum free medium- buffer (v/v, 1/1)(SFMB), (c) 20 µL particle-flubida incubated in cell with SFMB, (d) 20 µL particle-flubida-TAT incubated in cell with SFMB, (e) 20 µL particle-flubida incubated in SFMB, (f) 20 µL particle-flubida-TAT incubated in SFMB……...107

ABSTRACT

The objective of this Ph.D. study was to develop new and improved miniaturized particle-based optochemical sensors for the analysis of biological fluid and cellular components. This is highly important because current sensing systems can be biologically toxic and incompatible, invasive, and have limited responsiveness.

To accomplish this goal we defined three tasks. The first was to develop lipobead-based sensors for chloride. The halide-specific fluorescence dye, lucigenin, was immobilized into the phospholipid membrane of the lipobeads to enable chloride ion detection. The fluorescence intensity of lucigenin decreases with increasing chloride ion concentration due to dynamic quenching. To stabilize the lipobeads we co-immobilized hexadecanesulfonate molecules into the phospholipid membrane. We also immobilized the chloride ionophore [9] mercuracarborand-3 (MC-3) into the lipobeads membrane. The study resulted in a unique submicrometric chloride ion sensor, which is suitable for chloride ion measurements in biological fluids.

The second task was to develop for the first time lipobead-based biosensors. Urea was chosen as a model substance since the urea/urease biosensing system is well known. Fluorescence sensing lipobeads were characterized by coating carboxyl-functionalized silica microspheres with phospholipids for the measurement of urea in aqueous samples. The enzyme urease and the pH indicator Fluorescein-5-thiosemicarbazide were attached covalently to the phospholipid membrane of the lipobeads. We prepared improved fluorescence sensing lipobeads by utilizing covalent chemistry to bind the phospholipid membrane to the silica particles and the fluorophores to the membrane. It led to improvement in the stability of the newly developed urea sensing lipobeads compared to previously developed micrometric fluorescence sensors.

The final task of this study was to coat particle-based sensors with cell penetrating peptides to enable their permeation into cells. This step is essential for the use of particles as intracellular sensors. Streptavidin coated microspheres were modified by the strongest noncovalent interaction between avidin and biotin. Tat peptide and nonfluorescence indicator flubida were attached to the surface of the microspheres. These nanoparticles were delivered into MCF7 and Hela cancer cells for pH measurement. Before penetrating into the cells, flubida did fluoresce in cell medium; however it did not convert to fluorecein in Phosphate Buffered Saline (PBS) buffer.

CHAPTER I INTRODUCTION

1.1 Objectives and Aims

Previous work in synthesizing and developing analyte specific sensors in our lab has often encountered problems with reducing the size of particles for use as the sensing probes. Therefore, the main objective of my work was to develop new and improved miniaturized particle-based optochemical sensors for the analysis of biological fluid and cellular components. The specific aims of my work were: a) to develop lipobeads based sensors for chloride measurement, b) to develop lipobead sensors for urea measurement, and c) to demonstrate that these particles could also penetrate into cells to facilitate intracellular measurements.

1.2 Significance and Impact

There are numerous drawbacks for previously developed 100 times larger sensors when applied to biological systems. These include invasiveness that often leads to cell and tissue damage, slow response time and limited spatial resolution. Therefore, there is a need to develop new smaller sensors that have reduced or eliminated these drawbacks. In our lab we have developed submicrometric particle-based sensors which have greatly reduced much of the drawbacks listed above. The particle based sensors that were developed during my Ph.D studies generate significant improvements over previously developed particle based sensors such as improved physical stability, low cost of ingredients, reduction of carrier system leakage (e.g. drugs or probes leakage), increased ease of preparation, and improved yields, particularly for sensors that are used for hydrophobic indicators.

The newly developed particle-based sensors are phospholipids coated polymer particle, named lipobeads. Their successful preparation enabled their application in cellular studies requiring the use of non-invasive probes with high temporal and spatial resolution. Beyond the analytical impact of this Ph.D study, it is anticipated that this new sensing technology will enable better understanding of signaling events leading to the on-set of various pathologies including the genetic diseases cystic fibrosis (chloride sensors) and renal diseases (urea sensors). The ability to deliver sensing particles into cells as described in chapter 5 could lead in the future to the development of intelligent sensing systems with the capability to identify abnormal cells, permeate them and release drug molecules inside abnormal cells in response to a triggering signal sensed by the particles. This has the potential to revolutionize the ways currently used to deliver drugs in treating diseases.

1.3 Fluorescence Principle

1.3.1 Jabloński Diagram

Jabloński Diagrams describe light absorption and emission and demonstrate different molecular processes happening in the excited states during fluorescence. In a typical Jabloński Diagram, S_0 shows a singlet ground state, and S_1 and S_2 show first and second excited states, respectively. At each different state, the notation 0, 1, and 2 mean different vibrational energy levels. T_1 means the first triplet state. When a fluorophore absorbs light, it will excite from the singlet ground state to the first or second excited states. Internal convension usually occurs when the excited fluorophore molecules relax from the second excited state to the first excited state. This process normally happens before the emission starts, so generally we see the absorption and

emission spectra are the mirror images of each other because the electrons excited do not change the nuclear geometry. Intersystem crossing happens when the electrons in the first excited state S_1 transit to the triplet state T_1. This process will emit phosphorescence which is lower in energy compared to fluorescence. Figure 1.1 is an illustration of a typical Jabloński diagram.

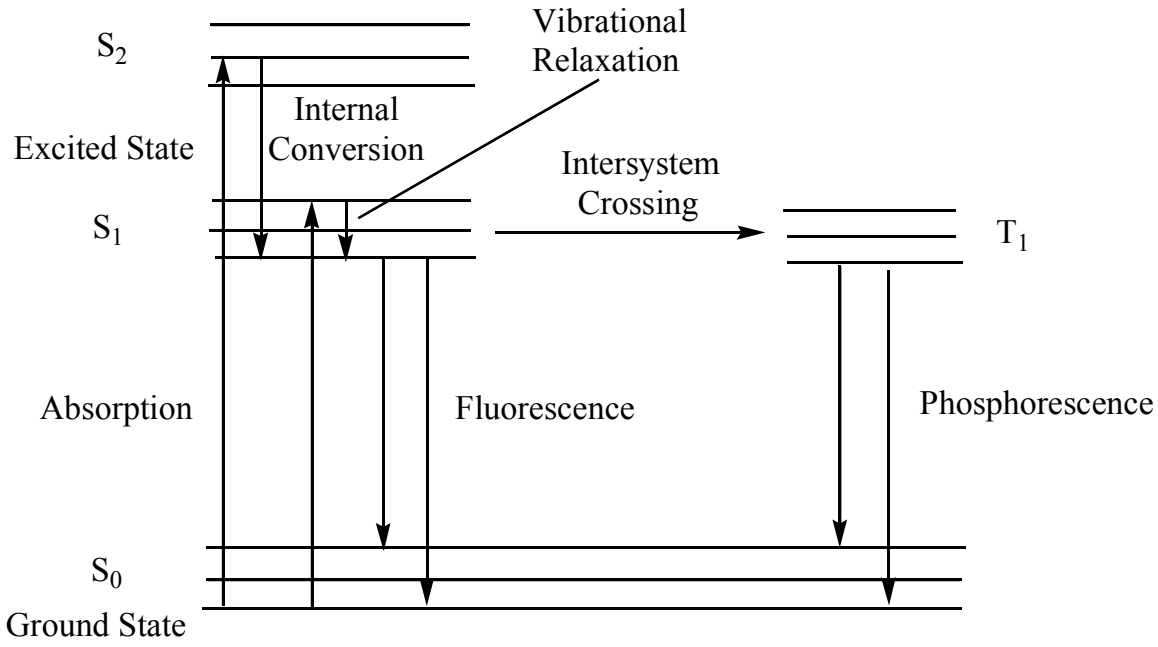

Figure 1.1 Jabloński Diagram.

1.3.2 Excitation and Emission Spectra

Fluorescence measurements typically involve recording excitation and emission spectra. In this study the fluorescence emission spectra were used often to characterize the sensing properties of particles and fluorophore solutions. Emission spectra depict the emission intensity as a function of wavelength when the sample is excited using a single wavelength. Excitation

spectra depict the fluorescence intensity at a fixed emission wavelength against the wavelength of the excitation light. Different fluorophores have variable excitation and emission spectra that are determined by the fluorophore's chemical structures and the solvent used.

1.3.3 Collisional Quenching

Fluorophore self-quenching, due to its own high concentration, is a fundamental phenomenon that is one type of fluorescence quenching. Fluorescence quenching occurs when the fluorescence intensity decreases due to an energy transfer process. The most widely used quenching is collisional quenching. Collisional quenching results in a fluorescence intensity decrease when the fluorophores in the ground state come in close proximity to the quencher, then return to the ground state without emitting fluorescence. Collisional quenching includes static and dynamic quenching. Static quenching occurs when nonfluorescent complexes form between the fluorophore in the excited state and a quencher. This complex returns the fluorophore in the excited state to the ground state without emitting fluorescence. Dynamic quenching happens when during the fluorophore's lifetime in the excited state; the fluorophore diffusively encounters a quencher and returns to its ground state without emitting photons. Quenching can be described by the following Stern-Volmer equation:

$$F_0/F = 1+K\,[Q] = 1+k_q\,\tau_0\,[Q] = 1+ K_D\,[Q] \qquad (1)$$

Where F_0 and F are the fluorescence intensities in the absence and presence of the quencher, respectively, and K is the Stern-Volmer quenching constant. For the static quenching, K is K_{sv}, which is Sten-Volmer constant, higher Stern-Volmer constant, higher sensitivity to chloride. For

the dynamic quenching, K represents K_D. [Q] is the quencher concentration, k_q is the bimolecular quenching constant, and τ_0 is the fluorophore lifetime in the absence of quencher. When we analyze the data, we plot F_0/F versus [Q]. The slope of the curve is equal to the Stern-Volmer quenching constant.

There are numerous ways to distinguish between static and dynamic quenching. The most direct way is to measure their fluorescence lifetimes. For the static quenching, the fluorophore's lifetime does not change with [Q] because the fluorophore-quencher complex does not emit fluorescence. However, for dynamic quenching, the fluorophore's lifetime changes with [Q]. As more collisions occur, lifetimes are shorter, and the fluorescence intensity is lowered. Quenching at different temperatures and viscosity will have different Stern-Volmer constants. When the temperature is higher, the quenching constant is lower for static quenching and higher for dynamic quenching .

1.4 Fluorescence Sensors

Two typical classes of fluorophores are intrinsic and extrinsic. The extrinsic fluorophores are primarily used to label nonfluorescent molecules while intrinsic fluorophores are utilized when analytes naturally fluoresce. Our discussion here involves extrinsic fluorophores that respond to certain substrates of interest.

1.5 Particle Based Fluorescence Sensors

1.51 Single Cell Analysis

In living organisms cells are the fundamental units. Different organs of mammals have different kinds of cells. The direct observation of single cells using fluorescence techniques has

become a powerful investigative tool for analyte measurement. It can dramatically help us understand cellular metabolism, signal transduction (1-5), gene transcription (6, 7), and intracellular transport and fate of delivered drugs. The methodologies used must provide sensitive and fast analysis for the single cell measurement due to the tiny amount of sample present inside the cell. Fluorescence microscopy and flow cytometry are the most popular cellular analysis techniques (8-11). In fluorescence microscopy the cell is excited with one wavelength of light and the emitted fluorescence from the excited fluorophores is collected by detection systems such as photomultiplier tubes. The flow cytometer uses a laser to light up cells going by in a stream. The incident light is diffracted by the cells and also absorbed by fluorophores in the cells. A photomultiplier tube is used to collect the emitted fluorescence from the fluorophores within the cells. These two techniques have the common feature that molecular fluorescent probes have to be employed to label the observed cells. Fluorescence microscopy is used for real-time continuous observation of cells. It is different in flow cytometry where each cell is observed only once as it flows through the detection system, even though it includes high-speed acquisition of information on the individual cells.

1.5.2 Phospholipids Properties

The components of cells are large molecules, among which lipids are one of the most important. In Greek, the word lipid comes from lipos, which means fat. The most widely used classification of the lipids includes simple lipids, compound lipids, and derived lipids (12). Simple lipids include neutral fats and waxes, compound lipids are composed of phospholipids which contain phosphate head groups, cerebrosides, gangliosides which involve a carbohydrate group, and sulphatides which are lipids having a sulphate residue. In this chapter we are

interested in phospholipids that we use to simulate the biological membrane for particle delivery into cells.

Phospholipids are the major components of biological membranes. Most phospholipids are made up of hydrophilic polar head groups and hydrophobic fatty acid chains. Although the structures of the various phospholipids are very similar, the differences among them still exists, which includes fatty acid compositions, acyl chain unstauration, and polar head groups. These small differences determine their membrane physical properties, their locations and their biological functions.

It is very important to understand phase transition and the fluidity of phospholipids membranes (13, 14). The different phospholipids membrane phases will demonstrate different ion permeability, ability to bind to proteins, degree of aggregation and fusion, and their biological behaviors. Phase transition means that at different temperature, the hydrocarbon chains of the phospholipids exhibit a different degree of molecular motion. One type of phospholipids can expand to have several phase temperatures. At the first transition point, the molecular motion of the fatty acid chain increases. With the temperature increase, the chain motion possibly involves molecular rotation, translation or diffusion. The phase transition is at low temperatures for the short chain length or unsaturated bonds. For the totally saturated long chain phospholipids, the phase temperature is higher. If the phospholipids have the same fatty acid chains and different head groups, their phase temperatures are still different.

We use artificial phospholipids membranes to simulate biological membranes. Some of the properties of artificial phospholipids membranes are similar to some of the biological membranes, e.g. water permeability, interfacial tension, and electrical capacitance. The artificial phospholipids membranes can be used to alternate ion conductivity for biochemistry reaction

transduction. The electrical charge would be induced due to a rapid structural change on the phospholipids membrane, and then an electrochemical signal can be generated on the phospholipids surface so an ion current can be provided for electrochemistry (15-17). However, the greatest disadvantage of artificial phospholipids membranes is it being impermeable to ions and some other hydrophilic compounds.

1.5.3 Lipobead Based Sensors

During the last 20 years, a series of fluorescent probes for cellular analysis have been developed. Most of the fluorescent probes are intracellular probes used for the measurement of pH and calcium cations in cells (19, 20). Some examples of probes that have been used for cellular analyses are PEBBLEs (probes encapsulated by biologically localized embedding) (21), liposomes (22-24), and lipobeads (25-27). PEBBLEs were first developed by Dr. Kopleman at the University of Michigan. PEBBLEs are optical nanosensors used for intracellular analyses. They are comprised of a polyacrylamide matrix which contains various fluorescent indicators. Their size ranges between 20 and 200 nm in diameter so that they are small enough to insert inside the cells without damage. This type of probe has demonstrated fast response times and high selectivity, while maintaining biocompatibility. Two disadvantages of PEBBLEs are the fact that they are limited to the use of only hydrophilic dyes, and structural problems that constrain their cellular sensing use. Liposome probes are different from PEBBLEs in that they are not made up of a solid core, but are comprised of an outer phospholipids layer forming a spherical vesicle that has an aqueous core (28). Liposomes can encapsulate fluorescent indicators which can be used for intra-cellular analyses. Due to the phospholipids outer layer, liposomes have been prepared as unilamellar (29), bilamellar (30), or multi-lamellar (31)

vesicles. Advantages include their ability to be used as probes which are non-invasive for tissues and individual cells (32-34), and are relatively nontoxic compared to polymeric nanoparticles (35). One of disadvantages of the liposomes is that when the probes are released from the vesicles, liposomes tend to fuse to the vascular system (36), the other is that due to the vesicle size and properties, reproducibility of liposomes are limited. These technological problems hinder the widespread use of liposomes. In our lab, we have developed one type of particle-based nanosensors called lipobeads that are polystyrene nanoparticles that are coated with a phospholipids membrane and hydrophilic or hydrophobic fluorescent indicators are absorbed outside or inside the phospholipids membrane (25-27, 37, 38). This type of nanosensor can be used for intracellular sensing in physiological conditions. Lipobeads are core-shell structured particles, where the core is made of water-dispersible solid microsphere beads. Their particle size ranges between 0.2 to 2.0 um in diameter. In our lab, the shell is composed of one monolayer of phospholipids molecules ideally. Other groups have studied a related nanosensor called lipospheres (39-50). These are composed of a hydrophobic fat core that has a surface monolayer of phospholipids which helps to stabilize the core (51). Their size is between 0.2 to 500 um in diameter. They have one disadvantage in that it is difficult to control the particle size because of their core composition, as compared to the production of lipobeads, which results in a uniform particle size. My continued research will expand the lipobead-based fluorescence sensing technology to new analytes of biological importance and greatly increase the ability of Dr. Rosenzweig's group to investigate cellular signaling processes at the single cell level.

1.5.4 Intra-Cellular Measurements

To measure intracellular ion concentration, we have to load the indicators-based material into the cell and quantitatively calibrate the free ion concentration inside the cell. There are many ways to load fluorescence labeled microspheres into cells such as mechanical loading, chemical reagent loading, and electroporation (52). Mechanical loading includes microinjection (53) which can be used to load indicators to specific area in neurons, Scrape loading (54) which can load macromolecules into the cytoplasm of cells, scratching to wound the culture (55), and mild sonication (56). The advantage of this type of methodology is that they are very simple and easy to operate; however, the disadvantage is that they are invasive to the cells.

Currently, the most popular method is to use chemical reagents. One type is cationic transfection reagents (57-59). This method can deliver submicron-sized particles with an implantation effiency of ~11% (60). In a typical experiment, certain amounts of submicron particles in serum free medium is mixed with the transfection agent well, incubated in serum free medium for 4 hrs, washed with complete growth medium, and then incubated with complete growth medium for another 24 hrs. The trick of this method is to let the submicron particle surface have negative charges. If the particle surface has no negative charges, it will lead to poor loading effiency.

Another method is to use cell-penetrating peptides. This is the method that we chose to use in our laboratory. Recent studies have shown that cell-penetrating peptides set up a new way for intracellular delivery of particles. This approach can deliver covalently bound particles (size up to 150 nm) into cells in vivo. In our experiment, we use commercially available avidin modified polystyrene beads that are covalently bound with biotin modified PEG. We then add the Tat peptide and fluorescein onto the surface of the particles. The negative charge of the Tat

peptide will interact with the cell membrane and the particles will get through the cell membrane and into cells. The trick of this method is that it has to have a spacer between the particles and Tat peptide.

After the particles have gotten inside the cells, we have to calibrate the free ion concentration in an accurate way. The calibration measurement needs to add some type of ionophore to equilibrate the external and internal ions of the cells, e.g. for pH measurement, we use Nigericin as a pH ionophore for intra and outside H^+ balance. Generally, we utilize a ratiometric calibration method for intracellular measurement. The advantage of this method is to avoid artificial variations such as nonuniform loading particles in different part of the cells, cell background fluorescence, indicator photobleaching, and instrument variations at different times.

1.6 Previous Work with Lipobead Based Sensors

In our lab, we have developed one type of particle-based nanosensors called lipobeads that are polystyrene nanoparticles that are coated with a phospholipids membrane and hydrophilic or hydrophobic fluorescent indicators are absorbed outside or inside the phospholipids membrane (25-27, 37, 38). This type of nanosensor can be used for intracellular sensing in physiological conditions. The idea of lipobeads is based on the core-shell structured of liposome. The core is made of solid microsphere beads instead of aqueous solution, the shell is composed of one monolayer of phospholipid molecules. Applications of the lipobead-based particles include murine macrophage lysosomal pH measurements (25), murine macrophage intracellular oxygen measurements (26), macrophage intracellular pH measurements (27), chloride ion measurements in aqueous solution (61), and a urease-based sensor for urea measurements (in manuscript).

1.7 Reference

1. Zell, Traci; Khoruts, Alexander; Ingulli, Elizabeth; Bonnevier, Jody L.; Mueller, Daniel L.; Jenkins, Marc K. *Proc. Natl. Acad. Sci. U.S.A.*, **2001**, 98(19), 10805-10810.
2. Guse, Andreas H. *FEBS Lett.* **1999**, 451(1), 85.
3. Berg, Hermann. *Bioelectrochem. Bioenerg.* **1998**, 46(2), 307-308.
4. Stickens, D.; Tao, W.; Verbelen, J.-P. *Plant Growth Regulation,* **1996**, 18(1-2), 149-54.
5. Civitelli, Roberto; Bacskai, Brian J.; Mahaut-Smith, Martyn P.; Adams, Stephen R.; Avioli, Louis V.; Tsien, Roger Y. *Journal of Bone and Mineral Research*, **1994**, 9(9), 1407-17.
6. De Billy, Francoise; Barker, David George; Gallusci, Philippe; Truchet, Georges. *Plant Journal,* **1991**, 1(1), 27-35.
7. Dianne, M. O'Dell; Tracy, K Mcintosh; James, H. Eberwine. *Arch Neurol,* **1999**, 56, 1453-1456.
8. Taylor, D. L.; Waggoner, A. S.; Lanni, F.; Murphy, R. F.; Birge, R. R.; EDS.; Alan R Liss:New York, **1986**.
9. Melamed, M. R., Mullaney, P. F., Shapiro, H. M. In Flow Cytometry and Sorting, 2nd ed; Melamed, M. R., Lindmo, T., Mendelson, M. L., Eds.; Wiley & Sons: New York, **1990**; Chapter 1.
10. Shapiro, H. M. *Practical Flow Cytometry*, 3rd ed.; Wiley: New York, **1995.**
11. Papavasilion, F.; Casellas, R.; Suh, H.; Qin, X.; Besmer, E.; Pelanda, R.; Nemazee, D.; Rajewsley, K.; Nussenzweig, M. C. *Science* **1997**, *278*, 298-300.
12. H.J. Deuel, The lipids, vol. 1, Interscience, New York, 1951, P3.
13. Ansell, G.B., Hawthorne, J.N., and Dawson, R.M.C., Form and Function of Phospholipids, Elsevier Scientific publishing Inc., vol.3, 1973, pp117-198.
14. New, R., Liposomes, IRL Press, 1990, pp1-31.
15. Dimitrios P., Nikolelis&Manolis G. Tzanelis, Ulrich J. Krull, *Biosensor&Bioelectronics* **1994**, 9, 179-188.
16. Krull, U.J., Brennan, J.D., Brown, R.S., Hosein, S., Hougham, B.D. &Vanderberg, E.T., *Analyst*, **1990**, 115, 147-153.
17. Brennan, J.D., Brown, R.S., McClintock, C.P. &Krull, U.J., *Anl. Chim. Acta.* **1990**, 237, 253-263.
18. Kallury, K.M.R., Lee, W.E., and Thomapson, M. *Anal. Chem.* **1993**, 65, 2459-2467.
19. Marc Cherlet, Patricia Franck, Pierre Nabet, and Annie Marc. *Biotechnol. Prog.,* **1999,** 15(4), 630 –639.
20. de Silva, A. P.; Eilers, J.; Zlokarnik, G. *Proc. Natl. Acad. Sci. U.S.A.* **1999**, 96, 8836-8837.
21. Heather A. Clark, Marion Hoyer, Martin A. Philbert, and Raoul Kopelman. *Anal. Chem,* **1999**, 71 (21), 4831 –4836.
22. Thuvan Nguyen, Zeev Rosenszweig. *Anal Bioana Chem*, **2002**, 374, 69-74.
23. McNamara, K.P.; Rosenzweig, N.; and Rosenzweig, Z *Mikrochim. Acta,* **1999**, 131, 57-64.
24. Verkman, A S; Takla, R; Sefton B; Basbaum C; and Widdicombe J H. *Biochemsitry*, **1989**, 28, 4240-4244.
25. Ji, J.; Rosenzweig, N.; Griffin, C.; Rosenzweig, Z. *Anal. Chem.* **2000**, 72(15), 3497-3503.
26. Ji, J.; Rosenzweig, N.; Jones, I.; Rosenzweig, Z. *Anal. Chem.,* **2001**, 73(15), 3521-3527.

27. McNamara, K. P.; Nguyen, T.; Dumitrascu, G.; Ji, J.; Rosenzweig, N.; Rosenzweig, Z. *Anal. Chem,* **2001**, 73(14), 3240-3246.
28. New, R. R. C. Liposome-A Practical Approach, IRL Press, Oxford University Press Inc., New York, **1990**.
29. Hope M.J.; Bally, M.B.; Webb, G.; Cullis, P.R. *Biochim. Biophys. Acta,* **1985**, 812, 55.
30. Kremer, J.M.H.; Van der Esker, M.W.J; Pharmanoharan, C.; Wiersema, P.H. *Biochemistry*, **1977**, 16, 3932.
31. Banghan, A.D.; Standish, M.M.; Watkins, J.C.; *J. Mol. Biol.*, **1965**, 13, 238.
32. Arvinate, T.; Wahl, P.; Nicolau, C. *Biochemistry,* **1987**, 26, 765.
33. Gutierrez-Merino, C.; Bonini de Romanelli, I.C.; Pietrasanta, L.I.; Barrantes, F.J. *Biochemistry,* **1995**, 34, 4846.
34. Liu, Y; Cheng, D.K.; Sonek, G.J.; Berns, M.W.; Tromberg, B.J. *Appl. Phys. Lett.,* **1994**, 65, 919.
35. Douglas S J; Davis S S; Illum L. *Critical Reviews in Therapeutic Drug Carrier Systems*, **1987**, 3(3), 233-61.
36. Lentz, B. R.; Carpenter, T. J.; and Alford, D. R. *Biochemsitry*, **1987**, 26, 5389
37. Kim Yumee, Lichtenbergova Lenka, Skitko Yana, and Cho Wonhwa. *Anal. Biochem.* **1997**, 259, 109-116.
38. Jin, T.; Pennefather, P.; Lee, P. I. *FEBS Letter,* **1996**, 397, 70-74.
39. Domb, A. J.; Bergelson, L.; Amselem, S. Lipospheres for controlled delivery of substances. In Microencapsulation, Bernita, S. (ed.), Marcel Dekker: New York, **1996**, 377-410.
40. Rita Cortesi, Elisabetta Esposito, Giovanni Luca, Claudio Nastruzzi. *Biomaterials,* **2002**, 23, 2283-2294.
41. Vyas, S. P.; Singh, R; Dimitrijevic, D. *Pharmazie*, **1997**, 52, 403-404.
42. Jenning, V; Thunemann, A. F.; Gohla, S. H. *Int. J. Pharm.,* **2000**, 199, 167-177.
43. Schwarz, C.; Mehnert, W. J. *Microencapsulation*, **1999**, 16, 205-213.
44. Khopade, A. J.; Shelly, C.; and Pandit, N. K. *Journal of Biomaterials Applications*, **2000**, 14, 389-398.
45. Westesen, K.; Siekmann, B. Biodegradable Colloidal Drug Carrier Systems Basedon Solid Lipids. In Microencapsulation, Bernita, S. (ed.), Marcel Dekker: New York, **1996**, 213-236.
46. Major, M.; Prieur, E.; Tocanne, J. F.; Betder D.; Sautereau, A. M. *Biochim. Biophys. Acta,* **1997**, 1327, 32-40.
47. Heiati, H.; Philip, N. C.; Tawashi, R. *Pharmc. Res.,* **1996**, 13(9), 1406-1410.
48. Műller, R.H.; Mäder, ak.; Gohla, S. *European J. Parmac. Biopharmac*, **2000**, 50, 161-177.
49. Amselem, S; Alving, C. R.; and Domb, A. J. *Polym. Adv. Technol,* **1992**, 3, 351-357.
50. Gasco, M.R.; Cavalli, R.; and Carlotti, M.E. *Pharmazie*, **1992**, 47, 119-121.
51. Rasiel, A.; Sheskin, T.; Bergelson, L.; and Domb, A. *Polym. Adv. Technol.* **2002**, 13, 127-136.
52. Tai-Kin Wong and Eberhard Neumann, *Biochem Biophys Res Commun* **1982**, 107, 584-587.
53. Jaiswall, J.K., Goldman, E.R., Mattoussi, H.& Simon, S.M., *Nature Methods,* **2004**, 1(1), 1-6
54. McVeil, P.L., Murry, R.F., Lanni, F., and Taylor, D.L., *J Cell Biol* **1984**, 98, 1556.
55. Joel A. Swanson; Paul L. McNeil, *Science*, **1987,** 238, 548-550.
56. Fechheimer, M., Denny, C., Murphy, R.F., Taylor, D.L. *Eur J Cell Biol*, **1986**, 40, 242-247.
57. Voura, E.B., Jaiswal, J.K., Mattoussi, H. & Simmon, S.M., *Nat. Med.* **2004**, 10, 993-998.

58. Kneuer, C., Sameti, M., Bakowsky, U., Schiestel, T., Schirra, H., Schmidt, H. and Lehr, C.M., *Bioconjugate Chem,* **2000**, 11, 926-932.
59. Sandhu, K.K., McIntosh, C.M., Simard, J.M., Smith, S.W. and Rotello, V.M., *Bioconjugate Chem*, **2002**,13, 3-6.
60. Zhao, Y., Sadtler, B., Lin, m., Hockerman, G.H. and Wei. A., *Chem. Commun.* **2004**, 784-785.
61. Ma, A., Rosenzweig, Z. *Anal. Chem.* **2004**, 76, 569-575.

CHAPTER II: EXPERIMENTAL

This chapter describes the general experimental information, which includes materials, reagents, instrumentation primarily used for the research, and the cell culture work that is described within this dissertation. The specific and detailed experimental procedures that pertain to any single application will be discussed in the appropriate chapter.

2.1 Material and Reagents

[9] mercuracarborand-3 (MC-3) was obtained from the laboratory of Dr. Eric Bakker of Auburn University. A 10% (solid percentage) suspension of polystyrene particles with an average diameter of 0.78 μm (± 3.8% variation), a 10% (solid percentage) suspension of carboxyl modified silica microspheres, averaging 1.7 ± 3% μm in diameter, and a 1% (solid percentage) suspension of streptavidin coated microspheres, averaging 0.12 ± 10% μm were obtained from Bangs Laboratory, Inc. (Fishers, IN). Lucigenin (bis-N-methylacridinium nitrate) and 5-((N-(5-(N-(6-(biotinoyl) amino) hexanoyl) amino) pentyl) thioureidyl) fluorescein (fluorescein biotin) were obtained from Molecular Probes (Eugene, OR). Flubida-2 was purchased from Biotium Inc. (Hayward, CA). Tat peptide was synthesized by Invitrogen Inc. (Carlsbad, CA). Dulbecco's modified Eagle's medium, Dulbecco's PBS buffer, Fetal bovine serum, Trypsin, L-glutamine, and sodium pyruvate were purchased from Invitrogen Inc. (Carlsbad, CA) Human breast cancer cell line (MCF-7) and Hela cell line were purchased from American Type Culture Collection (ATCC). Lab-Tek II chambered coverglass was purchased from Fisher Scientific. 1, 2-dimyristoyl-sn-glycero-3-phosphate (monosodium salt) (DMPA) and 1-palmitoyllysophosphatidyl ethanolamine was purchased from Avantilipids (Alabaster, AL).

Dihexadecyl phosphate (DP), sodium hexadecanesulfonate, sodium chloride, sodium bromide, sodium thiocyanate, sodium iodide Fluorescein-5-thiosemicarbazide (F-NH_2), N-hydroxysuccinimide, N, N'-dicyclohexylcarbodiimide, sebacoyl chloride, sodium bicarbonate, triethylamine, sodium hydroxide, hydrogen chloride acid, 4-dimethylaminopyridine, ethylenediaminetertaacetic acid disodium salt dehydrate (EDTA), urease (45,000U /g), Bovine Serum Albumin (BSA), poly-L-lysine and D-biotin were purchased from Sigma-Aldrich (St. Louis, MO). 5,10,15,20-Tetraphenyl-21H,23H-porphine manganese(III) chloride (Chloride ionophore I) and the sodium ionophore 4-tert-Butylcalix[4]arene-tetraacetic acid tetraethyl ester (sodium iononphore X) were purchased from Fluka (Ronkonkoma, NY). Buffer solutions were prepared from sodium hydroxide and either 3-morpholinopropanesulfonic acid (MOPS), or sodium phosphate monobasic, which were purchased from Sigma-Aldrich (St. Louis, MO). All aqueous solutions were prepared with 18 MΩ deionized water produced by a water purification system (Barnstead Thermolyne nanopure) and all chemicals were used as received without further purification.

2.2 Optical Measurement Instrumentation

2.2.1 Spectrofluorometer

The spectrofluorometer is one of the major instruments used in fluorescence applications. The light source of the fluorometer transmits the selected wavelength to the sample, which then emits fluorescence. The emitted fluorescence intensity is directly proportional to the sample concentration. The fluorometer spectra are presented as intensity vs. wavelength. For a set of known standards, the maximum fluorescence intensity at a given wavelength is regressed with the known concentration. The resultant linear relationship is used for samples where the

fluorescence intensity obtained from the spectra will correspond directly to the sample's concentration.

In our department we have two spectrofluorometers. One is PTI model QM-1 spectrofluorometer (PTI, Quantamaster, Ontario, Canada); the other one is LS 55 Luminescence spectrometer (Perkin Elmer, USA) which is relatively new and more accurate. Compared to the PTI model spectrofluometer, the LS 55 spectrometer is smaller and more compact. All of the optical components are under the same cover in contrast to the PTI which is multicomponent. The monochromatic slits are automatic and do not need to be changed manually. This important aspect increases the accuracy of the instrument. The instrument can change from a liquid sample to solid sample holder easily, which increases the versatility and application ability of the spectrometer. However, even though the spectrometer's response and accuracy are improved, the major components that make up a spectrometer do not fundamentally change. The major components include a light source, monochromators, and a photomultiplier tube (PMT) detector.

(a) Light Source

Both spectrometers, the PTI (not shown) and the Perkin Elmer, use a 75 W xenon (Xe) lamp. The lamp supplies a continuous light output from 250 to 700 nm, thus covering both the ultraviolet and the visible region of the spectrum. The lamp consists of two electrodes sealed under high pressure in a quartz bulb with Xe gas. When the power is turned on, a high voltage pulse is generated between the two electrodes, which will induce collisions between the Xe gas. The collisions ionize the Xe atoms by removing electrons. The recombination of the removed electrons with the ionized Xe atoms will result in a continuum of light.

(b) Monochromators

The purpose of the monochromator is to disperse a bunch of light into various colors of wavelengths. The spectrofluorometer has two monochromators; one is to select an excitation wavelength while the other is to select an emission wavelength

(c) Photomultiplier tube (PMT)

The purpose of the photomultiplier tube (PMT) is to amplify electrons, derived from incident photons entering the photomultiplier, to an extremely large number of electrons, thus increasing the analyte response many times fold. Photomultiplier tubes are used as the detector for most types of spectrofluorometers. A PMT output is taken as a current source by the instrument and the light intensity emitted by the analyte is proportional to the current, which is used to correlate concentration to fluorescence intensity.

Figure 2.1 illustrates the principle of photomultiplier tubes. Within the PMT vacuum area is a photocathode and a series of dynodes. Incident photons hit the surface of the photocathode where an electron will be ejected. The potential difference between the photocathode and dynode will accelerate the ejected electrons to the first dynode. Several additional electrons are ejected by the differential potential. This process continues along the dynode chain, where more electrons are ejected and collected. When a new current pulse arrives at the cathode, a new cycle of this process is started again. By this process, amplification of the electrons is generated that represents amplification of the incident signal.

The PTI spectrofluorometer specifically utilizes digital photon counting detector with a discriminator and high-voltage power supply. At constant high voltage, the PMT is very

sensitive. The measurement is performed when each photon hits the photocathode of the photomultiplier tube. Individual photon results in a count at the anode which can be detected. The light hitting on the photomultiplier detector is proportional to the count rate which is the number of counts per second. The detector is usually operated with a discriminator to discriminate a low level noise signal from a higher level signal from the incident photons.

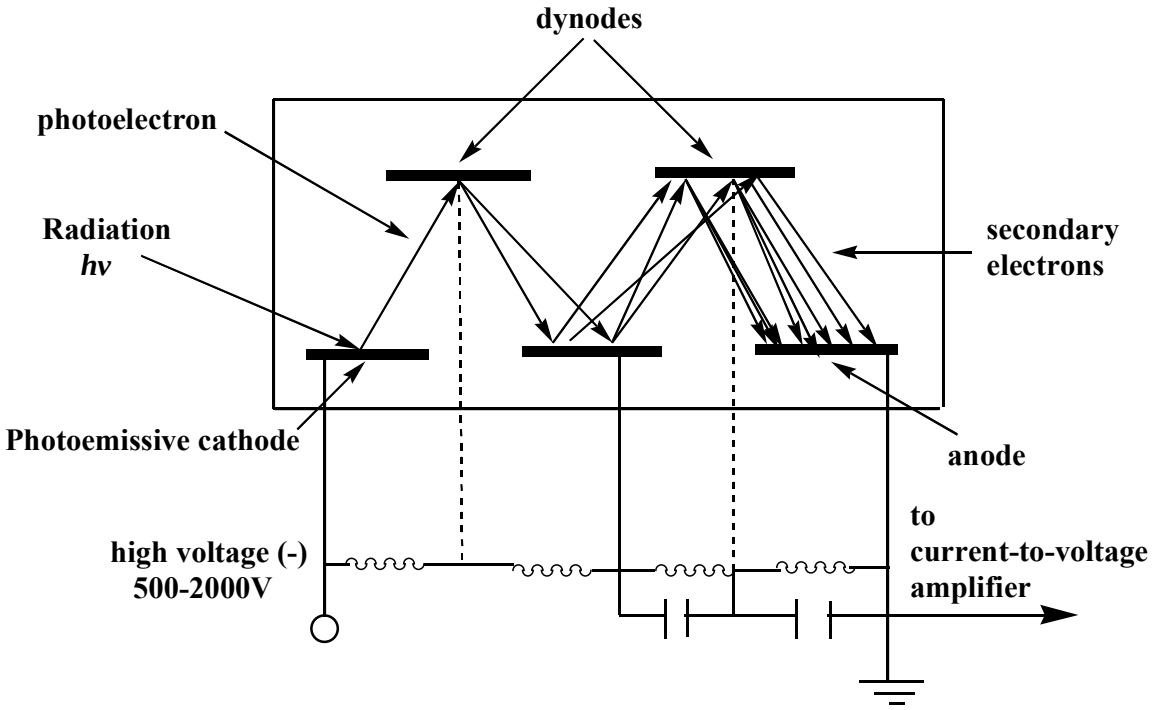

Figure 2.1. Schematic of a Photomultiplyer Tube.

2.2.2 Multidetection Microplate Reader

The design and function of the SpectraMax M2 microplate reader (Molecular Device, Inc.) performs similarly to a spetrofluorometer. However, this is the only system that can provide both dual-mode measurement for a cuvette port and 6-384 microplate reading. The major components of a multidetection microplate reader are similar to the spectrofluorometer such as

the light source, the monochromator, and the photodetector. There is slight difference between the two such as the light source for the microplate reader uses a 50 watt xenon flash lamp (versus a 75 W for the spectrofluorometer). It has very similar functions for the monochromator. The dual monochromators of the microplate reader are flexible to select any absorbance wavelength range between 200-1000 nm, any excitation wavelength between 250-850 nm and any emission wavelength from 360 to 850 nm.

The multidetection microplate reader can measure and obtain endpoint and kinetic spectra, and multi-point well-scanning for fluorescence and absorbance. It can be applied to the field of biochemistry, cell biology, immunology, nuclear biology and microbiology. A schematic diagram of the multidetection microplate reader is shown in Figure 2.2.

2.2.3 Digital Fluorescence Microscopy

Digital fluorescence imaging microscopy system is highly sensitive enable of single molecule observation, and specific tool for fluorescent measurement. It can distribute to a single molecule measurement and visualize specific fluorescent molecules in intracellular locations. Primarily used instrument in the research work is inverted fluorescence microscopy (Olympus IX-70). Figure 2.3 illustrates a typical digital fluorescence microscope used in this dissertation. The major components in a microscope are the light source, filter cubes, objectives and grating, and a charge-coupled device (CCD), which are individually described next.

1. Light Source

The fluorescence microscope is a very sensitive instrument that requires a bright, white light source. A 100 watt mercury arc lamp is the most commonly used light source. This type of lamp provides a bright, continuous emission across the visible range from 400 to 750 nm,

plus a UV range of 200 to 399 nm. Mercury lamps also have very distinct and sharp emission lines that are very importantly used to characterize the mercury arc lamp and calibrate the spectra.

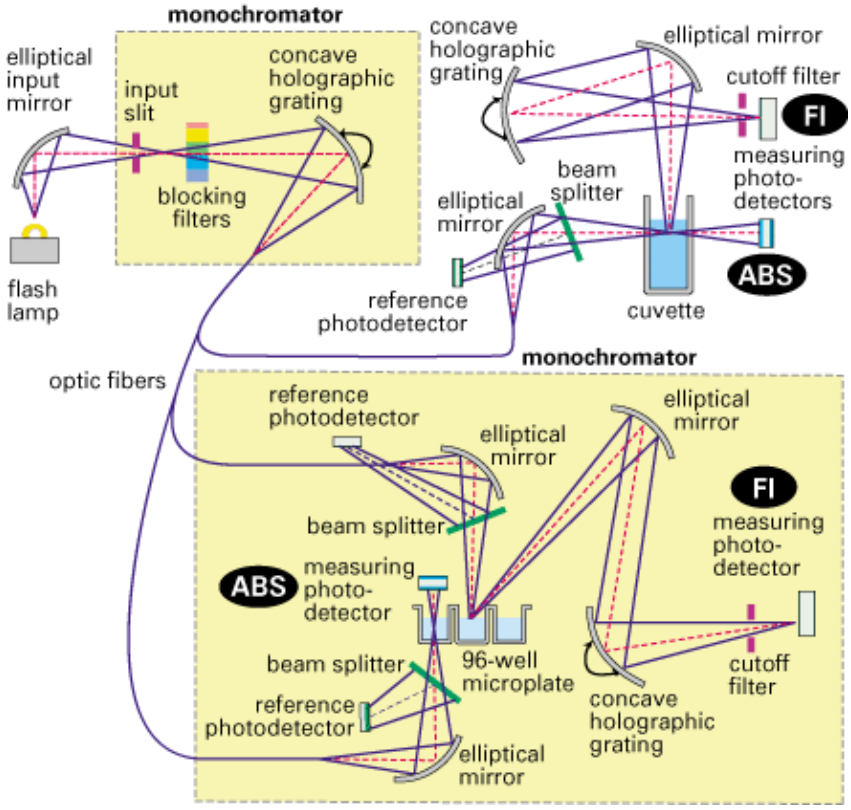

http://www.moleculardevices.com/pages/instruments/spectramax_m2.html

Figure 2.2. Diagram of the Spectramax Microplate reader.

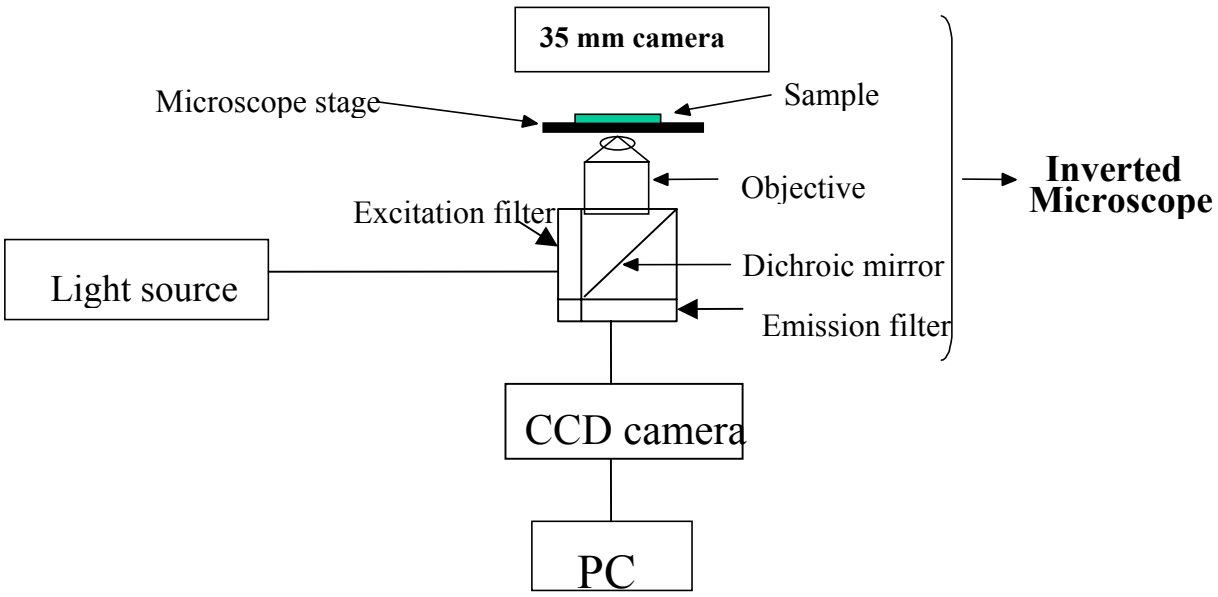

Figure 2.3. Diagram of a typical digital fluorescence microscope.

2. Filter Cube

To deliver the light to the specimen from the lamp, then collect the emitting fluorescence and form a fluorescence image, the proper filter cube need to be selected. A filter cube is typically made up of an excitation filter, a dichromic mirror, and an emission filter. The excitation filter is used to excite the specimen by selectively transmitting a narrow band of wavelengths. The dichromic mirror is used to reflect the excited light to the specimen and to transport the collected emission to the CCD detector. The emission filter is used to transmit the emission fluorescence from the specimen and block the residual excited light. Figure 2.4 illustrates the filter cube components.

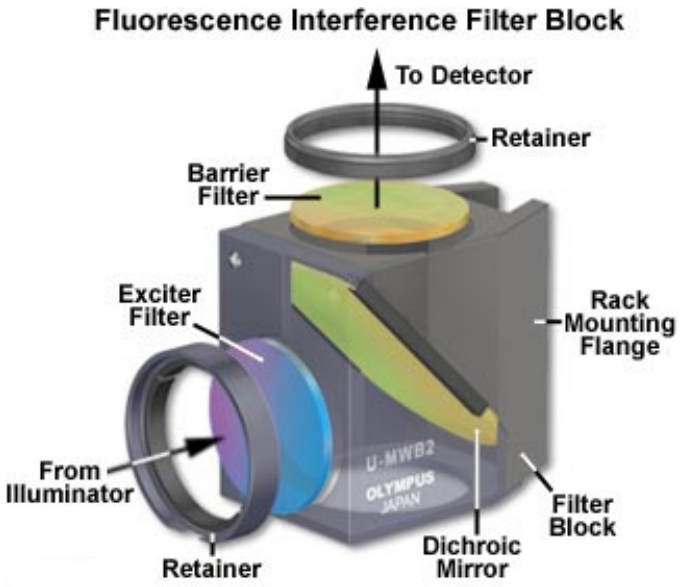

http://www.olympusmicro.com/primer/techniques/fluorescence/filters.html

Figure 2.4. Filter cube and its components

3. Objectives and Grating

The objective is often considered the most important part of the microscope because the image qualities are produced by it. The objective is positioned between the specimen and the filter cube. Its function is to transmit the fluorescence inducing light (excitation wavelength) to the specimen from the dichromic mirror while allowing passage of the emitted fluorescence to the CCD camera for images or spectra. In the lab, we have 10x, 20x, and 40x objectives with a numerical aperature of 0.5 or 0.9.

The diffraction grating is used to separate the mercury light into individual wavelengths and can be used as a monochromator and as a spectrograph in microscopy. In one of our microscopes, we use a triple grating to achieve efficiency light throughput over a broad spectral region, which is equipped with 150 blz (blaze), 300 blz at an optimum wavelength (Acton Research, Inc.).

4. Charged Couple Device (CCD)

A charged couple device (CCD) is a photon detector used in digital CCD cameras. It is made up of thousands, or millions, of pixels, which are silicone diode photosensors. Pixels can store information from incident photons that are used to comprise the microscope image. Pixels are semiconductor materials that can trap and hold photon-induced electrons (photoelectrons) derived from incident photons. A pixel is coupled to a charge storage region that will accumulate and store the photoelectrons. This storage region is connected to one amplifier that reads out the amount of accumulated charge. The stored charge is transferred through the parallel registers to a linear serial register and then to an output mode adjacent to the read-out amplifier.

The three types of CCD designs are full-frame CCD, frame-transfer CCD, and interline transfer CCD. Figure 2.5 illustrates two types of charge-coupled device architectures, namely frame-transfer CCD and interline transfer CCD.

(a) Full-frame CCD

One of our microscope uses full-frame CCD which is supplied by Andor Tehcnology, Inc. In this design, every pixel of the CCD surfaces corresponds to the image being collected. During image collection, exposures are usually controlled by an electrochemical shutter.

(b) Frame-transfer CCD

In this design, one half of the CCD chip is masked and used as a storage space. After exposure, all of the pixels in the image side are transferred to pixels on the storage side. No camera shutter is needed because transferring time for the image is only a fraction of the exposure time.

(c) Interline Transfer CCD

In this design, imaging rows and masked storage transfer rows are parallel pixels of columns. Camcorders and video cameras typically use interline transfer CCDs because they provide high quality images and can be read out at video rate. This type of CCD can be used for dim fluorescent specimens because of the low camera read noise and improvement in camera electronics. Interline transfer CCDs can be very fast and they do not require a shutter to control the exposure. With current technologies, the spatial resolution and light-collecting efficiency can reach those of a full-frame CCD.

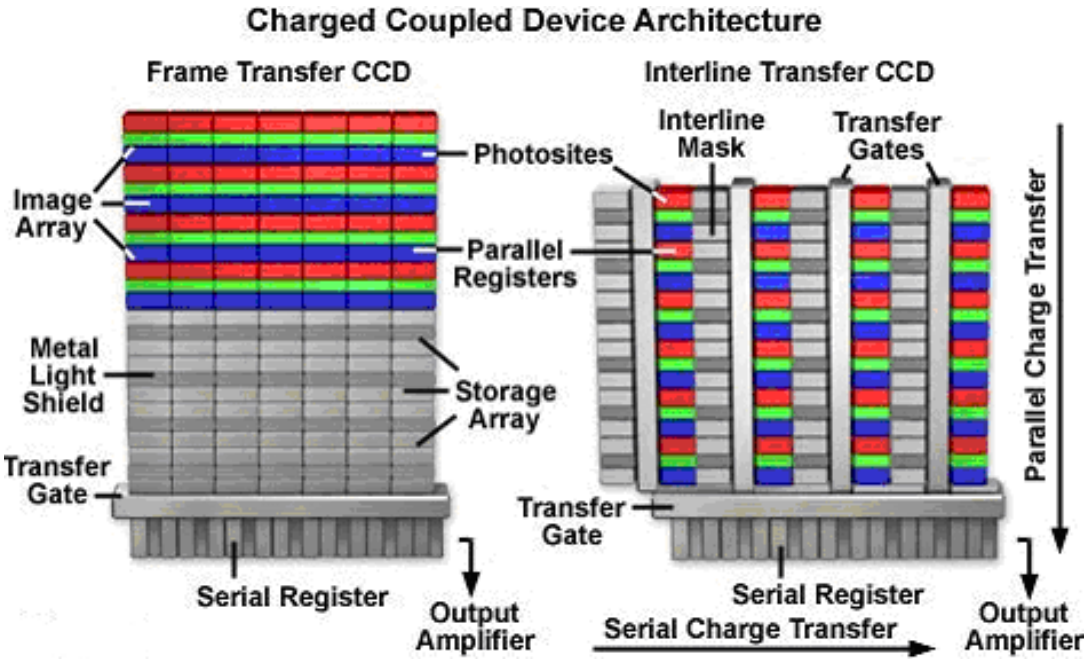

http://www.olympusmicro.com/primer/digitalimaging/digitalimagingdetectors.html

Figure 2.5. Frame transfer CCD and Interline transfer CCD.

2.3 Cell Culture of Hela and MCF7 Cells

MCF 7 cell is one type of breast cancer cells isolated from female and Hela cell is one type of cancer cellines isolated from female. These two cancer cells were used in the cell delivery experiments. An in-house protocol, developed by Dr. Nitsa Rosenzweig, was used to maintain these two different types of cell cultures. MCF 7 cells are cultured in Dulbecco's Modified Eagle Medium (DMEM) (Invitrogen Incorporate, Carlsbad, California) with 10% fetal bovine serum, 2 mM antibiotic-antimycotic, 8 mM L-glutamine, and 0.1 mM non-essential amino acids. Hela cells are cultured in Minimum Essential Medium (MEM) (Invitrogen. Incorporate, Carlsbad, California) with 10% fetal bovine serum, 2% antibiotic-antimycotic, 4 mM L-glutamine, and 1 mM sodium pyruvate. The cells are grown at 37^0 C under 5% CO_2. The medium was changed when there was a lot of cellular debris accumulating, when the medium changed color, or in general after two days have past.

Cell cultures were planted in a 4 well chamber. The following procedures describe the cell preparation steps of splitting the cells, counting the cells, and planting the cells.

To split the cells, the cells are detached from the surface of a T75 tissue culture bottle by adding 2 mL of trypsin. The trypsin treated bottle was then placed into an incubator for 10 min. The trypsin treated T75 bottle was then removed from the incubator and 20 mL of growth medium was added. The cells were mixed with the growth medium by a glass pipette.

To count the cells, it is always best to count right after splitting them. 500 μL of the cell suspension solution was mixed with 0.5 mL of trypan blue in a 1 mL Eppendorf tube. 12 μL of the mixed solution was then injected into the hemacytometer. The hemacytometer was then placed under the microscope to observe the 9 squares. If the cells number counting on the hemacytometer are #a, the number of the cells/mL are calculated by #a multiplying by 20,000.

From the calculated number of cells/mL the cells can be plated. The number of cells/well needed is known, then to determine how much volume in mL of the cell suspension is needed to add to each plate. For a 4 chamber well plate, we add 0.15 mL of the cell suspension (~1×10^6 cells/mL) to each well, and 0.7 mL of growth medium. The cells are incubated to attach and grow onto the wells at 37^0 C under 5% CO_2. Typically 70-90% confluency is achieved in one day for Hela cells or 3 days for MCF7 cells.

CHAPTER III SUBMICROMETRIC LIPOBEAD-BASED FLUORESCENCE SENSORS FOR CHLORIDE ION MEASUREMENTS IN AQUEOUS SOLUTION

3.1 Introduction

Chloride is one of the major anions in biological fluids. A number of physiological mechanisms that regulate cellular physiochemical properties like cell volume and pH, as well as membrane transport properties, involve chloride ion transport across cell membranes. An example of the importance of chloride ion transport is found in the disease Cystic Fibrosis where a defective transport of chloride anions across the plasma membrane of epithelial cells is often observed (1). A number of techniques have been used to detect chloride anions in biological systems. These include colorimetric titration (2), patch-clamp (3, 4), microelectrode (5, 6), fiber optic chloride ion sensor (7 Kopelman) and x-ray microanalysis (7). These approaches are invasive and generally lack sufficient sensitivity and selectivity. There is a need for less invasive and more sensitive methods for anion detection in biological systems.

Molecular fluorescence probes have emerged in the last two decades as useful tools for ion analysis in biological fluids. Most of the fluorescence probes were developed for the measurement of pH, and cations in cells (8, 9). Recently, these and other molecular fluorescence probes were immobilized to particles that were used as intracellular sensors. These particles include PEBBLEs (probes encapculated by biologically localized embedding) (10), liposomes (11-13), and lipobeads (14-16). Currently developed by Kopelman and co-workers PEBBLEs consist of a hydrophilic polymer matrix, e.g. polyacrylamide, which contains various fluorescence indicators. PEBBLEs have shown to be highly selective and sensitive. Due to their nanometric dimensions they exhibit fast response times in the millisecond time scale. Liposome-based sensors enable the encapsulation of hydrophilic and hydrophobic indicators in their

membranes and exhibit high biocompatibility (17-20). However, high leakage rate of fluorophores from liposomes is often observed, which negatively affect their analytical sensing properties (21). In our laboratory, we recently developed a new type of particle-based nanosensors termed lipobeads. Lipobeads are submicrometric polystyrene nanoparticles that are coated with a phospholipid membrane. Hydrophilic or hydrophobic fluorescent indicators can be immobilized to the phospholipid membrane (14-16, 22, 23). Previously we showed that lipobead-based fluorescence sensors could be used for intracellular pH and oxygen sensing under physiological conditions. Other groups have studied similar nanosensors termed lipospheres (24-27). Lipospheres consist of a hydrophobic fat core that is coated with a monolayer of phospholipids (28). While formulations of lipobeads show consistency in diameter and narrow size distribution it is more difficult to control the particle size and size distribution of lipospheres. Often, a heterogeneous sample of lipospheres ranging between 0.2 and 500 μm is obtained. Both lipobeads and lipospheres have similar advantages such as high physical stability, and low leakage rate of encapsulated probes and drugs. They are particularly attractive when hydrophobic indicators are used as sensing probes.

This paper reports the synthesis, characterization, and optimization of fluorescence-based submicrometric chloride ion sensing lipobeads. A unique chemistry is used in their design, which enables for the first time stable non-covalent immobilization of hydrophilic sensing dyes in their membrane.

3.2 Experimental

3.2.1 Preparation of Lucigenin- Hexadecanesulfonate Ion Pairs

The lucigenin- hexadecanesulfonate ion pair was synthesized following a method previously described by Wolbeis et al (29) with slight modifications. 2.6 mg lucigenin were dissolved in 4 mL phosphate buffer at pH 7.0. 3.3 mg of sodium hexadecanesulfonate dissolved in 2 mL methanol were added to the buffer solution. The resulting mixture was incubated at room temperature for 1 hour. The formed lucigenin- hexadecanesulfonate ion pair was then extracted with 15 mL chloroform. The chloroform solution was reduced to dryness by a gentle stream of nitrogen. The lucigenin-hexadecanesulfonate ion pair was then reconstituted in 0.5 mL chloroform resulting in a 10 mM lucigenin- hexadecanesulfonate solution**.**

3.2.2 Synthesis of Nanometric Fluorescent Lipobeads

The synthesis of the lipobeads was carried out using an oil-in-water microemulsion method. A 50 mM lipid stock solution was prepared with a 9:1 molar ratio mixture of 1,2-dimyristoyl-sn-glycero-3-phosphate (monosodium salt) (DMPA) and dihexadecyl phosphate (DP) in chloroform/methanol/H_2O (65:25:4 v/v/v). Microemulsion was formed when 90 μL of the phospholipid solution and 30 μL of the 10 mM lucigenin- hexadecanesulfonate ion pair dissolved in chloroform were added to 100 μL aqueous suspension of polystyrene microspheres averaging 780 ± 3.8% nm in diameter. The microemulsion was transferred to a 50 mL round bottomed flask in which the mixture was evaporated by a rotary evaporator. The microemulsion had to be dried completely to avoid subsequent aggregation of the lipobeads. The dried lipobeads sample was then resuspended in 5 mL of MOPS buffer at pH 7.4 and gently stirred for 5 hours. The formed lipobeads were washed three times using slow speed centrifugation (4000

rpm for 15 minutes) to remove excess fluorescent indicator and phospholipid molecules and unreacted polystyrene microspheres. Lipobeads coupled with indicators were suspended in 10 mL of MOPS buffer (pH 7.4) and stored in glass vials covered with aluminum foil at 4 ^{0}C until used.

3.2.3 Incorporation and Comparison of Ionophores

The ionophores [9] mercuracarborand-3 (MC-3), the manganese based ionophore 5,10,15,20-Tetraphenyl-21H, 23H-porphine manganese (III) chloride (Chloride Ionophore I), and the sodium ionophore 4-tert-Butylcalix [4] arene-tetraacetic acid tetraethyl ester (Sodium Ionophore X), were each incorporated into the lipobeads for ion response comparative studies. The hydrophobic ionophores were easily incorporated into the phospholipid membrane by adding the ionophores to the phospholipid solution used for the preparation of the lipobeads. The lipobeads containing the three ionophores were tested for their response to millimolar concentrations of Cl^-, Br^-, I^-, and NCS^- using a Photon Technologies Inc. fluorimeter (PTI, Canada). For calibrating the chloride ion sensitive lipobeads, 1 mL lipobeads suspension was placed in a cuvette and its emission at 500 nm (ex = 430 nm) was measured using the spectrofluorometer. Under constant stirring, microliter aliquots of 1 M NaCl in a MOPS buffer solution at pH 7.4 were added to the cuvette to obtain increasing concentrations of chloride ions. Each data point was repeated three times.

3.2.4 Response Time of the MC-3 Lipobeads

The response time of the MC-3 lipobeads was measured by monitoring the change in fluorescence intensity upon the addition of a chloride solution to a solution of the chloride sensing lipobeads suspended in a phosphate buffer solution at pH 7.0. The fluorescence intensity

was measured as a function of time using excitation wavelength of 430 nm and an emission wavelength of 500 nm. To conduct the measurement 1.8 mL of lipobead solution was placed in a 3 mL quartz cuvette (1 cm pathlength). The sample was placed in the fluorometer and its emission was monitored until obtaining a stable baseline. Then, 10 μL of a 3 M NaCl solution was injected into the cuvette while the lipobead solution was stirred. The emission measurement was continuously recorded until a stable baseline was observed.

3.2.5 Digital Fluorescence-Imaging Microscopy

The experimental setup used for fluorescence measurements of the lipobeads based sensors consisted of an inverted fluorescence microscope (Olympus IX-51) that is attached to a high performance charge coupled device (CCD) camera (Andor Technology, DV434-BV). A 100-W mercury lamp was used as the light source for excitation. The fluorescence was collected through a 40X microscope objective with N.A=0.9. A filter cube containing suitable excitation filters, dichroic mirrors, and emission filters was used to ensure spectral purity. The exposure time used in most experiment was 0.5 seconds. The software Image Pro+ (Media cybernetics inc.) was used for image analysis.

3.3 RESULTS AND DISCUSSION

3.3.1 Choice of Fluorescence Indicator

A number of fluorescent indicators were used previously for chloride ion analysis in aqueous samples (30). Table 3.1 is a compilation of the spectroscopic properties of widely used Cl^- sensitive chromophores (monique) (31). For our lipobead based sensors we chose lucigenin (N,N'-dimethyl-9,9'-bisacridinium dinitrate), as the chloride sensitive fluorophore. Lucigenin is

a heterocyclic compound with quaternized nitrogen atoms that is highly sensitive to chloride quenching. Figue 3.1 illustrates the lucigenin structure (32). Its maximum excitation and emission wavelengths (λex = 430 nm, λem = 500 nm) are longer than the excitation and emission wavelengths of other chloride ion fluorescence indicators like 6-methoxy-*N*-(3-sulfopropyl) quinolinium (SPQ) (33). Lucigenin is characterized by a relatively high emission quantum yield of 0.67 and it is pH insensitive between pH 5 and 8 (34). Its fluorescence is minimally quenched by inorganic anions like sulfate, nitrate and phosphate, organic anions like bicarbonate and citrate, and monovalent and divalent cations that are abundant in biological fluids (33). Figure 3.2(a) shows the fluorescence quenching response of free lucigenin in solutions of increasing chloride ion concentrations. The fluorescence intensity at 490 nm (λex=430 nm) decreases by approximately 10 fold as the chloride ion concentration increases from 0 to 50 mM. Figure 3.2(b) shows a Stern-Volmer plot describing the chloride ion concentration dependence of the ratio F_0/F of free lucigenin, where F_0 is the fluorescence intensity at chloride free solution while F is the fluorescence intensity at a given chloride ion concentration. The Stern-Volmer quenching constant, K_{sv}, was determined to be 225 M^{-1}, with a correlation coefficient of 0.9945.

	Absorbance		Fluorescence			
	Peak abs (nm)	Molar extinct. coeff. (M^{-1} cm^{-1})	Excitation (nm)	Emission (nm)	Quantum yield	K_{halide} (M^{-1})
SPQ	318/345	5,400/3,450	322/350	450	0.69	118 (Cl^{-1})
MEQ	318/344	5,700/4,100	322/350	440	0.70	140 (Cl^{-1})
MQAE	320/350	4,850/2,800	355	460	0.75	200 (Cl^{-1})
TMAPQ	318/348	5,800/3,700	325/355	450	0.73	310 (Cl^{-1})
Lucigenin	368/455	34,200/7,400	368/455	506	0.67	390
LMQ	428	9000	428	533	0.47	70 (Cl^{-1})
Bis-DMXPQ	324/342/440	36,200/26,800/7,000	342/364/440	450/560	0.40 (450 nm) 0.04 (560 nm)	82 (Cl^{-1})

SPQ: N-sulfopropyl-quinolinium; MEQ: 6-methoxy-N-ethylquinolinium iodide; MQAE: *N*-(ethoxycarbonylmethyl)-6- methoxyquinolinium bromide; TMAPQ: 6-Methoxy-N-93-trimethylammoniumpropyl)quinolimium dibromide; Lucigenin: N,N`-Dimethyl-9,9`-biacridinium dinitrate; LMQ: 4-aminopyrido[2,1-h]-Pteridin-11-ium-5-olate; Bis-DMXPQ: *trans*-1,2-bis[4-(1-α'-MQ-1'-α'-DMAQ-xylyl)-pyridinium] ethylene

Table 3.1. Properties of chloride indicators.

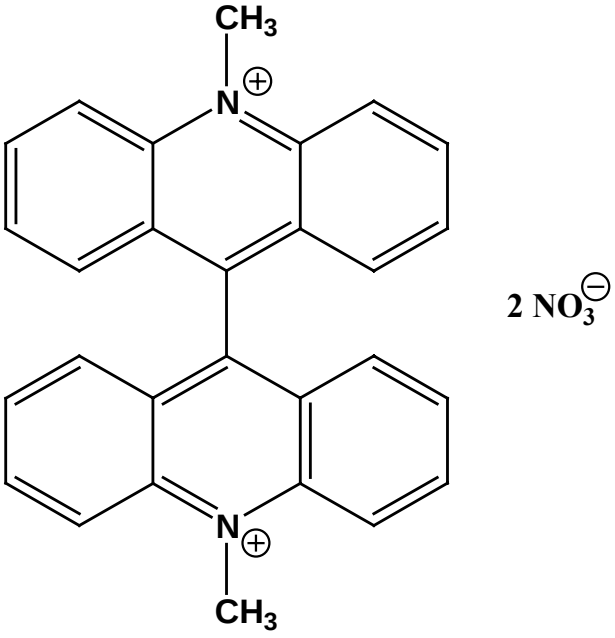

Figure 3.1. Lucigenin structure.

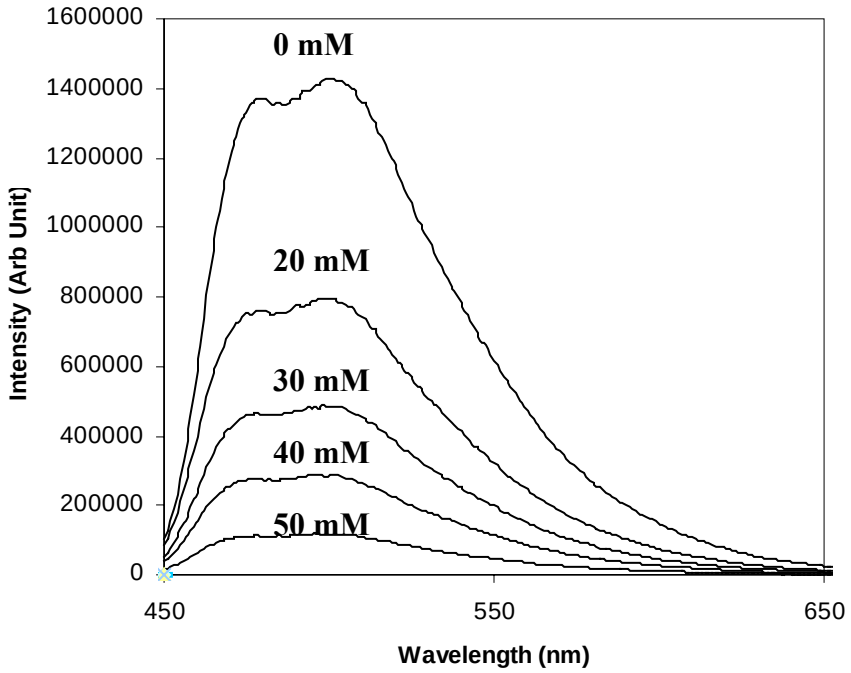

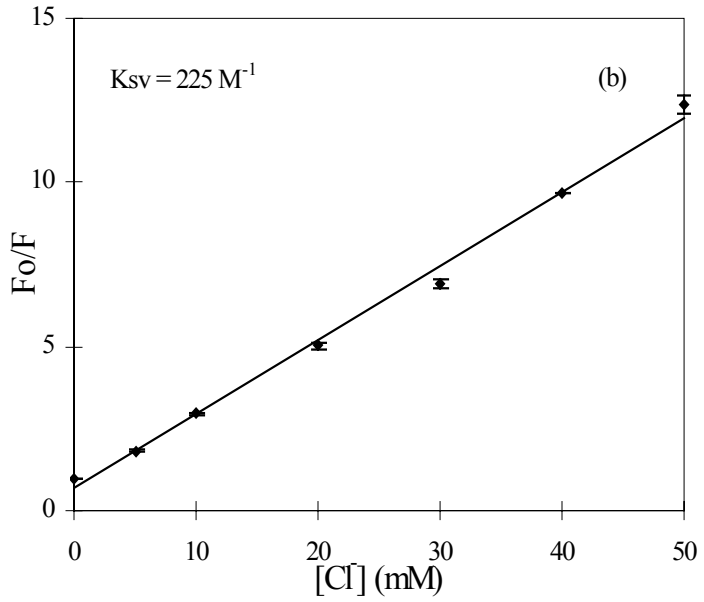

Figure 3.2 -(a) Fluorescence spectra of lucigenin in phosphate buffer solutions at pH 7.4 with increasing chloride ion concentrations from 0 to 50 mM (λex=430 nm) (b) A Stern-Volmer plot describing the ratio between the initial fluorescence (F_0) intensity and the fluorescence intensity at a given chloride ion concentration (F) against chloride ion concentration. The Stern-Volmer constant, K_{sv}, was determined to be 225 M^{-1}.

3.3.2 Incorporation of Ion-Pair into the lipobeads

Lipobeads that only contain lucigenin were ineffective as chloride ion sensors due to poor partition of the water-soluble lucigenin molecules into the phospholipid membrane and high leakage rate of the immobilized lucigenin molecules to the aqueous medium. To stabilize the chloride ion sensing lipobeads, hexadecanesulfonate molecules were co-immobilized into the phospholipid membrane. Scheme 3.1 illustrates the formation of the ion pair between lucigenin and hexadecansulfonate. The negatively charged hexadecanesulfonate molecules are attracted electrostatically to the positively charged nitrogen atoms of the lucigenin molecules. The complex becomes more hydrophobic and could partition into the phospholipid membrane at a higher rate compared to the partition of free lucigenin molecules. To determine if the incorporation of the ion pair would have a detrimental effect on the luminescence properties of lucigenin we compared the absorbance and emission spectra of lucigenin dissolved in aqueous solution and lucigenin-hexadecanesulfonate ion pair dissolved in chloroform. Figure 3.2 shows that the formation of the lucigenin-hexadecanesulfonate ion pair had minimal effect on the absorption and fluorescence of lucigenin. The shape of the absorption spectrum remained similar except for an increased absorption between 400 and 450 nm (figure 3.3a). The fluorescence spectrum (figure 3.3b) shows no apparent shifts or change in peak shape except for minor features at 470 nm. Digital fluorescence images of lipobeads containing free lucigenin and lucigenin-hexadecanesulfonate ion

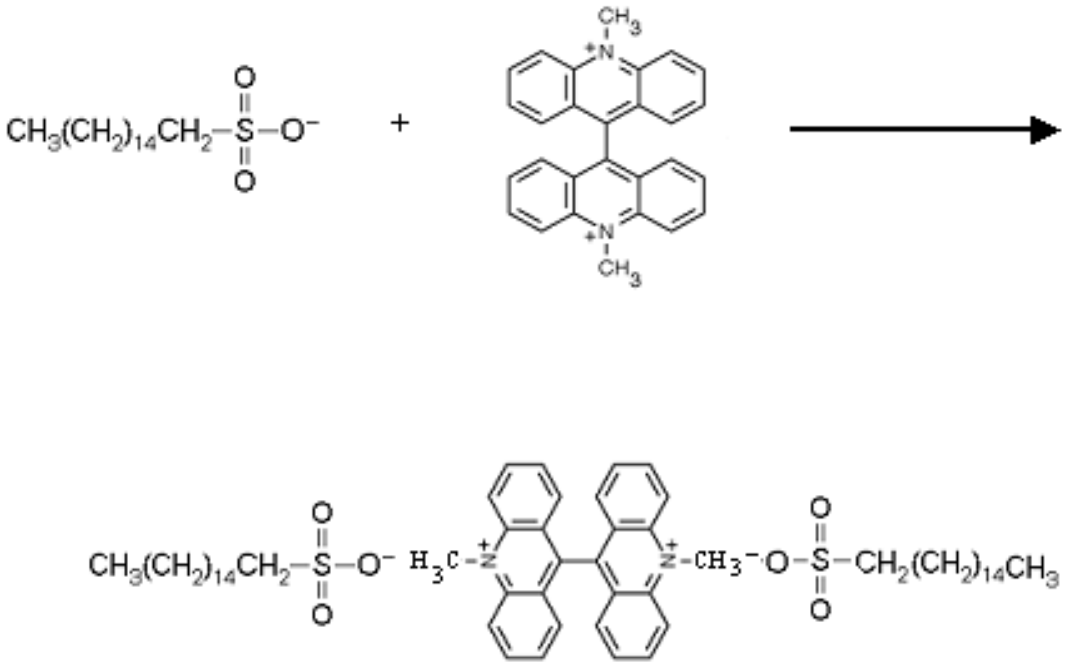

Scheme 3.1 - A proposed mechanism for the incorporation of the ion-pair into the phospholipid membrane. The lucigenin molecules partition effectively into the phospholipid membrane due to the formation of ion pairs with hexadecanesulfonate.

pairs are shown in figures 3.4a and 3.4b respectively. Both images reveal that the lipobeads were monodispered in aqueous solution. However, the lipobeads that contain lucigenin-hexadecanesulfonate appear brighter than lipobeads that contain free lucigenin. To quantify the difference in brightness we measured the signal to background ratio in these images.

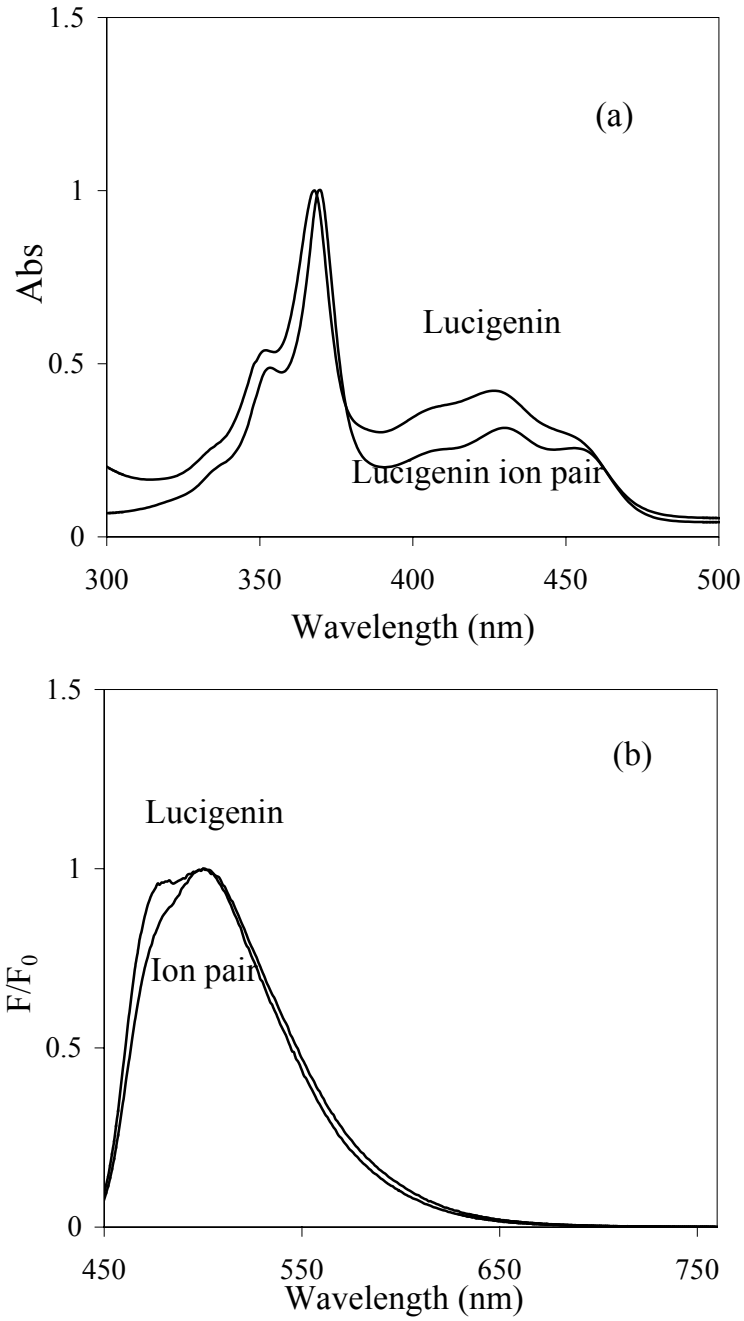

Figure 3.3 - Absorption spectra (a) and fluorescence spectra (b) comparing the spectroscopic properties of free lucigenin in aqueous solution and the lucigenin- hexadecanesulfonate ion pair dissolved in chloroform. The ion pair formation had minimal effect on the spectroscopic properties of lucigenin.

We first defined the boundaries of the particles and measured their fluorescence intensity. We then measured the background signal by defining areas near the measured particles that occupied the same number of pixels and measured the fluorescence intensity of these areas. The average signal to background ratio in figure 3.4b (lucigenin-hexadecanesulfonate lipobeads) is about 100 while the signal to background ratio in figure 3.4a is about 13 (free lucigenin lipobeads). It is fair to conclude that the formation of ion pairs between hexadecanesulfonate and lucigenin decreased the hydrophillicity of the dye and increased its partition rate into the membrane. This resulted in a largely increased brightness of the particles. We also characterized the effect of ion pair formation on the leaking stability of the chloride ion sensing lipobeads. A lipobeads sample suspended in 10 ml MOPS buffer solution at pH 7.4. The particles were precipitated daily using slow speed centrifugation (4000 rpm for 15 minutes) and the fluorescence of the supernatant was measured to test for leakage of fluorophores from the membrane of the particles. No significant leakage was observed over a period of two weeks. In contrast, lipobeads containing free lucigenin were largely unstable loosing over 50% of their fluorescence during the first 24 hours of storage. We concluded that the formation of the lucigenin- hexadecanesulfonate ion pairs largely increased the leakage stability of the lipobeads. We also tested the photobleaching rate of the lucigenin containing lipobeads. Lipobeads samples were placed on a microscope slide and were illuminated constantly for 30 minutes using the 100W mercury lamp of the microscope. We found that the excitation intensity must be reduced to minimize photobleaching of the particles. Using a neutral density filter of 1.0 we found that the fluorescence of the lipobeads lost less than 10% of the original fluorescence signal during

(a)

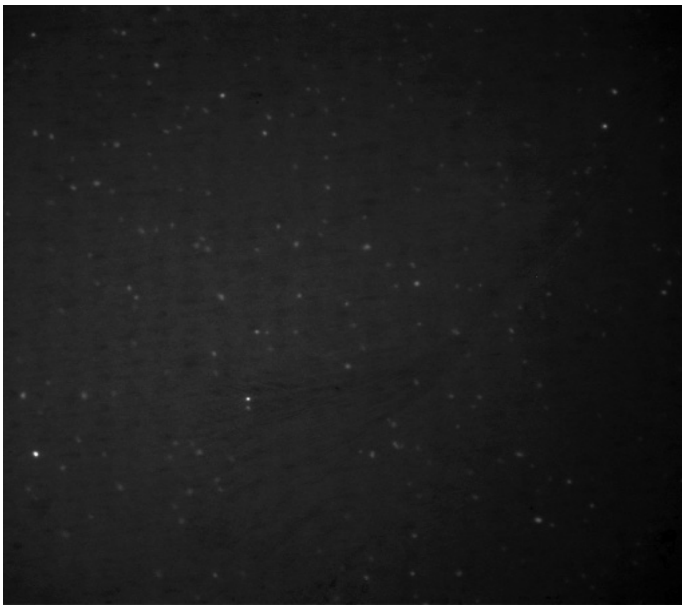

(b)

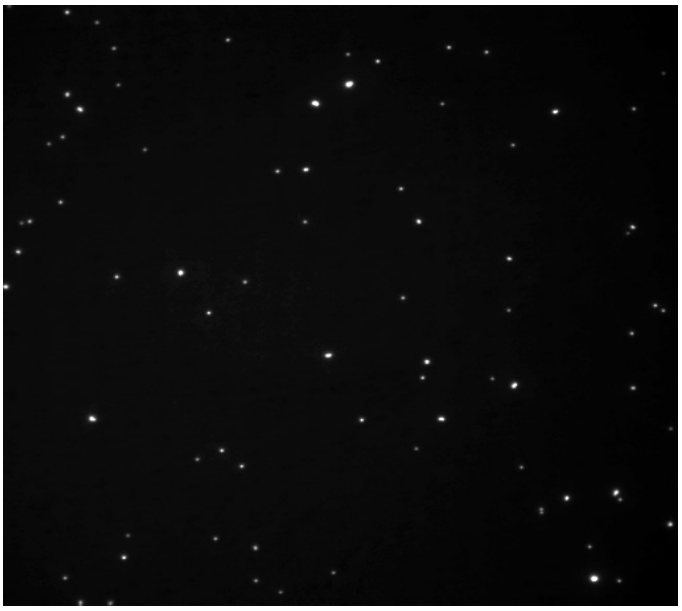

Figure 3.4 - Digital fluorescence images of (a) lipobeads containing free lucigenin, (b) lipobeads containing the lucigenin- hexadecanesulfonate ion pair. The signal to background ratio improves from 13 (image 3.4a) to about 100 (image 3.4b).

30 minutes of continuous illumination. It should be noted that in microscopy experiments the lipobeads are exposed to excitation light only during the actual exposure time of the CCD camera used for imaging. In a typical experiment the lipobeads are exposed to the excitation light for less than 1 minute.

3.3.3 A Comparison Between Ionophores

To further improve the selectivity of the lipobeads, ionophores (34) were incorporated into the phospholipid membrane of the lipobeads. Due to their inherent hydrophobicity, the ionophores used in this study were easily incorporated into the phospholipid membrane, simply by adding the ionophores to the phospholipid cocktail used in the microemulsion. Figure 3.5 illustrates the transport mechanism of the analyte by the ionophore into the lipobeads membrane. In our experiments we compared the performance of three ionophores. [9] mercuracarborand-3 (MC-3)(35-37) and the manganese based Chloride Ionophore I are known for their chloride ion selectivity (38). We also utilized the Sodium Ionophore X as an ionophore in our system. As previously mentioned chloride ionophores selectively transport chloride anions into the membrane. This is followed by the permeation of counter cations into the membrane (e.g sodium) to balance the membrane charge. Sodium ionophores transport sodium cations into the membrane, which is followed by the permeation of counter anions to balance the membrane charge. It was expected that a membrane containing sodium ionophore would show lower selectivity towards chloride ions since all the anions in the analyte solution could permeate the membrane following sodium ion transport. The chloride ion selectivity of this system was based on the lucigenin selectivity and on the difference between the permeation rate of chloride

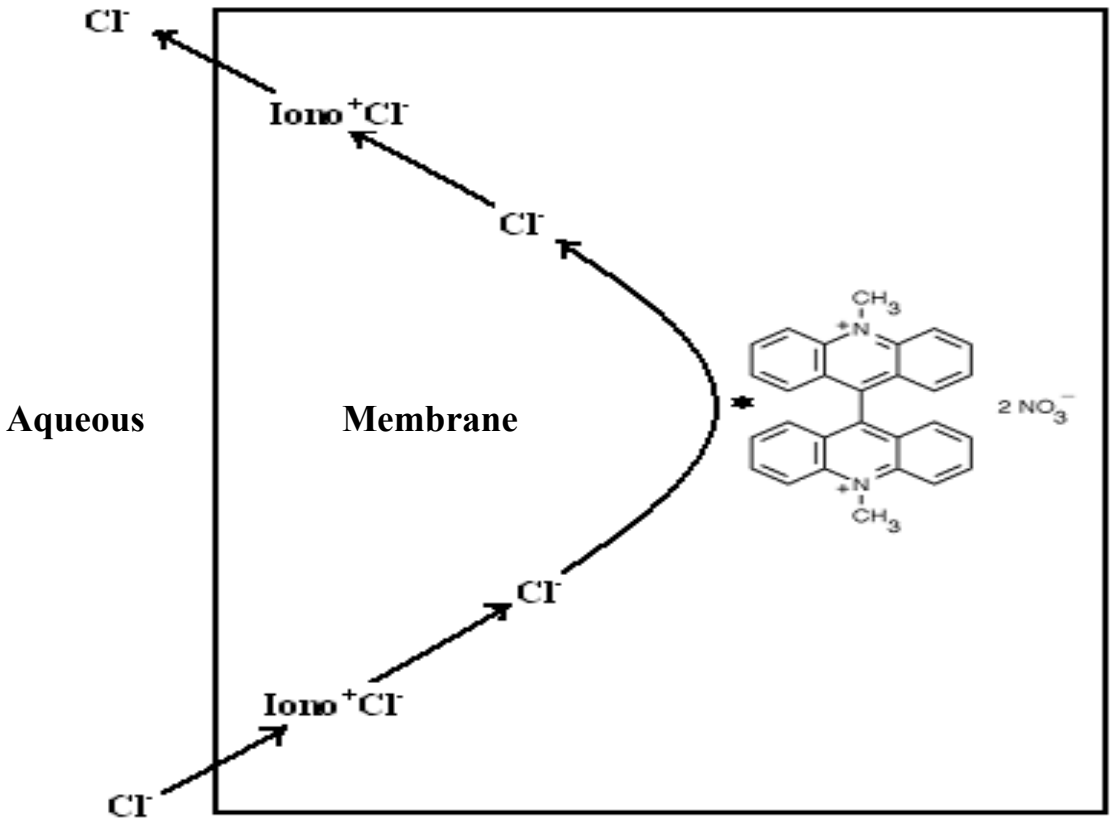

Figure 3.5 - Mechanism of the phase transport of chloride ions from the aqueous phase, by the ionophore, into the lipobead membrane. $Iono^+$ is the ionophore, Cl^- the anion analyte, and $Iono^+Cl^-$ the ionophore:analyte complex. The ionophore transports the anion from the aqueous phase into the phospholipid membrane, thus allowing the chloride to quench the fluorescence of lucigenin.

ions and other ions into the membrane. On the other hand, membranes containing chloride selective ionophores were expected to show higher chloride ion selectivity since chloride ions were selectively transported into the membrane and lucigenin selectively responded to chloride ions. However, some interference from other halides, particularly iodide, was still observed. It should be noted however that in biological fluids the level of chloride is 4 or more orders of magnitude higher than the level of other halides. Our studies revealed that the ionophore MC-3 was about twice more selective to chloride ions than to other halides and showed 50% lower response to iodide. Figure 3.6 shows the structure of the chloride ionophore MC-3. Both MC-3 and the chloride ionophore I did not respond to other competing ions like phosphate and bicarbonate. Phospholipid containing MC-3 were slightly more stable than lipobeads containing the chloride ionophore I. We therefore focused our experiments on MC-3 containing lipobeads. Figure 3.7 describes the fluorescence response of chloride sensitive lipobeads as a function of MC-3 concentration in the lipobeads preparation solution. The chloride ion response is defined as F_0/F_{50mM} where F_0 is the fluorescence intensity of the lipobeads in a chloride free MOPS buffer solution at pH 7.4, and F_{50mM} is the fluorescence intensity of the lipobeads when the chloride ion concentration in the same lipobeads solution is raised to 50 mM. At low concentrations MC-3 did not effectively transport chloride ions into the membrane. The chloride ion response of the lipobeads increased with increasing chloride ion concentrations. The lipobeads exhibited the highest chloride ion sensitivity when the concentration of MC-3 in the lipobeads preparation solution was about 5 mM. However, the response decreased sharply as the concentration of the ionophore exceeded 5 mM. This is attributed to a

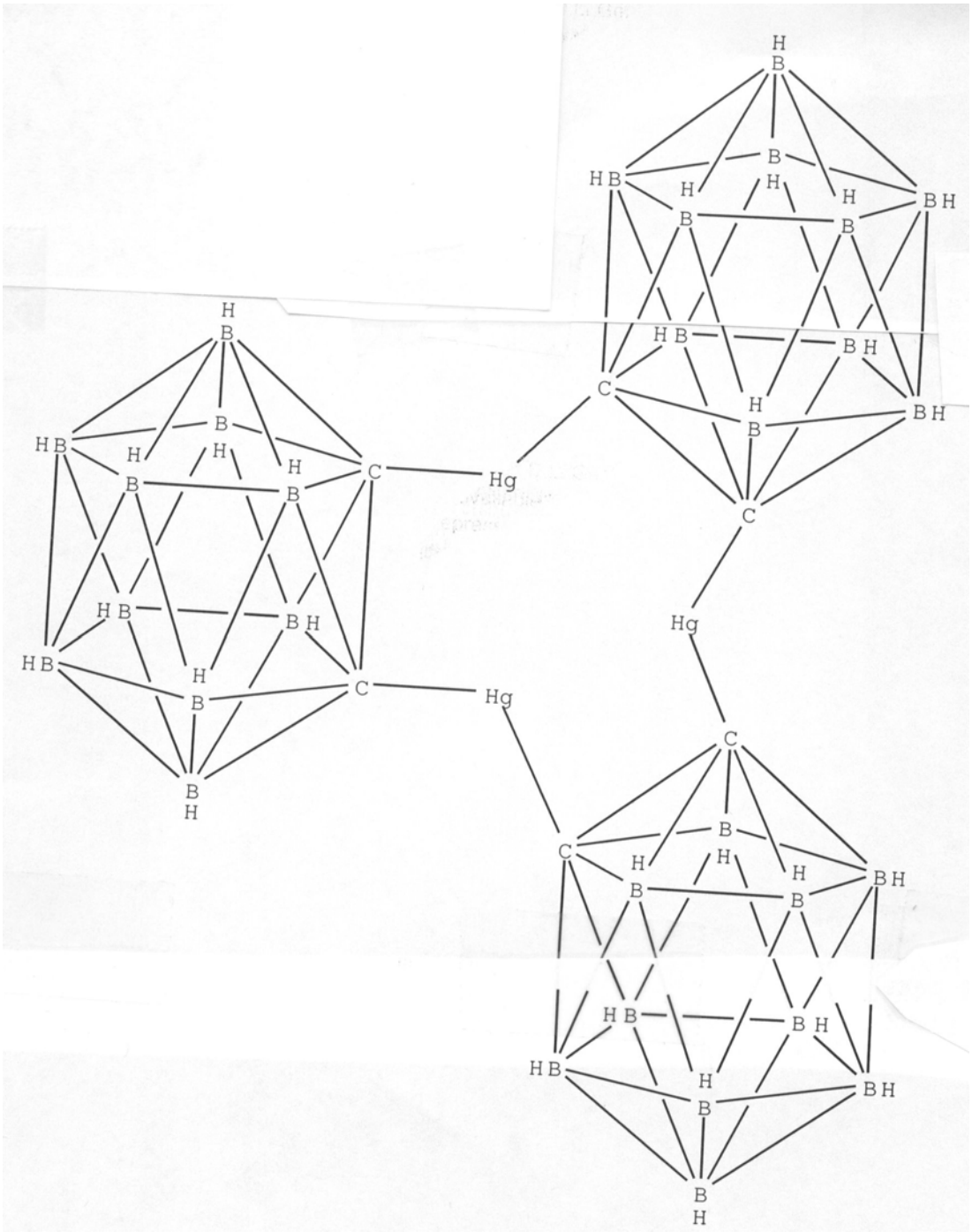

Figure 3.6. Structure of the chloride ionophore MC-3.

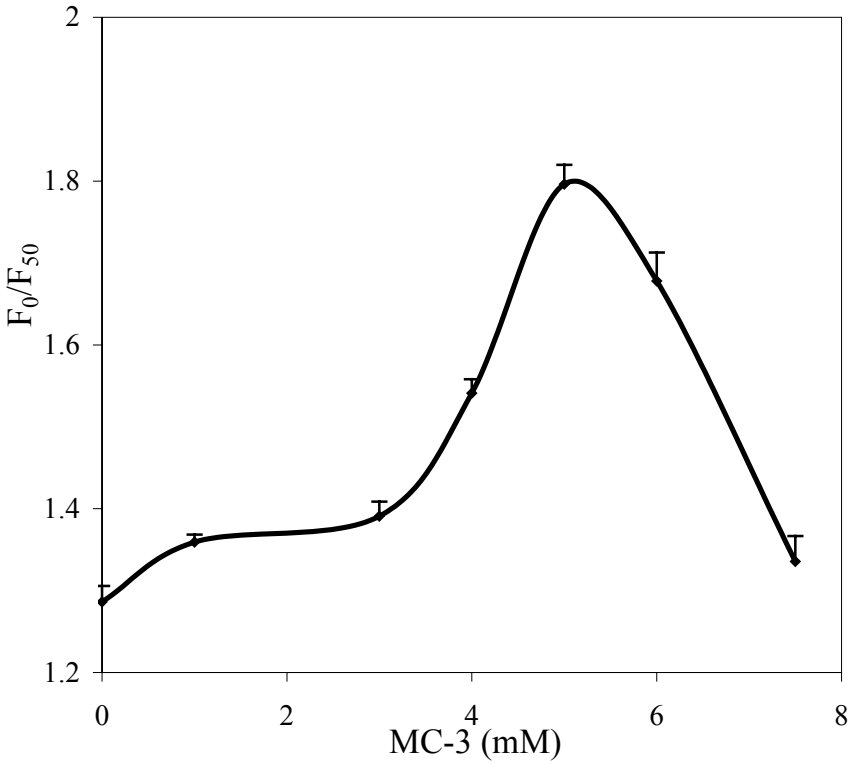

Figure 3.7 – The chloride response of MC-3 containing lipobeads (F_0/F_{50mM}) as afunction of MC-3 concentration. F_0 is the fluorescence intensity of MC-3 containing lipobeads in a chloride free phosphate buffer solution at pH 7.2. F_{50mM} is the fluorescence intensity of the lipobeads solution when the chloride ion concentration is raised to 50 mM. It can be seen that the optimal MC-3 concentration in the phospholipid solution used to prepare the lipobeads is 5 mM.

competition between the ionophore molecules and the lucigenin- hexadecanesulfonate ion pairs on the limited number of hydrophobic pockets in the phospholipid membrane. Indeed, the fluorescence intensity of the lipobeads as well as the chloride ion response decreased with

increasing concentrations of MC-3 in the phospholipid solution that was used to prepare the lipobeads.

3.3.4 Analytical Properties of the MC-3 Lipobeads

Figure 3.8 shows a Stern-Volmer plot of chloride sensing lipobeads that contain the lucigenin- hexadecanesulfonate ion pair and MC-3 with increasing chloride ion concentrations. Similarly to other fluorescence quenching based sensors a significant variation from linearity is observed. This is attributed to heterogeneity in the microenvironment of fluorescence indicators within the supportive matrix of solid-state sensors (39,40)**.** In our system, there are a limited number of lucigenin molecules that are stably immobilized to the surface of the phospholipid membrane. These molecules are more accessible to chloride ions than lucigenin ion pairs that are embedded in the hydrophobic region of the phospholipid membrane. As a result, the Stern Volmer constant, K_{sv}, at chloride ion concentrations below 2 mM is higher than K_{sv} at higher concentrations. Furthermore, additional variation from linearity is observed at concentrations higher than 30 mM due to saturation. The change in K_{sv} values is clearly seen in Figure 3.8 where the three concentration zones are characterized by dashed lines of decreasing K_{sv}. The K_{sv} between 2 and 50 mM, which the biologically relevant concentration zone, is about 17 M^{-1}, which is an order of magnitude lower than the Stern-Volmer constant of free lucigenin in solution. This is typically observed in solid-state sensors since the analyte of interest must permeate through the solid-state support, in our case the phospholipid membrane, to interact with the sensing fluorophores. Nevertheless, the chloride ion sensitivity of the chloride sensing lipobeads is sufficient to quantify chloride ion levels often found in the millimolar range in biological fluids.

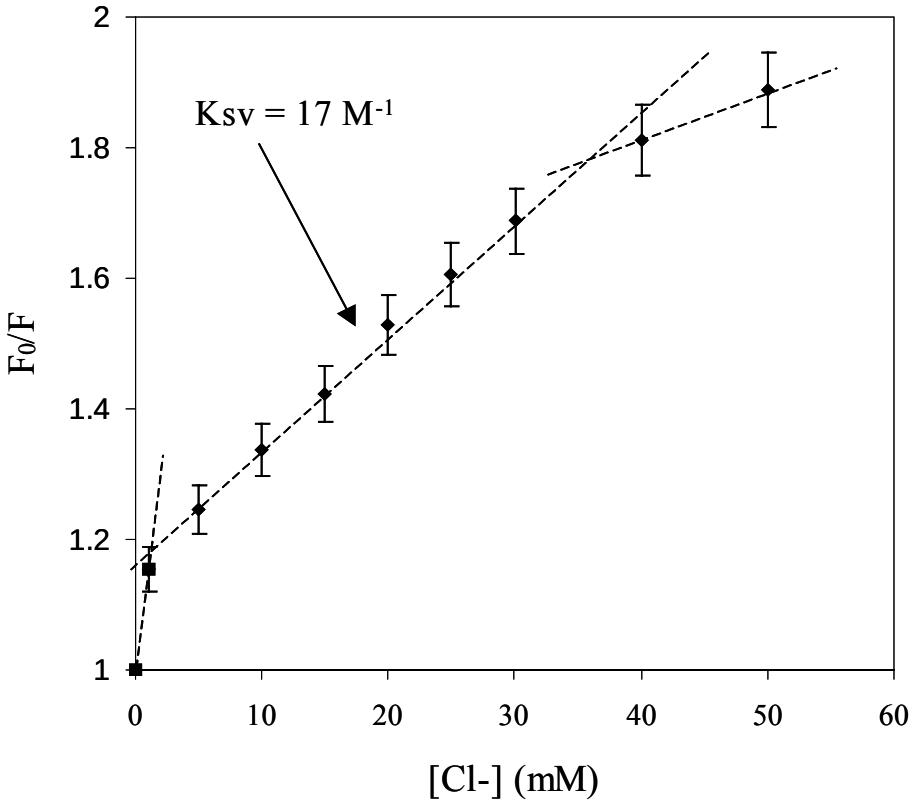

Figure 3.8 - A Stern-Volmer plot describing the chloride ion response F_0/F with increasing chloride ion concentrations. F0 is the fluorescence intensity of the lipobeads in a chloride free phosphate buffer solution at pH 7.2. F is the fluorescence intensity of the lipobead solution at a given chloride ion concentration. Typical variations from linearity are observed at chloride ion concentrations lower than 2 mM and higher than 30 mM.

Previous studies in our laboratory with oxygen sensing lipobeads showed that the response time of individual lipobeads was in the sub-second time scale. However, oxygen readily permeates through the phospholipid membrane of the lipobeads while chloride ions, as previously discussed, require an active transport mechanism by an ionophore to effectively interact with the sensing fluorophore. Response time measurements of the chloride sensing lipobeads are shown in figure 3.9. The fluorescence of a lipobeads solution was measured using the fluorometer at 500 nm (λ_{ex} = 430 nm). The fluorescence dropped sharply when an aliquot of concentrated chloride solution was injected into the constantly stirred lipobeads solution. Since each data point represents a time interval of 1 second the response time could be estimated to be about 5 seconds. It was difficult to obtain the recovery time of the lipobeads since diluting the sample with an aqueous sample diluted the number of lipobeads in the sample and decreased the fluorescence intensity of the solution. Adding aqueous solution containing lipobeads at the original lipobeads concentration was problematic as well since such injection often resulted in an intensity spike due to light scattering. Full reversibility studies would require immobilization of the lipobeads to a solid-state support (e.g. glass). A procedure to immobilize the fluorescence sensing lipobeads to a glass support through silane chemistry is currently developed in our laboratory.

3.4 CONCLUSIONS

This paper reports the development of unique chloride ion sensing lipobeads of submicrometric dimensions with the capability to quantify chloride ion levels in aqueous samples and biological fluids. Several new advances are reported: First, the use for the first time

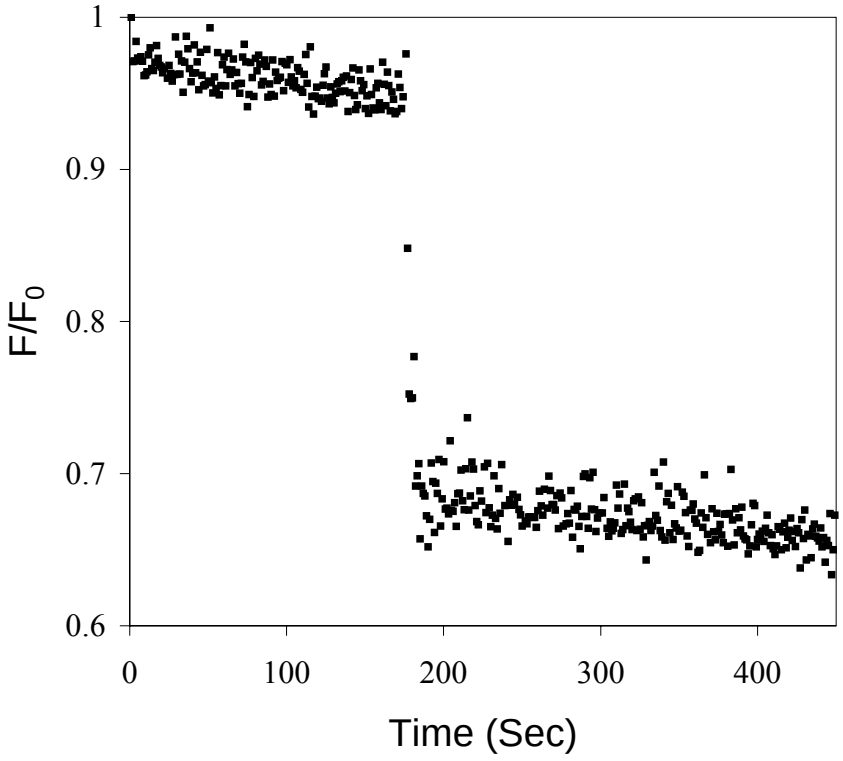

Figure 3.9 - Characterization of the response time of the chloride ion sensing lipobeads- the fluorescence intensity of the lipobeads prior and following the injection of an aliquot of concentrated chloride solution is shown.

of an oil-in-water microemulsion method to prepare the lipobeads resulted in lipobead formulations of smaller lipobead diameters with minimal aggregation compared to previous studies in our laboratory and compared to other submicrometric particle-based sensors. Secondly, the paper describes the first lipobead based anion sensor. To realize this task the naturally hydrophilic chloride sensitive dye lucigenin was ion paired with alkyl hexadecanesulfonate to decrease its hydrophilicity. This resulted in greater partition rate of the lucigenin dye into the membrane of the lipobeads and decreased the leakage of lucigenin from the sensing particles. The formation of lucigenin- hexadecanesulfonate ion pairs and their incorporation into the phospholipid membrane did not affect the luminescence properties of lucigenin. However, due to poor permeability of chloride into the membrane the lucigenin containing lipobeads were ineffective as chloride ion sensors in the absence of an active mechanism for chloride ion transport from the solution into the membrane. The incorporation of the chloride ionophore [9] mercuracarborand-3 (MC-3) into the phospholipid membrane provided the required transport mechanism. The chloride sensing technique presented in this paper is different than previously described chloride ion sensors that were based on the co-immobilization of a chloride selective ionophore and a pH sensitive dye in thin films or larger particles. The transport of chloride ions into the film or particles resulted in a proton gradient that was sensed by the pH sensitive dye. Such systems have been limited in their application to solutions of strong buffering capacity, as pH changes in the solution would surely elucidate a response from the chloride ion sensor. The use of the chloride sensitive dye lucigenin instead of a pH sensitive dye is a departure from this pH based sensing technology. Moreover, the use of lucigenin provides an additional selectivity dimension since both the ionophore MC-3 and lucigenin are chloride ion selective. However, while chloride ionophores are insensitive to

biologically important anions like phosphate and bicarbonate there is still a room for improvement in their chloride ion selectivity particularly against other halides. Currently available anion selective ionophores are not as effective as cation selective ionophores such as the ones available for sodium and calcium. The development of anion selective ionophores will continue to be the bottleneck for the development of anion sensors in the foreseeable future. Nevertheless, even with their current analytical properties our newly developed chloride sensing lipobeads provide an effective technique for the measurement of chloride ions in biological fluids.

ACKNOWLEDGMENT

The authors gratefully thank Dr. Eric Bakker for providing us with the ionophore [9] mercuracarborand-3 (MC-3). This work was supported by NSF Grant CHE-0314027.

3.5 REFERENCES

1. Jayaraman, S.; Biwersi, J.; and Verkman, A.S. Am.J. Physiol.., **1999**, 276, C747-757.
2. Koneke, J.; Tepel, M.; Kisters, K. Trace Elements and Electrolytes, **2001**,18(1), 7-12.
3. Fischer, Horst; Machen, Terry E. Biophysical J. **1996**, 71(6), 3073-3082.
4. Ray, D. E.; Sutharsan, S.; Forshaw, P. J. Neurotoxicology, **1997**, 18(3), 755-760.
5. Ishibashi, K.; Sasaki, S.; and Yoshiyama, N. Am. J. Physiol., **1988**, 255, F49-F56.
6. Stanton, B. A. Am. J. Physol., **1988**, 254, F80-F86.
7. Acker H; Pietruschka F; Zierold K In Vitro Cellular and Developmental Biology, **1985**, 21(1), 45-8.
8. Cherlet, M, Franck, P, Nabet, P, and Marc, A. Biotechnol. Prog., **1999** 15 (4), 630 –639.
9. de Silva, A. P.; Eilers, J.; Zlokarnik, G. Proc. Natl. Acad. Sci. U.S.A. **1999**, 96, 8836-8837.
10. Clark H. A., Hoyer M, Philbert M A., and Kopelman R. Anal. Chem, **1999**, 71 (21), 4831 –4836.
11. Nguyen T, Rosenszweig Z. Anal Bioana Chem, **2002**, 374, 69-74.
12. McNamara, K.P.; Rosenzweig, N.; and Rosenzweig, Z Mikrochim. Acta, **1999**, 131, 57-64.
13. Verkman, A S; Takla, R; Sefton B ;Basbaum C; and Widdicombe J H. Biochemsitry, **1989**,28,4240-4244.
14. Ji, J.; Rosenzweig, N.; Griffin, C.; Rosenzweig, Z. Anal. Chem. **2000**, 72(15), 3497-3503.
15. Ji, J.; Rosenzweig, N.; Jones, I.; Rosenzweig, Z. Anal. Chem., **2001**, 73(15), 3521-3527.
16. McNamara, K. P.; Nguyen, T.; Dumitrascu, G.; Ji, J.; Rosenzweig, N.; Rosenzweig, Z. Anal. Chem, **2001**, 73(14), 3240-3246.
17. New, R. R. C. Liposome-A Practical Approach, IRL Press, Oxford University Press Inc., New York, **1990**.
18. Hope M.J. ;Bally, M.B.; Webb, G.; Cullis, P.R. Biochim. Biophys. Acta, **1985**,812,55.
19. Kremer, J.M.H.; Van der Esker, M.W.J; Pharmanoharan, C.;Wiersema, P.H. Biochemistry, **1977**, 16, 3932.
20. Banghan, A.D.; Standish, M.M.; Watkins, J.C.; J. Mol. Biol., **1965**,13,238.
21. Lentz, B. R.; Carpenter, T. J.; and Alford, D. R. Biochemsitry, **1987**, 26, 5389.
22. Kim Y, Lichtenbergova L, Skitko Y and Cho W. Anal. Biochem., **1997**, 259, 109-116.
23. Jin, T.; Pennefather, P.; Lee, P. I. FEBS Letter, **1996**, 397,70-74.
24. Domb, A. J.; Bergelson, L.; Amselem, S. Lipospheres for controlled delivery of substances. In Microencapsulation, Bernita,S. (ed.), Marcel Dekker: New York, **1996**,377-410.
25. Vyas, S. P.; Singh, R; Dimitrijevic, D. Pharmazie, **1997**,52,403-404.
26. Schwarz, C.; Mehnert, W. J. Microencapsulation, **1999**, 16, 205-213.
27. Gasco, M.R.; Cavalli, R.; and Carlotti, M.E. Pharmazie, **1992**,47, 119-121.
28. Rasiel, A.; Sheskin, T.; Bergelson, L.; and Domb, A. Polym. Adv. Technol. **2002**,13,127-136.
29. Mohr, G.J.; Werner, T.; Oehme, I.; Preininger, C.; Klimant, I.; Kovacs, B.; and Wolfbeis, O.S. Adv. Mater., **1997**, 9, 1108-1113.
30. Jayaraman, S;Verkman, A.S. Biophys. Chem, **2000**, 85, 49-57.

31. Mansoura, M.;Biwersi, J.; Ashlock, M.A. and Verkman, A.S. Human Gene Ther., **1999**, 10, 861-875.
32. Verkman, A.S. and Biwersi J., Methods in Neurosci., **1995**, 27, 328-339.
33. Wissing, F.; and Smith, J.A.C. Membrane Biol., **2000**, 177, 199-208.
34. Johnson, R.D.; and Bachas, L.G. Anal Bioanal Chem, **2003**, 376, 328-341.
35. Badr, I.H.A.; Diaz, M.; Hawthorne, M. F.; and Bachas, L.G. Anal. Chem., **1999**, 71, 1371-1377.
36. Badr, I.H.A.; Johnson, R.D.; Diaz, M.; Hawthorne, M. F.; and Bachas, L.G. Anal. Chem., **2000**, 72, 4249-4254.
37. Ceresa, A. ; Qin, Y.; Peper, S.; and Bakker, E. Anal. Chem., **2003**, 75,133-140.
38. Cha, M..J; Shin, J.H. ; Oh, B. K. ; Kim, C.Y. ; Cha, G.S. ; Shin, D.S. ; and Kim, B. Anal. Chem. Acta, **1995**, 315, 311-319.
39. Schoenfisch MH, Zhang H, Frost MC, Meyerhoff ME. Anal Chem. **2002**;74, 5937-5941.
40. Mao L, Xu F, Xu Q, Jin L. Anal Biochem. 2001; 29, 94-101.

CHAPTER IV: LIPOBEAD-BASED FLUORESCENCE BIOSENSOR FOR UREA

4.1 INTRODUCTION

There is a growing interest in the development of optochemical miniaturized sensors with the capability to measure minute chemical changes in volume-limited and complex microenvironments. Recently, molecular fluorescence dyes were entrapped in submicrometric particles that were used as fluorescence sensors in volume limited samples like single cells. PEBBLEs (probes encapsulated by biologically localized embedding) first developed by Kopelman and coworkers were composed of a hydrophilic polymer matrix, e.g. polyacrylamide with fluorescence indicators copolymerized or physically entrapped in the polymeric matrix (1,2). They show high selectivity, sensitivity and fast response time in the millisecond time scale. In our laboratory, we encapsulated hydrophilic and hydrophobic indicators in phospholipids vesicles (liposomes) and employed them as fluorescence sensors (3-6). However, poor stability of liposomes prevented their application as sensors in biological fluids. Recently we prepared an advanced version of liposome-based sensors that was based on the use of fluorescent lipobeads. Lipobeads are polymer particles ranging from 0.2 to 2 μm in diameter that are coated with a phospholipid membrane. The phospholipid membrane could be used to immobilize hydrophilic fluorescent indicators through covalent attachment to the phospholipids' head-groups of the membrane. It could also be used to immobilize hydrophobic fluorescent indicators through physical adsorption to the hydrophobic region of the phospholipids membrane (7-10). We showed that fluorescence sensing lipobeads could be used for intracellular pH and oxygen measurements (8, 9). We also developed lipobead-based sensors for chloride ions in aqueous samples (10).

Previously, lipobead-based sensors were prepared in our laboratory by coating polystyrene particles with phospholipids and physically immobilize fluorescent indicators to the phospholipid membrane (7-10). Typically, lipobeads solutions could be stored for up to two weeks without substantial loss of activity due to leakage of phospholipids or fluorescent molecules to the storage solution. It was also preferable that a hydrophobic indicator would be immobilized to the lipobeads to increase their stability toward leakage. This limited the scope of analytes that could be detected using this sensing technique. In this paper, we describe a new approach for the synthesis of fluorescence sensing lipobeads. Micrometric carboxyl-modified silica particles replaced the polystyrene particles as a supportive core matrix. Amino-functionalized phospholipids replaced the non-functionalized phospholipids like 1, 2-dimyristoyl-sn-glycero-3-phosphocholine (DMPC) that were previously used to form the phospholipid membrane of the lipobeads. Furthermore, the fluorescent indicators and enzyme molecules were attached covalently to the phospholipid membrane. The resulting new lipobeads exhibited higher chemical stability since all the molecular components were attached covalently to the sensing particles.

To demonstrate the capability of the new lipobead based fluorescence sensors we developed fluorescence biosensing lipobeads for urea. Urea has been frequently a target for biosensor development since abnormal urea levels in urine are indicative of urinary tract infections. Normal urea levels in urine are from 30 to 80 mM (11), and normal urea levels in serum are around 6.2 mM (12). High levels of urea in blood are related to renal diseases like pre-renal azotemia, post-renal azotemia and kidney function abnormalities (13, 14**)**. A fluorescence biosensor for urea was first developed by Guilbault and coworkers as early as 1969 (15). It was based on the co-immobilization of the enzyme urease hydrolase and a fluorescent indicator to a

solid-state support. Urease hydrolase catalyzes the conversion of urea to ammonia, which results in a pH increase in the analyte sample.

$$NH_2CONH_2 + 2H_2O + H^+ \xrightarrow{\text{Urease hydrolase}} 2NH_4^+ HCO_3^-$$

Since then, different types of transducers were applied in urea biosensors to detect increasing pH or ammonium ion levels in the presence of urea. These include chromophores (16), fluorophores (17-22), pH and ion selective electrodes in voltammetric (23-25) or amperometric modes (26-28), and field effect transistors (29). The performance limiting factor has often been the immobilization of the enzyme to the sensing support. Successful immobilization of enzymes or other bioactive molecules leads to minimal loss of activity and increased stability toward denaturization. While efficient immobilization is important for successful fabrication of large sensors, it is critical for successful fabrication of micrometric sensors since the number of enzyme and fluorescence sensing molecules per sensor is limited. This paper describes the preparation and analytical properties of micrometric sensing lipobeads for urea that were prepared using our new covalent approach for lipobead synthesis.

4.2 EXPERIMENTAL

4.2.1 Synthesis of Silica Lipobead

Phospholipid coated silica particles (silica lipobeads) were synthesized following a method previously developed by Thompson et al (30, 31) for the attachment of phospholipids to a glass surface. The multi step synthesis is shown in schemes 1, 2, and described in the following sections:

4.2.2 Activation of Carboxylic Surfaces of Silica Microspheres

0.1 ml of a 10% solution of 1.7 μm silica microspheres were dried under nitrogen. Then, 1 ml 0.1 M N-hydroxysuccinimide and 0.1 M N, N'-dicyclohexylcarbodiimide in dimethyl formamide (DMF) were added to the dry powder and the suspension was stirred overnight. The activated silica microspheres were washed with DMF by centrifugation at 4000 rpm for 5 min and re-suspended in DMF.

4.2.3 Covalent Binding of 1-Palmitoyllysophosphatidyl-ethanolamine to the Silica Microspheres

The activated silica microspheres were esterified with 1 mL 0.02 M 1-palmitoyllysophosphatidyl-ethanolamine in DMF and 0.4 mL triethylamine. The reaction mixture was stirred for 48 hours at room temperature. The resulting modified lipobeads were washed with DMF and dried under nitrogen.

4.2.4 Acylation of the sn-2 Hydroxyl of the Immobilized Lipids

The dried lipobeads were acylated with 1 mL 0.01 M sebacoyl chloride and 0.1 mL 0.1 M 4-dimethylaminopyridine in tetrahydrofuran (THF) and stirred overnight. The resulting lipobeads were washed with THF and dried under nitrogen.

4.2.5 Conversion of the Terminal Acid Chloride to Acidic Moiety

1 mL Saturated sodium bicarbonate in a methanol:deionized water (5:1) solution were added to the 0.1 mg lipobeads powder. The suspension was incubated for three hours. The

lipobeads solution was washed with deionized water by centrifugation at 4000 rpm and dried under nitrogen.

4.2.6 Choice of Fluorescent Indicator

Fluorescein is the earliest pH probe used in fluorescent microscopy. Fluorescein emits fluorescence only in the monoanion and dianion forms. Fluorescein equilibrates with different ions at different pH. Above pH 9.0, the phenol and carboxylic function groups of fluorescent indicator are totally anized. When we first acidify the aqueous solution, the dianions will convert to the monoanion with the phenol function group protonation. The reason why the phenol group protonates first because the pK_a of phenol is ~ 6.4, while the pK_a of the carboxylic acid is less than 5.0. When the aqueous solution further acidifies, the monoanion will change to the neutral form that is not fluorescent itself. If the fluorophore environment becomes more acidic, it will go to the cation form with no fluorescence emitting. If we dissolve the fluorescein in organic solvent such as acetone, the fluorescein will form lactone that is not fluorescent at all. Figure 4.1 shows the ionization forms of fluorescein. The fluorescent intensity changes demonstrate the equilibrium of the monoanion and dianion forms of the fluorescein.

The specific fluorescein used was fluorescein-5-thiosemicarbazide. Its first pK_a is 6.5 and it can dissolve in dimethylfloride (DMF) and basic aqueous buffer solution. Figure 4.2 shows the structure of this fluorophore (64). In aqueous solution, the excitation and emission of this fluorescein-5-thiosemicarbazide is 490 nm and 515 nm, respectively. The advantage of the excitation spectrum is to allow ratiometric pH measurement at 450 nm and 490nm due to its long excitation wavelength, which will avoid nonuniform dye loading, photobleaching, dye leakage

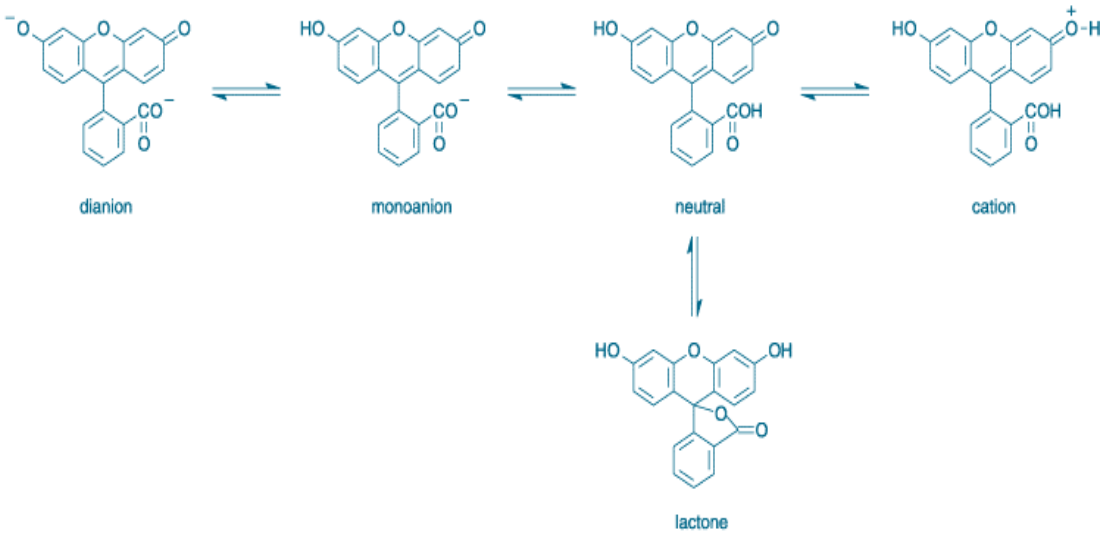

www.probes.com/handbook/figures/0571.html

Figure 4.1. Ionization forms of fluorescein.

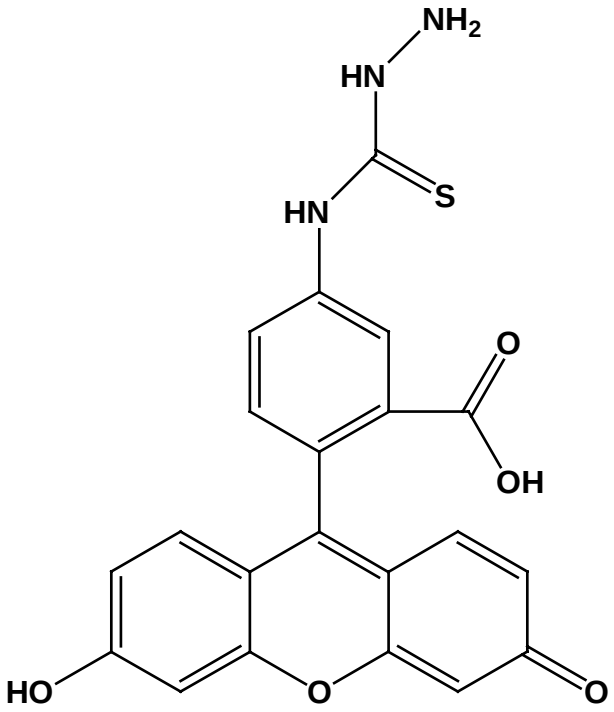

Figure 4.2. Structure of Fluorescein-5-thiosemicarbazide.

and cell background fluorescence. Fluorescein-5-thiosemicarbazide has a primary amine functional group that is convenient to use for covalently binding during synthesis of the bead sensing system. We use this advantage to apply carboxylate cross-linking to the amine to form amide and avoid fluorophore leaking from the lipobeads.

4.2.7 Covalent Binding of Urease and Fluorescein-5-thiosemicarbazide to the Lipobeads

The acylated lipobeads were activated with 1 mL 0.1 M N-hydroxysuccinimide and 1 mL 0.1 M N, N'- dicyclohexylcarbodiimide in DMF. The activated lipobeads were added to 0.2 mM EDTA solution containing 100 μg urease (45,000 U per g) and 500 μL 1 mM fluorescein-5-thiosemicarbazide at pH 6.0. The reaction mixture was stirred for 48 hrs at 4 ^{0}C. The mixture was washed with the EDTA buffer to remove excess urease and fluorescein-5-thiosemicarbazide. The particles were then dried and stored in a glass vial coated with aluminum foil at 4 ^{0}C until used.

4.2.8 pH Reversibility of the Urea Sensor

The pH reversibility of the lipobead-based urea biosensors was measured by monitoring the change in fluorescence intensity when weak acids or bases were added to a solution of fluorescence sensing lipobeads. The fluorescence intensity was measured as a function of time using an excitation wavelength of 490 nm and an emission wavelength of 520 nm. To conduct the measurement, 2 mL of lipobead solution was placed in a 3 mL quartz cuvette (1 cm pathlength). The sample was placed in the fluorimeter cuvette holder and its emission was monitored until obtaining a stable baseline. Then, different amounts of weak acid or base

solution were injected into the cuvette while the lipobeads solution was stirred. The emission measurement was continuously recorded until a stable baseline was observed.

FTIR Spectroscopy - Fourier transform infrared (FTIR) spectra of lipobeads solutions at 25 ^{0}C were collected using a Bomem MB-104 FTIR spectrometer equipped with a KBr transmission window. The spectral range was from 700 to 4000 cm^{-1}, with a resolution of 8 cm^{-1}. The spectrometer used Win-Bomem software to record the spectra. 32 scans were accumulated for each spectrum. Samples were collected and measured from each synthesis step.

4.2.9 Digital Fluorescence-imaging Microscopy

The experimental setup used for fluorescence measurements of the lipobeads based sensors was reported previously (10). The system consisted of an inverted fluorescence microscope (Olympus IX-70) equipped with three detection ports. A 100-W mercury lamp was used as the light source for excitation. The fluorescence was collected by a 40 x microscope objective. A filter cube containing 460/50 nm excitation filter, 500 nm dichroic mirror, and 515 nm longpass emission filter was used to ensure spectral purity. A high-performance ICCD camera (Roper Scientific, model 256HB) with a 512 x 512 pixel array was used for digital fluorescence imaging of the samples. The software image Pro+ (Media Cybernetics Inc.) was used for image analysis. The exposure time used in most experiments was 0.1 seconds.

4.3 RESULTS AND DISCUSSION

4.3.1 Synthesis of Lipobead-based Urea Biosensors

Carboxyl-modified silica microspheres were used as the supportive matrix of the urea biosensors. The abundance of carboxyl groups enabled the covalent binding of phosphatidyl

ethanolamine to the particles through a condensation reaction between the amino groups of the phospholipid molecules and the activated carboxyl groups on the silica particles to form stable amide bonds. Scheme 4.1 describes the first steps of the urea biosensor synthesis. The carboxyl groups on the silica particles surface were first activated with N-hydroxysuccinimide to facilitate the formation of amide bonds when the particles were mixed with amino functionalized phospholipids. The second step of the synthesis involved the acylation of the sn-2 hydroxyl groups of the immobilized phosphatidyl ethanolamine with sebacoyl chloride. This placed a terminal carboxylic acid chloride group at the sn-2 position of the immobilized phospholipids. The lipobeads were then treated with sodium bicarbonate to convert the terminal acid chloride to an acidic moiety in order to enable the covalent conjugation of enzyme and fluorescent molecules to the lipobeads. The carboxylic acid groups were activated with N-hydroxysuccinimide. Then, a solution containing the enzyme urease and fluorescein-5-thiosemicarbazide was added to the reaction mixture. The enzyme and fluorescent molecules were attached covalently to the sn-2 acyl chain carboxyl moieties through their free amino groups. The ratio between the enzyme and fluorescent molecules was optimized to realize maximum enzyme activity and maximum fluorescence response to urea. First, we optimized the concentration of urease in the lipobead preparation solution. The activity of the lipobeads increased with increasing enzyme concentration up to a level of 4.0 U/mL. Increasing the concentration above this level decreased the enzymatic activity of the lipobeads, which could be attributed to steric interactions due to excess of enzyme molecules in the lipobeads membrane. To determine the efficiency of the covalent attachment of urease to the phospholipid membrane of the sensing particles we monitored the residual fluorescence of the lipobead preparation

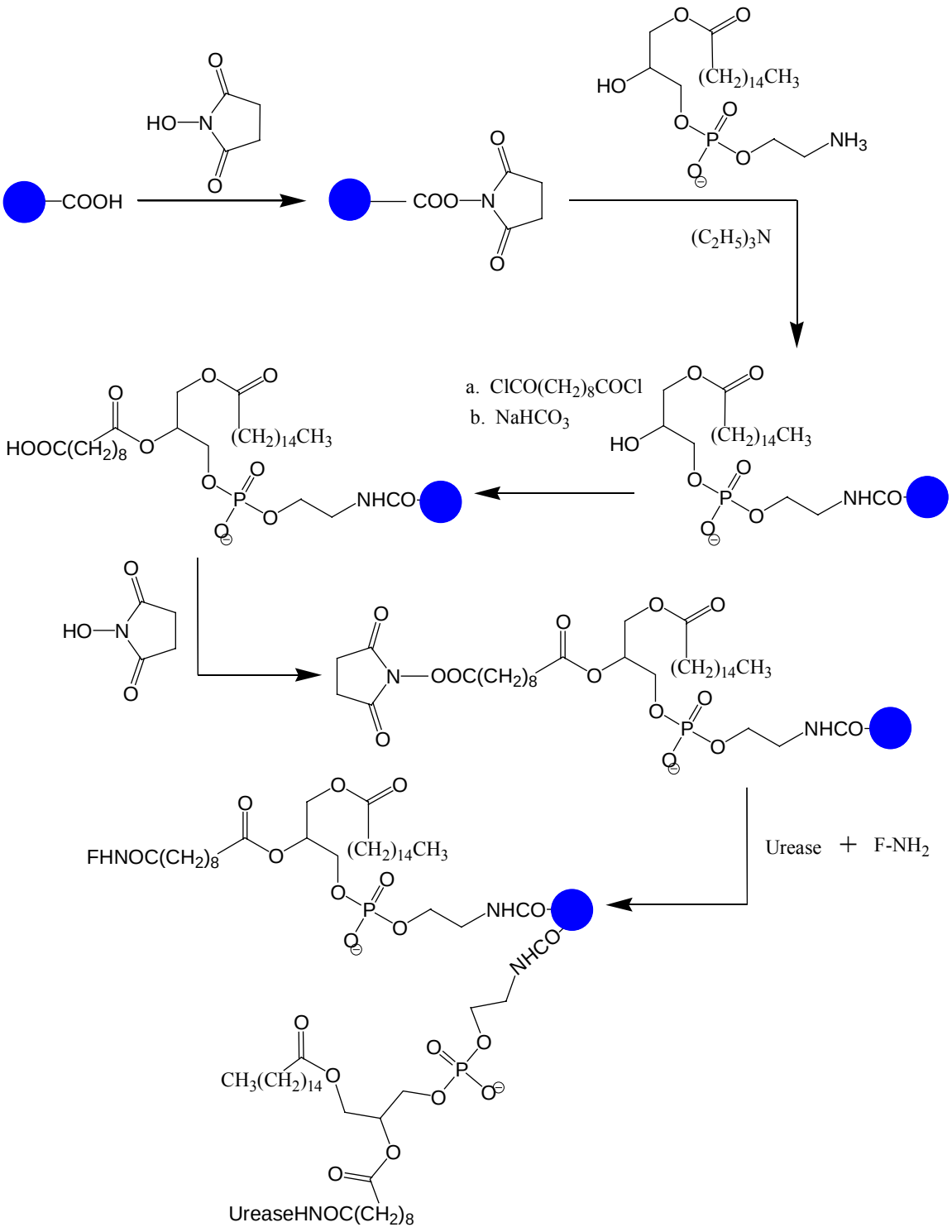

Scheme 4.1 – Synthesis of activated lipobeads.

solution following precipitation of the enzyme-bound lipobeads by slow speed centrifugation. Urease molecules fluoresce at 360 nm when excited at 290 nm due to the presence of the aromatic amino acid tryptophan in the protein sequence (32). Figure 4.3 describes the fluorescence intensity of free urease as a function of urease concentrations ranging from 1 to 0.08 mg/mL. The percentage immobilization curve exhibits considerable non-linearity the insert shows linear response in urease concentrations ranging from 1 to 0.02 mg/mL with a correlation coefficient of 0.990. In the immobilization experiments we used lipobeads concentration of 1.6 mg/mL. Based on the fluorescence intensity of the supernatant prior to and following enzyme immobilization we found that for a reaction mixture containing 0.09 mg/mL urease the residual urease concentration in the solution was 0.02 mg/mL indicating that about 80% of urease molecules were immobilized to the lipobeads under these conditions. The concentration of fluorescein-5-thiosemicarbazide in the lipobeads preparation solution was optimized as well. The fluorescence intensity of the lipobeads increased with increasing dye concentration up to a level of 0.75 mM. Increasing the dye concentration above this level resulted in a decrease of the fluorescence intensity and pH sensitivity of the lipobeads, which could be attributed to self fluorescence quenching of the fluorescein moieties when excessively immobilized to the membrane. In our experiments, we used a dye concentration of 0.45 mM in the lipobeads preparation solution. This dye concentration resulted in sufficiently bright lipobeads with signal to background ratio of ~50. This was done to maximize the number of binding sites on the membrane for the conjugation of urease to the lipobeads. It should be noted that washing the lipobeads to remove excess dye was technically difficult since fluorescein-5-thiosemicarbazide

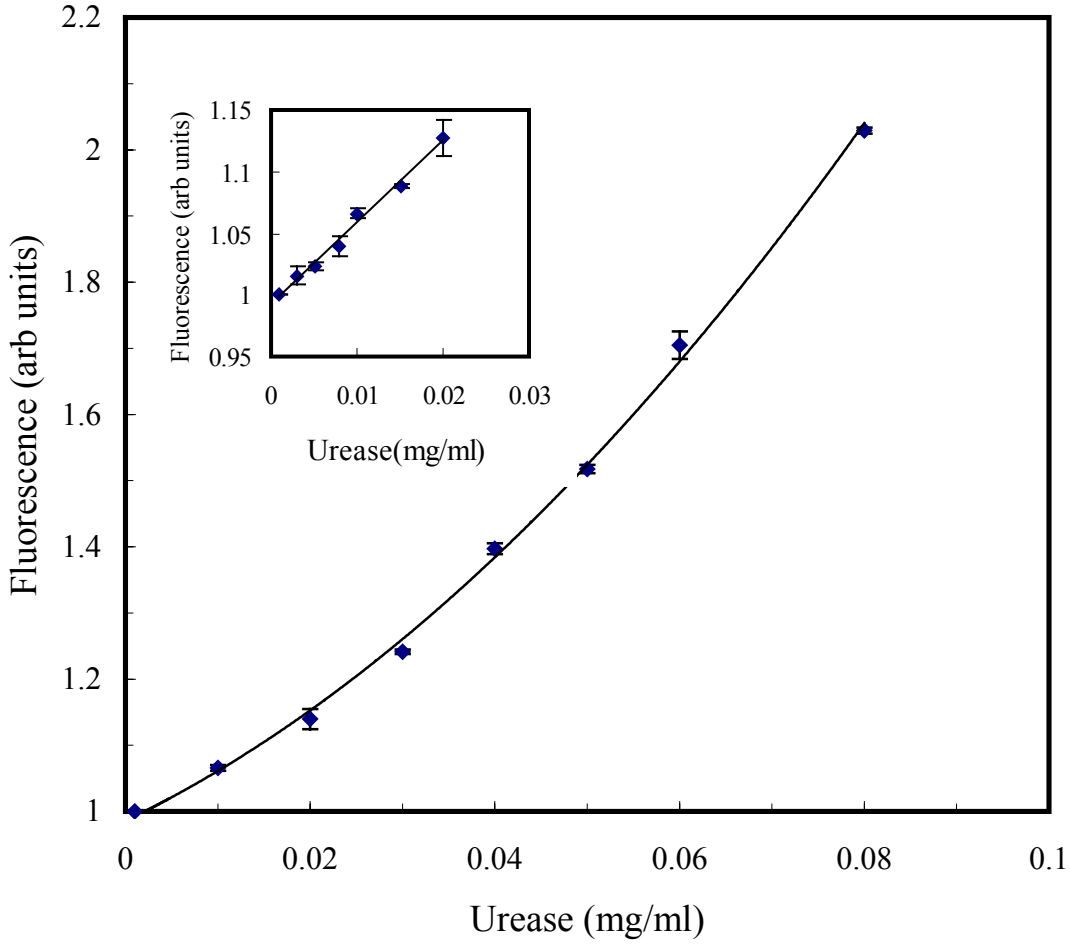

Figure 4.3 – A calibration curve of free urease fluorescence versus urease concentrations ranging from 0 to 0.1 mg/mL. The shape of the large concentration spanning curve is nonlinear. Insert - linear plot of urease fluorescence against. urease concentrations ranging from 0 to 0.02 mg/mL.

has limited solubility in aqueous solution. The lipobeads were washed repeatedly until their fluorescence intensity remained constant. This indicated that only covalently attached fluorophores remained in the lipobeads membrane.

4.3.2 FTIR Monitoring of Biosensor Synthesis Steps

Steps in the synthesis of the lipobead biosensors were monitored using FTIR spectroscopy. Figure 4.4a shows an FTIR spectrum of commercially available silica beads dispersed in chloroform. Two characteristic absorbance bands at 1640 cm^{-1} for the carboxylic groups and at 1105 cm^{-1} for the Si-O stretch of the silica beads can be seen. Figure 4.4b shows an FTIR spectrum of silica lipobeads dispersed in toluene. The spectrum contains absorbance bands indicative of phospholipids. New bands are observed in the spectrum at 1227 cm^{-1} for the phosphate groups, at 1468 cm^{-1} for secondary amines, and at 1731 cm^{-1} for the palmityl fatty ester group of the phospholipids. Finally, Figure 4.4c shows the spectrum of the lipobeads collected after the acylation of the sn-2 hydroxyl groups of the immobilized phosphatidyl ethanolamine with sebacoyl chloride, and subsequent acid chloride conversion to the terminal carboxylic acid with sodium bicarbonate. The lipobeads were dispersed in chloroform. The spectrum shows absorbance bands at 1086 cm^{-1} for the silica groups, at 1220 cm^{-1} for the phosphate group, and a weak band at 1731 cm^{-1} for the ester group. As expected, the spectrum shows a decrease in the intensity of the ester band at 1731 cm^{-1} and an increase in the intensity of the weak acid band at 1648 cm^{-1}. A new absorbance band at 1563 cm^{-1} for the carboxylate ion also confirmed the successful completion of this synthesis step.

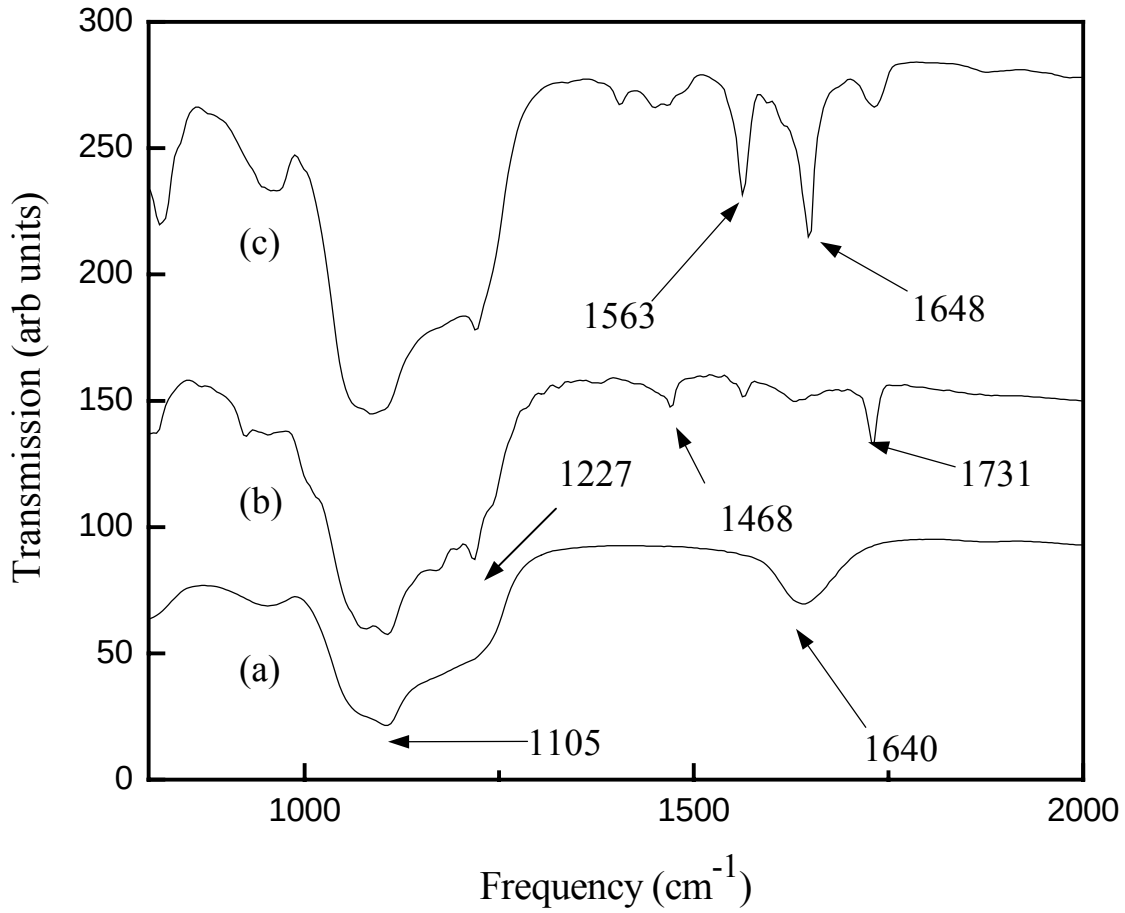

Figure 4.4 – FTIR spectra monitoring different steps of the lipobeads synthesis: (a) bare silica beads, (b) silica lipobeads prior to acylation, and (c) silica lipobeads following acylation with sebacoyl chloride.

4.3.3 Scanning Electron Microscopy (SEM) and Digital Fluorescent Images of the Lipobeads

An SEM image of the silica beads is shown in Figure 4.5a. The mono-dispersed particles appear spherical in shape with an average diameter of 1.7 μM ± 3%. Figure 4.5b shows an SEM image of lipobeads containing urease and flurescein-5-thiosemicarbazide. There are no significant differences between the SEM images of the bare silica particles and the lipobeads as the resolution of SEM is not sufficient to observe the phospholipid layer. However, the mono-dispersity and shape of the lipobeads indicate that coating the silica particles with a phospholipid membrane did not affect the size and shape of the particles, and more importantly did not induce particle aggregation. Figure 4.5c shows a digital fluorescence image of lipobeads. The lipobeads appear bright with a signal to background ratio of 50 ± 15%. The intensity variations between lipobeads are attributed to heterogeneity in the excitation light intensity in the microscope field of view and to variations in the membrane coating of the lipobeads.

4.3.4 pH Sensitivity and Reversibility of the Lipobeads

Fluorescein-5-thiosemicarbazide is a pH sensitive fluorescent indicator. Studies were performed to determine whether the immobilization of fluorescein-5-thiosemicarbazide to the membrane of the lipobeads affected the pH sensitivity of the fluorescent indicator. Figures 4.6a and 4.6b depict the pH dependent emission spectra of free and immobilized fluorescein-5-thiosemicarbazide in aqueous solutions buffered with 0.2 mM EDTA at pH 6.0 and 8.0 respectively. The spectra were measured at a fixed excitation wavelength of 490 nm and the fluorescence intensity was measured at 520 nm. The fluorescence intensity of both free dye and

(a)

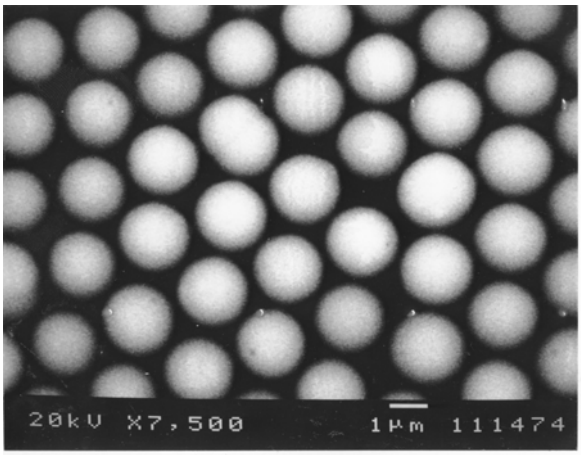

(b)

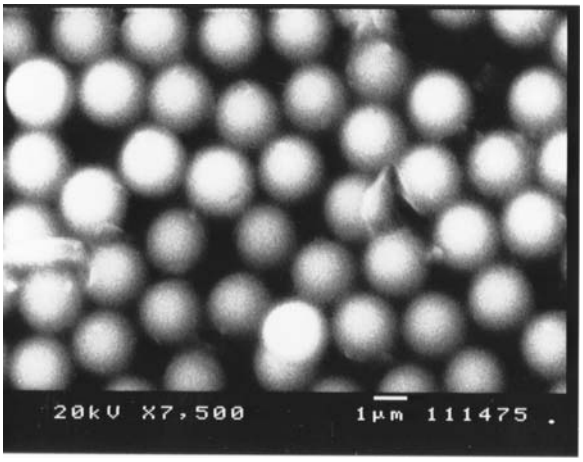

(c)

Figure 4.5 – Scanning electron microscopy (SEM) image of (a) bare silica beads, (b) Silica lipobeads. Both images reveal that the particles are spherical, evenly dispersed, and average 1.7 ± 3% μM in diameter with narrow size distribution. (c) A digital fluorescence image of the lipobeads. The signal to noise ratio is about 50 ± 15%.

dye-containing lipobeads solutions increased by about 2-fold when the pH increased from 6.0 to 8.0. This indicated that the covalent immobilization of fluorescein-5-thiosemicarbazide to the lipobead membrane did not significantly alter its pH sensitivity. Figure 7 describes the pH reversibility of the lipobeads. First, the pH was increased from 6.0 to 6.8 by adding drops of diluted sodium hydroxide. As expected, an increase in fluorescence intensity was observed. The pH was further increased from 6.8 to 7.9. Again, a fluorescence intensity increase was recorded. The solution was adjusted back to pH 6.8 and then to pH 6.0 by adding drops of diluted hydrochloride acid. Each step brought the fluorescence intensity back to the original value. This clearly demonstrated the pH reversibility of the fluorescent sensing lipobeads.

4.3.5 Catalytic Properties of the Urease Lipobead Biosensor

Using the well-known classical enzyme kinetics model of the Michaelis-Menten (33, 34), the Michaelis-Menten constant K_m was calculated for the free enzyme, and for the sensing lipobeads. Digital fluorescence images and spectra of the particles were taken at different time intervals when the urea sensing lipobeads were exposed to solutions of increasing urea concentrations. Figure 4.8 is a Lineweaver-Burke plot describing the invert of the initial reaction rate versus the invert of substrate concentration between 0 and 4 mM. K_m of the sensing lipobeads was calculated as 7.0 ± 1.8 mM. For free urease, K_m was calculated as 1.9 ± 0.04 mM. This is in agreement with the literature K_m values that range between 1 and 8 mM for free urease in solution (35). It should be noted that the error in the Km determination of the lipobeads is significantly higher than the error in the determination of K_m in free urease solutions. This is attributed to the small number of lipobeads, about 50, in the images and spectra used to determine the rate of the enzymatic reaction. Increasing the lipobead concentration would make

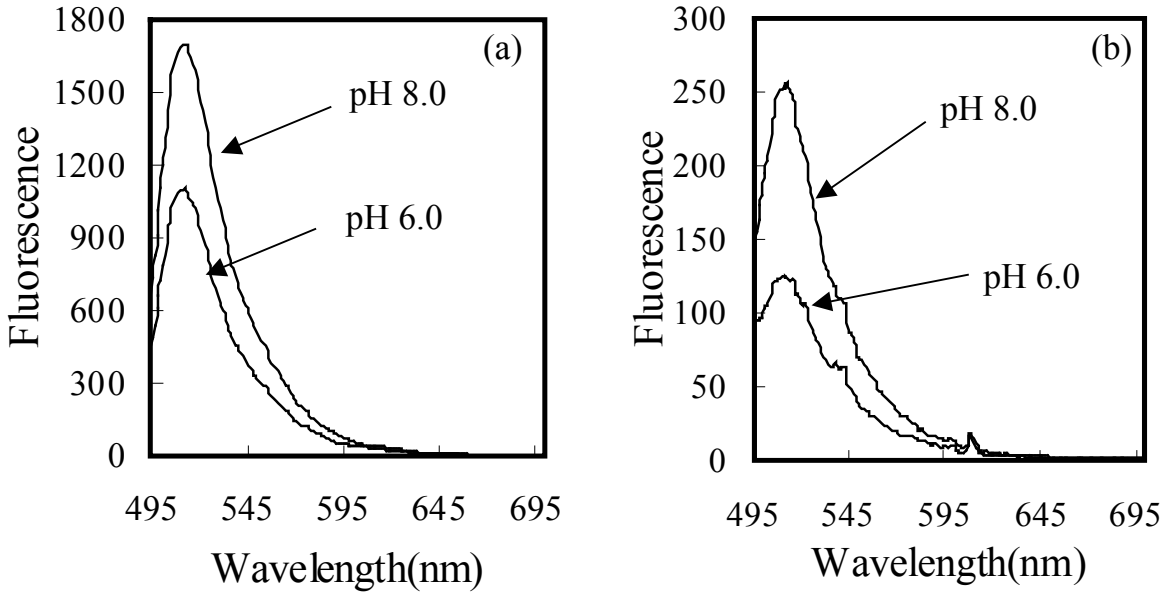

Figure 4.6 –The pH dependent emission spectra of (a) 0.05 mM fluorescein-5-thiosemicarbazide in 0.2 mM EDTA solution and (b) lipobeads solution containing fluorescein-5-thiosemicarbazide between pH 6.0 and 8.0 in a 0.2 mM EDTA solution. The spectra were measured at a fixed excitation wavelength of 490 nm and the fluorescence intensity was measured at 520 nm.

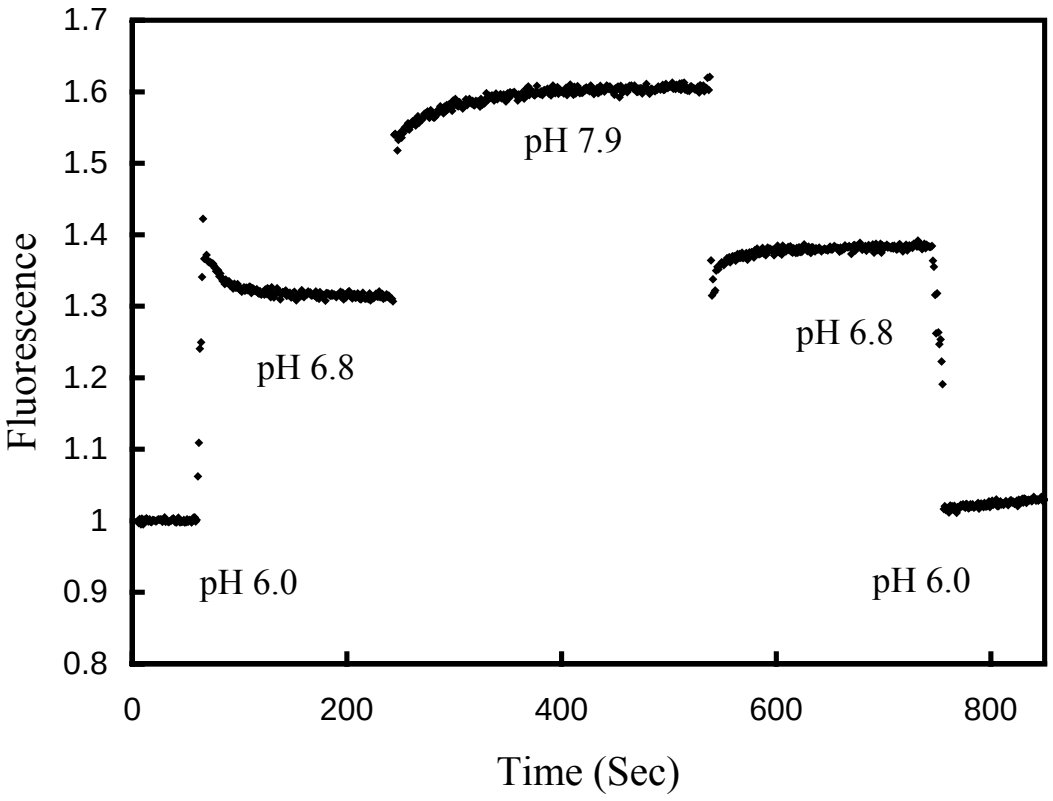

Figure 4.7 – pH reversibility study describing the fluorescence intensity of the urea sensing lipobeads versus time at different pH levels.

it difficult to discriminate between the responses of individual particles. On the other hand, spectro-fluorimetry measurements of urea sensing lipobeads in solution did not significantly reduce the error in the K_m analysis due to added scattering noise. It is fair to conclude that the variability in membranal coating and enzyme immobilization remained the performance limiting parameters of the lipobead-based biosensors. Another interesting observation was the relatively large K_m of the urea sensing lipobeads compared to the K_m of urease in solution. In enzyme kinetics, K_m is a measure of the enzyme-substrate binding affinity where a large K_m indicates low binding affinity since a high substrate concentration ([S]) is required to reach $V_{max}/2$. On the other hand, a small K_m indicates higher binding affinity since a lower [S] is required to reach $V_{max}/2$. The higher K_m value of 7.0 ± 1.8 mM for the lipobeads compared to 1.9 ± 0.04 mM for free urease indicates that the reaction rate decreased for the urea sensing lipobeads. This is also reflected in the two orders of magnitude lower V_{max} of the lipobeads compared to that of free urease. The increase in K_m and decrease in V_{max} are attributed to the additional diffusion barrier, which must be overcome by the urea molecules when permeating through the phospholipid membrane. Figure 4.9 shows a semi-log calibration curve of the response of the lipobead-based urea biosensors to increasing concentrations of urea. Each data point was the average of three replicate measurements. The error bars were calculated based on the standard deviation of the three replicate measurements. The dynamic range of the urea sensing lipobead was between 0.1 and 4 mM which is comparable with previously developed large fluorescence-based urea biosensor (22). With the proper dilutions, the urea sensing lipobeads should be applicable to the measurement of urea in both serum and urine. The urease activity is the only performance of limiting parameter by the newly developed lipobead-based urea biosensors. The covalent

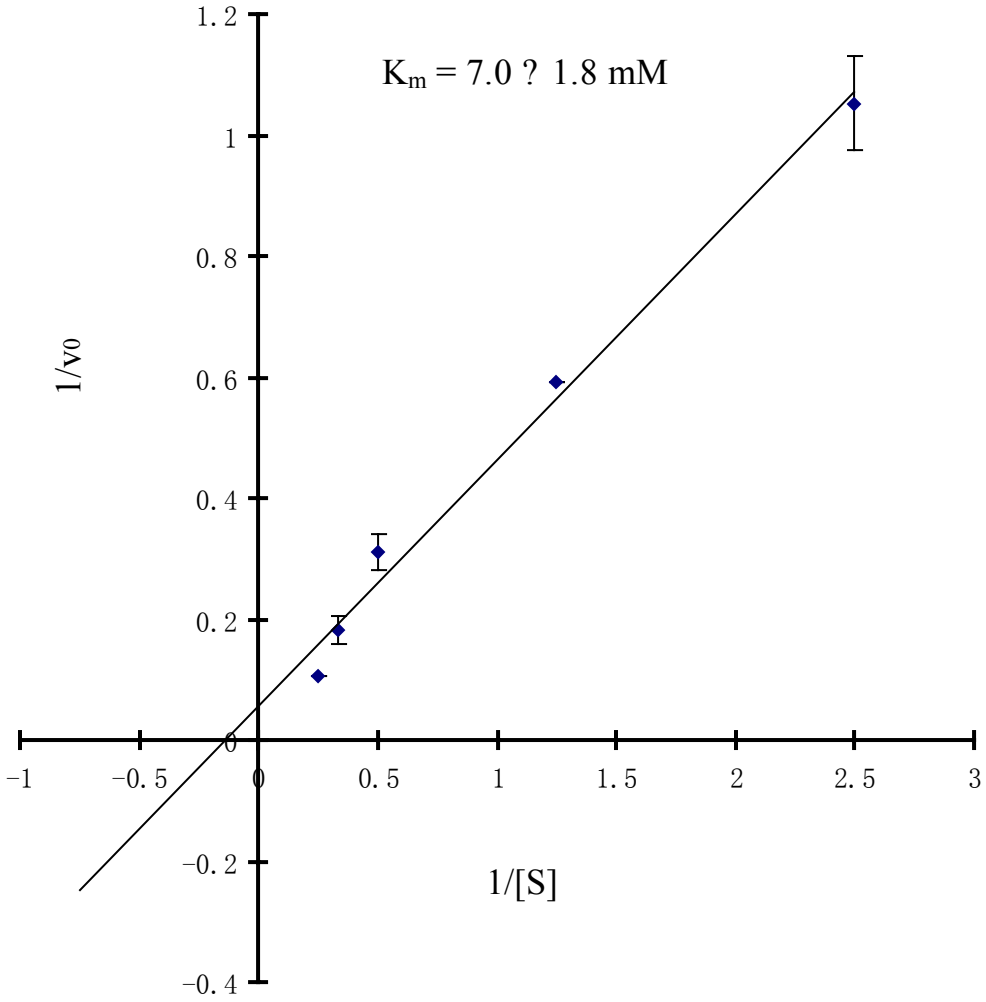

Figure 4.8 – A Lineweaver-Burk plot of the invert of the initial reaction rate versus invert substrate concentration. K_m was calculated at 7.0 ± 1.8 mM for the urea sensing lipobeads.

coupling of the fluorescent indicator and urease to the lipobeads eliminated stability problems related to dye and enzyme leakage from the lipobead membrane. After two months in storage only 10% loss in activity was observed demonstrating the extended stability of the urea sensing lipobeads.

4.4 CONCLUSIONS

This paper describes an improved synthesis protocol for the fabrication of fluorescence biosensing lipobeads. Silica particles modified with carboxyl groups were used to prepare the lipobeads. They were coated with functionalized phospholipids to form the membrane coated beads. The enzyme urease and the pH sensitive indicator fluorecein-5-thiosemicarbazide were attached covalently to the lipobeads membrane. SEM and digital fluorescent images showed that the synthesized lipobeads were bright and evenly dispersed, and no apparent aggregation was observed. This work represents a departure from the previous use of polystyrene particles as a supporting matrix for fluorescence sensing lipobeads. Polystyrene particles of different surface functionalities (NH2, COOH, SH) are available commercially. Furthermore, there is large body of work in the literature that describes the conjugation of fluorophores and biomolecules to polystyrene particles. However, our recent studies indicated that size reduction of polystyrene particles to submicrometric dimensions often led to their aggregation. Additionally, polystyrene particles undergo shape deformations in different solvents and ionic strength, which decrease their leaking stability. Polystyrene particles were also shown to be quite toxic. On the other hand, silica particles have been recently used as drug carriers without noticeable side effects. This paper describes the use for the first time of submicromteric silica particles as the core of

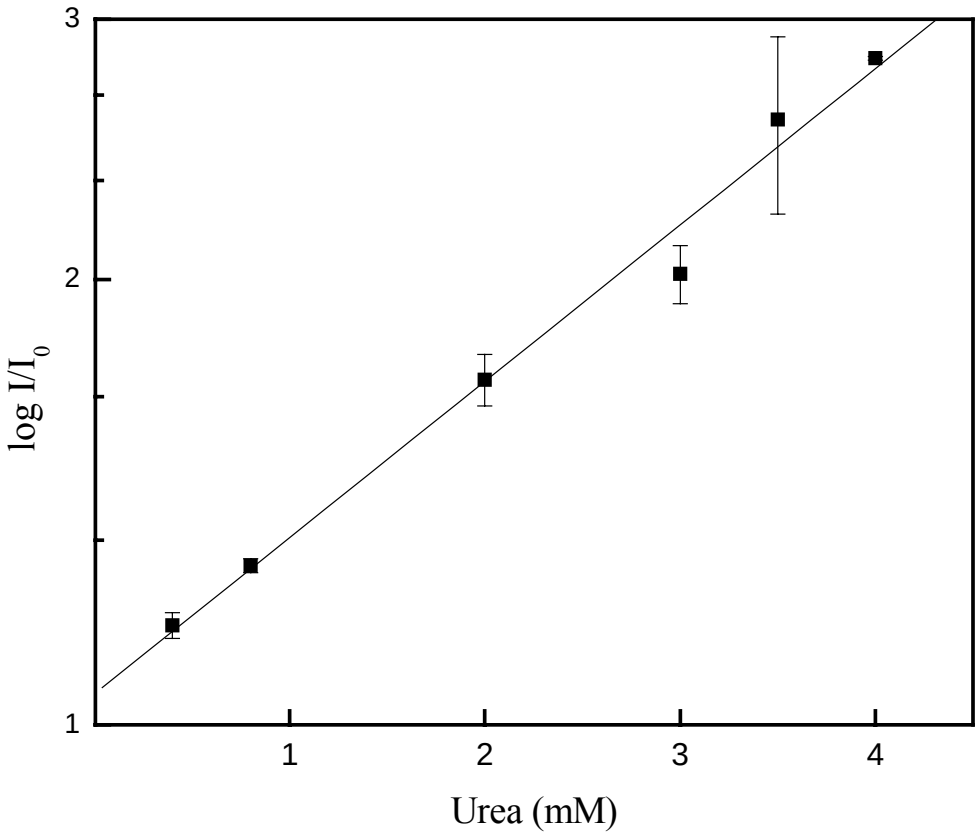

Figure 4.9 – A semi-log plot describing the fluorescence intensity of the urea sensing lipobeads against increasing urea concentrations.

urea sensing lipobeads. Tests performed to determine the effect that immobilization of the fluorescent indicator to the lipobeads had on the pH sensitivity of the fluorescent indicator demonstrated that the response of the immobilized pH indicator did not change appreciably due to immobilization. The working range of the immobilized fluorescein-5-thiosemicarbazide indicator was between pH 6 and 8.5. Reversibility studies indicated that the lipobeads responded to pH increase or decrease with high reproducibility. The dynamic range of the lipobeads-based urea biosensors was determined to be from 0.1 mM to 4 mM. Through the use of Lineweaver-Burke plots, the Michaelis-Menten constant K_m for the lipobeads particles was calculated to be 7.0 ± 1.8 mM, 3.7 fold higher than the K_m of free urease. This indicated that immobilization of urease to the membrane of the lipobeads decreased the rate of the hydrolase conversion of urea into ammonia. This was expected due to the membrane addition of a diffusion barrier in the lipobeads. However, the dynamic range and sensitivity of the lipobeads are still sufficient to measure normal and elevated urea concentrations in diluted biological fluids. In addition to increased stability compared to previously reported particle-based sensors, the lipobead-based biosensors could prove useful in *in-vivo* experiments where preventing particle endocytosis would be essential for long term monitoring of urea in serum. The phospholipid coating of the particles was previously shown to be effective in lowering endocytotic rate. Future studies will focus on the application of fluorescent biosensing lipobeads in *in-vitro* and *in-vivo* measurements.

ACKNOWLEDGMENTS

The authors give special thanks to Dr. Andriy Ya. Vovk for his assistance in obtaining SEM images of the sensing particles. This study was supported by NSF Grant CHE-013427.

4.5 REFERENCES

1. Clark, H. A.; Hoyer, M.; Philbert, M. A.; Kopelman, R. Anal. Chem. **1999**, *71* (21), 4831 –4836.
2. Brasuel, M.; Kopelman, R.; Miller, T.J.; Tjalkens, R.; Philbert, M.A. Anal. Chem. **2001**, *73*, 2221-2228.
3. Nguyen, T.; Rosenzweig, Z. Anal Bioana Chem., **2002**, *374*, 69-74.
4. Nguyen, T.; McNamara, K.P.; Rosenzweig, Z. Anal. Chim. Acta, **1999**, *400* (1-3), 45-54.
5. McNamara, K.P.; Rosenzweig, N.; Rosenzweig, Z. Mikrochim. Acta, **1999**, *131*, 57-64.
6. McNamara, K.P.; Rosenzweig, Z. Anal. Chem., **1998**, *70* (2), 4853-4859.
7. Ji, J.; Rosenzweig, N.; Griffin, C.; Rosenzweig, Z. Anal. Chem. **2000**, *72* (15), 3497-3503.
8. Ji, J.; Rosenzweig, N.; Jones, I.; Rosenzweig, Z. Anal. Chem., **2001**, *73* (15), 3521-3527.
9. McNamara, K. P.; Nguyen, T.; Dumitrascu, G.; Ji, J.; Rosenzweig, N.; Rosenzweig, Z. Anal. Chem., **2001**, *73* (14), 3240-3246.
10. Ma, A.; Rosenzweig, Z. Anal. Chem. **2004**, *76*, 569-575.
11. Snyder, C.H., in The Extraordinary Chemistry of Ordinary Things, 2nd edition, John Wiley & Sons, Inc., New York, **1992**,164.
12. Huang, C.T.; Chen, M.L.; Huang, L.L.; Mao, I.F.; Chin, J. Physiol. **2002**, *45* (3), 109-15.
13. Lee, W.; Kim, S.; Kim, T.; Lee, K.; Shin, M.; Park, J. Anal. Chim. Acta, **2000**, *404*, 195-203.
14. Eckfeldt, J. H.; Levine, A. S.; Greiner**,** C**.;** Kershaw, M. Clin. Chem. **1982**, *28*, 1500.
15. Guilbault, G.G.; Smith, R.K.; Montalvo, J.G. Anal. Chem. **1969**, *41*, 600.
16. Koncki, R.; Lenarczuk, T. Radomska; Glab, S. Analyst, **2001,** *126*, 1080-1085.
17. Koncki, R.; Mohr, G.J.; Wolfbeis, O.S. Biosensors & Bioelectronics, **1995**, *10*, 653-659.
18. Marcos, S.; Hortigűela, R.; Galbán, J.; Castillo, J.R.; Wolfbeis O.S. Mikrochim. Acta. , **1999**, *130*, 267-272.
19. Krysteva, M.; Hallak, M. Biotechnol & Biotechnol Eq., **2002**, *16* (1), 161-164.
20. Luo, S.; Walt, D.R. Anal. Chem., **1989**, *16* (10), 1069-1072.
21. Fuh, M.S.; Burgess, L.W.; Christian, G.D. Anal. Chem., **1988**, *60* (5), 433-435.
22. Xie, X.; Suleiman, A.A.; Guilbault, G.G. Talanta., **1991**, *38* (10), 1197-1200.
23. Wang, J.; Chou, J.; Sun, T.; Hsiung, S.; Hsiung, G. Sensors and Actuators B, **2003**, *91*, 5-10.
24. Adeloju, S.B.; Shaw, S.J.; Wallace, G.G. Anal. Chim. Acta, **1993**, *281*, 611-
    a. 627.
25. Walcerz, I.; Glab, S.; Koncki.R. Anal. Chem. Acta, **1998**, *369*, 129-137.
26. Adeloju, S.B.; Shaw, S.J.; Wallace, G.G.; Gordon, G. Anal. Chim. Acta, **1996**, *323* (1-3), 107-113.
27. Vostiar, I.; Tkac, J.; Sturdik, E.; Gemeiner, P. Bioelectrochemistry, **2002**, *56* (1-2), 113-115.
28. Cho, W.; Huang, H. Anal. Chem., **1998**, *70* (18), 3946-1951.
29. Melo, J.V.; Cosnier, S.; Mousty, C.; Martelet, C.; Jaffrezic-Renault, N. Anal Chem., **2002**, *74*, 4037-4043.
30. Kallury, K.M.R.; Lee, W.E.; Thompson, M. Anal. Chem., **1992**, *64*, 1062-1068.
31. Kallury, K.M.R.; Lee, W.E.; Thompson, M. Anal. Chem., **1993**, *65*, 2459-2467.
32. Ruan, K.; Tian, S.; Lange, R.; Balny, C. Biochem. Biophys. Res. Commun. **2000**, *269*, 681-686.

33. Michaelis, L; Menten, M.L. Biochemische Zeitschrift, **1913**, *49*, 333-369.
34. Briggs, G.E.; Haldane, J.B.S. Biochem. J., **1925**, *19*, 338-119.
35. Lynn, K. R. Biochim. Biophys. Acta **1967**, *146*, 205-218.

CHAPTER V DELIVERY OF PARTICLES INTO CELLS FOR INTRACELLULAR MEASUREMENTS

5.1 Introduction

Loading nanosensors and macromolecules into cells, by transfection or translocation through the cellular membrane, to probe biological systems is an evolving area of research for probe sensing and drug delivery. Numerous methods exist for loading fluorescence labeled sensing particles into cells such as mechanical loading, chemical reagent loading, and electroporation (1). Mechanical loading includes direct microinjection methods (2) or "gene gun" methods (3) which can be used to load indicators to specific area in cells. Mechanical loading methods require harsh conditions which often lead to either cell injury, cell death, or both. Scrape loading, which has been demonstrated to load large nanoparticles of similar dimensions to nanoparticles into the cytoplasm of cells (4), was also observed to be a fatal method when applied to fibroblasts. Mild agitation was the alternative method used which demonstrated that scrape loading is not amicable to all cell types. Receptor-mediated endocytosis has also been reported for intracellular nanoparticle delivery, however, it is not effective for particles greater than 100 nm (5,6). Mild sonication has also been reported for large macromolecules os similar dimensions to nanoparticles delivery into cells, but is primarily limited to loading cells that are in a suspension (7). Cationic transfection reagents such as TransIT®-293, GenePORTER™, and GeneJuice® have also been successfully used for intracellular nanoparticle delivery (8-10). This method can deliver submicron-sized particles with efficiency of ~11% (11). In a typical experiment, certain amounts of submicron particles in serum free medium is mixed with the transfection agent, incubated in serum free medium for 4 hrs, washed with complete growth medium, and then incubated with complete growth medium for another 24 hrs. However, for this

method to work the submicron particle surface must have negative charges. If the particle surface has no negative charges, it will lead to poor loading efficiency (2). Another associated charge problem can arise when polyanion species are present, such as heparin or dextran sulphate, as contaminants, which are known to inhibit the transfection efficiency. Also reported has been the difficulty of removing particles that were adhered to the cell surface without damaging the cells (12).

Recently, an alternative approach for cellular uptake of nanoparticles has been developed, which involves the use of cell-penetrating peptides (CPPs) (13). CPPs such as the Tat peptide, polyarginine, and penetratin have membrane translocating properties which allow them to enter into cell (14). The mechanism by which the CPPs are internalized into cells has been ascribed to both endocytosis and to free energy passage directly through the lipid bilayer of the cell membrane. However, it is the second mechanism of a direct transport through the lipid bilayer of cell membrane that has been the most widely accepted mechanism for internalization of CPP's. Recently, Richard et al. (13), reevaluated the uptake mechanism for the CPP's Tat $_{48\text{-}60}$ and $(Arg)_9$. Their findings showed that past measurement methods based on fluorescence-activated cell sorting (FACS) analysis and fluorescence microscopy on fixed cells required adjustments for proper determination of CPP internalization. Following adjustments to the methodologies, they reported the observance of a direct role of endocytosis for cationic CPP internalization. CPPs are derived from the "protein-transduction domains" of proteins like HIV-1 Tat, HSV-1 VP22, and *Drosophilia* Antennapedia homeoprotein (15). The active peptide domains of CPPs contain as major residues the basic amino acid arginine and lysine (16). At physiological pH CPP's are highly cationic (17), and often have a conformation that is alpha helical (18). Intracellular studies using CPPs include: tracking the differentiation and distribution of stem and progenitor

cells (19), the transportation into cells of heterologous proteins (20), gene delivery systems which are nonviral (21), and delivery of antibody fragments for tumor-targeting (22,23).

Recent work to internalize nanoparticles using the Tat cell penetrating peptide has been reported using magnetic nanoparticles for in vivo tracking and recovery of progenitor cells (24), for hepatic permeability studies in rats (25), for cellular uptake studies in mice spleen lymphocytes (26), and uptake studies in HeLa cells (27). The magnetic nanoparticles were iron oxide crystals comprised of ~2000 iron atoms, and averaged less than 10 nm in diameter. The Tat peptide has also been coupled to liposomes to study the internalization of liposomes into cancer cells (28). The liposomes were used as drug or DNA delivery vesicles. They have averaged in diameter 200 nm. Liposomes, however, are not rigid body particles and may be able to deform their shape during the internalization process. Quantum dots, which have diameters smaller than 10 nm, were also coupled to the amphipathic peptide Pep1 to facilitate their cellular internalization (2). The objective of our studies was to determine whether CPPs could facilitate the permeation of larger particles into single cells.

5.2 EXPERIMENTAL

5.2.1 Digital Fluorescence-imaging Microscopy

The experimental setup used for fluorescence measurements of the nanoparticles based sensors was reported previously (29). The system consisted of an inverted fluorescence microscope (Olympus IX-70) equipped with three detection ports. A 100-W mercury lamp was used as the light source for excitation. The fluorescence was collected by a 40 x microscope objective. A filter cube containing 470-490 nm excitation filter, 505 nm dichroic mirror, and 515 nm longpass emission filter was used to ensure spectral purity. A high-performance ICCD

camera (Roper Scientific, model 256HB) with a 512 x 512 pixel array was used for digital fluorescence imaging of the samples. The software image Pro+ (Media Cybernetics Inc.) was used for image analysis. The exposure time used in most experiments was 0.1 seconds.

5.2.2 Synthesis of Tat Peptide and Flubida Coated Nanoparticles

Streptavidin-beads will absorb onto Eppendorf tubes very easily so the tubes are coated with a 10 mg/mL bovine serum albumin (BSA) solution to avoid the nonspecific absorption. The BSA is dissolved in Dulbecco's PBS buffer and added to the disposable tubes to make a final concentration of 10 mg/mL. The BSA solution is incubated overnight in the tube and then rinsed with PBS buffer to prepare for the next step. The streptavidin is also coated with BSA to inhibit non-specific absorption onto the beads surface. 6 μL beads suspension is mixed with 1 mL Dulbecco's PBS buffer, mixed well, then 10 μL of a 100 mg/mL BSA dissolved in PBS solution is added to the mixture and incubated for 20 min. The beads are then washed 3 times by centrifuge at a speed of 14000 rpm for 15 min. The longer reaction time may reduce the beads binding capacity for biotin because it is possible that BSA eventually becomes absorbed onto the beads surface and block the specific biotin binding. The supernatant is then dispersed in 200 μL PBS buffer and mixed with 8 μL 200 μM flubida-biotin and 8 μL 200 μM biotin for control experiments, or the beads solution mixed with 8 μL flubida-biotin and 8 μL 200 μM Tat peptide solution, overnight. The beads are then washed three times with PBS buffer. To avoid photobleaching of the dye, the processed beads in their final vial are always covered by aluminum foil and stored in a refrigerator at 4 ^{o}C until used.

5.2.3 Permeation of Nanoparticles into Cells

We have tested the Tat peptide mediated uptake of nanoparticles by using two different cell lines, MCF 7 and Hela cancer cells under varying incubation times. All of the experiments were performed at 37 ^{0}C under a 5% CO_2 atmosphere. After initial growth in tissue culture flasks, the cells were collected and diluted into 1×10^6 cells/mL cell growth medium. Standard hemacytometry was used to determine the cells concentration and viability with trypan blue staining (30,31). The cells were planted and incubated in coverslip covered chamber wells for 80% confluency. The cells were washed with serum free medium, or Dulbecco's PBS buffer, then mixed with nanoparticles in a sterilized hood environment and incubated at varied times. After incubation, the cells were washed with PBS buffer (pH 7.2) to remove extra nanoparticles and analyzed by digital fluorescence microscopy, spectrofluorimeter, and microplate reader.

5.3 Results and Discussion

5.3.1 Choice of Fluorescence Indicator

The probe chosen for fluorescent labeling of the sensor under development was flubida-2, which is a conjugate between fluorescein diacetate and biotin. This fluorophore is non-fluorescent before penetrating into cells under physiological pH conditions. Figure 1 illustrates the structure of flubida-2 (32). The advantage of this indicator is that there is no background fluorescence from extra flubida-2 being present during intracellular measurements because it is non-fluorescent under physiological pH conditions. The mechanism responsible for activation of the flubida-2 fluorescence is controlled by enzymatic activity where after the flubida-2 has penetrated into the cells, the esterase enzyme will catalyze the diacetate to acid, changing the fluorescein diacetate to fluorescein, which then emits fluorescence. The mechanism for the

conversion of flubida-2 to fluorescein is shown below. In the developed sensor the flubida-2 is covalently bound to the avidin microspheres. With the aide of the Tat peptide, which acts as a cell penetrating peptide, the microspheres will penetrate into the cells and emit fluorescence. Thus allowing the sensing and subsequent measurement of the pH in the cytoplasm.

To determine whether the modification of flubida-2 would have an affect on its pH dependant fluorescence properties, we scanned the emission spectra of free flubida-2 and flubida-2 modified polystyrene particles in a physiological pH 7.4 solution and in a pH 10 basic solution. The flubida-2 concentration used in the tests was 2 ųM. Figure 5.2(a) illustrates that the free flubida fluorescence intensity was observed to increase after changing the pH from 7.4 to 10. After modifying flubida-2 onto the polystyrene particles, the fluorescence intensity still increased with increasing pH, as illustrated in Fig. 5.2(b), demonstrating that the pH dependant fluorescence properties had not changed.

5.3.2 Coupling of Tat Peptide and Flubida to Nanoparticles

Although the avidin-biotin binding is known to be a very strong noncovalent binding, streptavidin was used in the development of the bead sensor instead of avidin. Streptavidin shows less nonspecific binding to the particles compared to avidin. Streptavidin is very similar to avidin in structure. It has four subunits, each can bind to a single biotin molecule. Both streptavidin and avidin are resilient proteins that can tolerate a variety of buffer conditions, different pH values, and many chemical modifications. To optimize the amount of flubida biotin and Tat peptide conjugated to the particles, control experiments were performed in which flubida biotin was replaced with the fluorescent dye 5-((N-(5-(N-(6-(biotinoyl) amino)

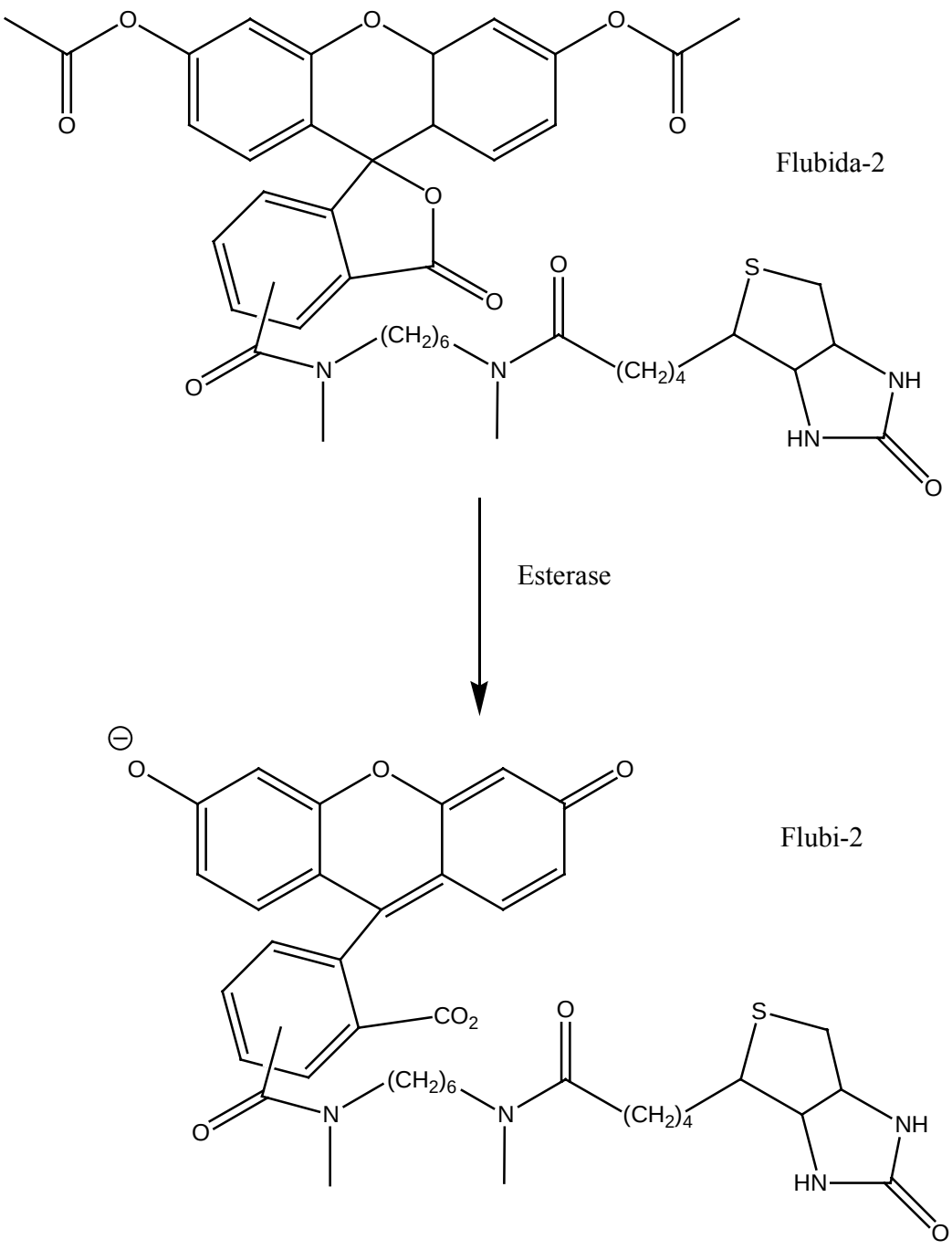

Figure 5.1. Flubida structure and esterase conversion to the fluorescent species (32).

hexanoyl)amino)pentyl)thioureidyl)fluorescein (fluorescein biotin), and the Tat peptide was replaced with biotin (multiple control experiments using the Tat peptide are prohibitive due to high cost). The fluorescence intensity of fluorescein biotin was quenched when the dye was bound to the streptavidin coated nanoparticles. The fluorescence quenching could be attributed to the formation of nonfluorescent aggregates on the particle surface due to interaction of the fluorescein molecules with unsaturated steptaviding binding sites (33). To overcome this problem, 200 μM biotin was added to the fluorescein biotin and beads solution. This minimized the fluorescence due to the decreasing availability of streptavidin binging sites

5.3.3 Microscopy Studies of Nanoparticls Permeation into Cells

The particle-based sensors in our experiments averaged 120 μm in diameter. To determine whether these particles can penetrate into MCF7 cells, the particles were incubated with the cells, in a controlled environment incubator, for 4 hours at 37 ^{0}C under a 5% CO_2 atmosphere. The samples were then removed from the incubator and washed with Dulbecco's PBS buffer three times. The chambered coverglasses containing the cells and particles were then monitored by digital fluorescence microscopy. If the particles have penetrated into the cells, only the cells should fluoresce. There should be minimal background fluorescence from particles outside of the cells since flubida-2 is non-fluorescent under physiological conditions. Figure 5.3 illustrates the digital images of nanoparticles incubated with MCF 7 cells where (a) is the MCF 7 cells transmission image, and (b) is the digital fluorescence image of MCF 7 cells and particles.

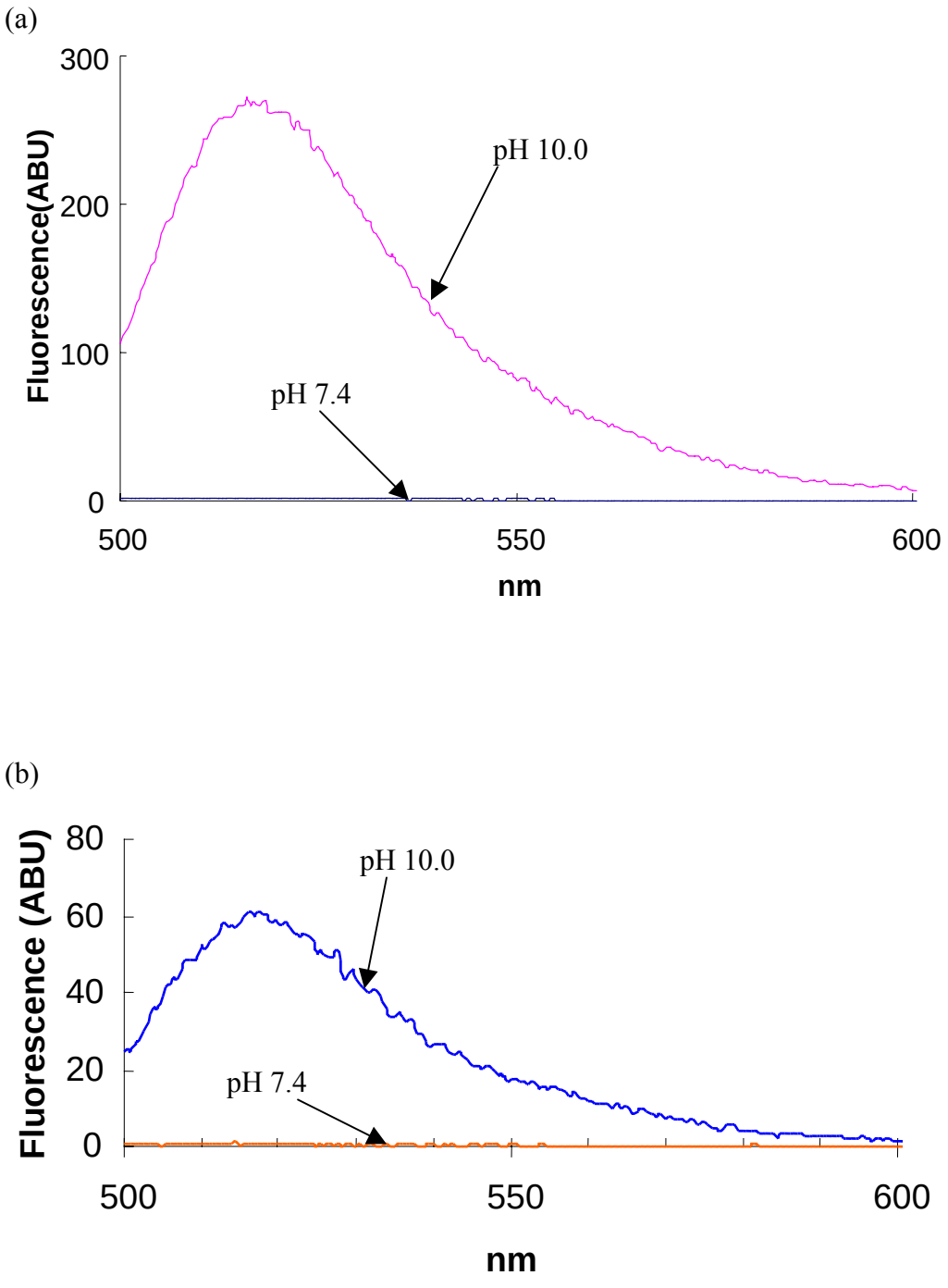

Figure 5.2. (a) 2 uM flubida-biotin at pH7.4 and pH10.0. (b) 6 uL 120 nm streptavidin microspheres at pH7.4 and pH10.0.

(a)

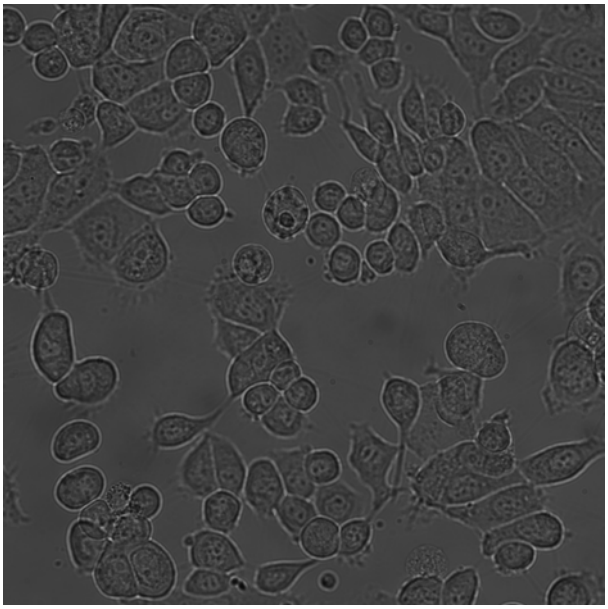

(b)

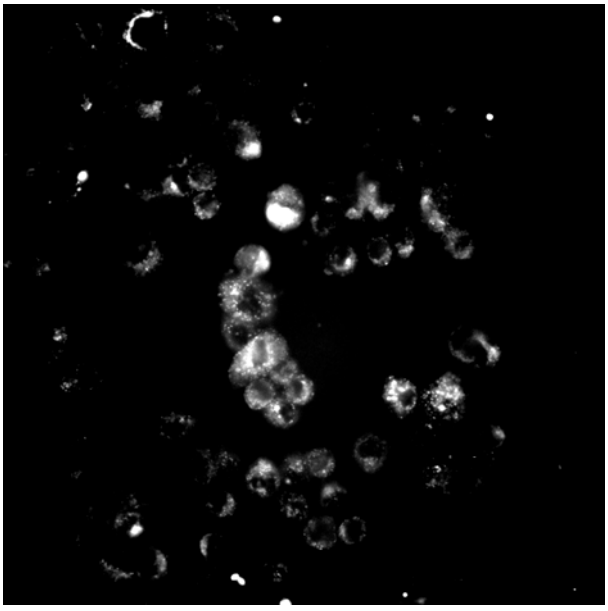

Figure 5.3. Digital images of particles with MCF 7 cells where (a) is the MCF 7 cells transmission image, and (b) is the digital fluorescence image of MCF 7 cells and particles.

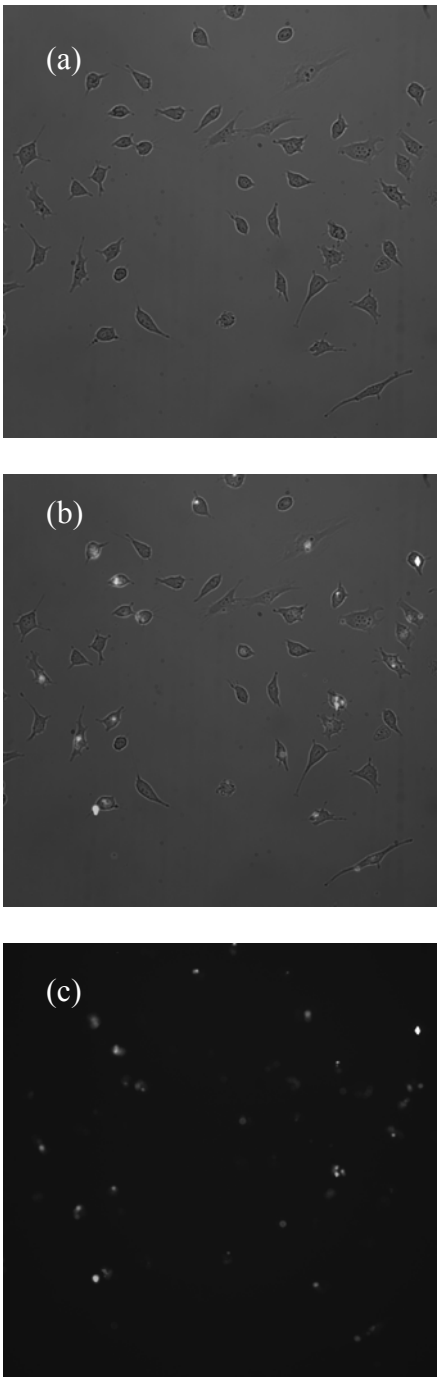

Figure 5.4 Digital images used to determine whether the particles are penetrating into the Hela cells. (a) Hela cells transmission image, (b) overlap of the transmission-fluorescence image of the Hela cells, and (c) digital fluorescence image.

The images do not readily demonstrate whether the particles have penetrated into the cells or not. But Figs 5.3 (a) showed 70-80% cells confluency and MCF 7 cells were alive which was confirmed with trypan blue. Figs 5.3 (b) demonstrated that some cells fluoresce indicating nanoparticles internalization or attachment of flubida into the cells. To determine if penetration has taken place, experiments were performed that attempted to compare MCF 7 and Hela cells for particle penetration confirmation. The first experiment involved incubating the particles with Hela cells under the same condition as was performed for the MCF 7 cells. Generally, Hela cells are known to more easily engulf an intruder such as the sensors than the MCF 7 cells. Figure 5.4 shows the digital images of the experiment to determine whether the particles are penetrating into the Hela cells. In Figure 5.4, (a) is the Hela cells transmission image, (b) is an overlap of the transmission-fluorescence image of the Hela cells, and (c) is the digital fluorescence image. Figs 5.4 (a) demonstrated the Hela cells were smaller than MCF7 cells and Hela cells had 40-50% confluency, Figs 5.4 (b), (c) illustrated that less labling were showed in Hela cells than in MCF 7 cells, However, the images still did not demonstrate that the particles have penetrated inside the cells.

5.3.4 Proving That the Microscopy Results are an Artifact

From the digital microscopy images shown above for the penetration experiments, it could not be determined whether the particles had penetrated inside the cells. Under the above described experiment of incubating the particles in a suspension of cells for 4 hours at 37 ^{0}C under 5% CO_2 atmosphere and measuring the fluorescence by fluorimeter, the comparison of the fluorescence intensity before and after the particles were incubated with cells was done. However, the fluorescence intensity change was too small to prove that the particles were inside

the cells. To illustrate this, Figure 5.5 shows a plot of the emission spectra comparing the particles in a suspension of Hela cells where (a) is the mixture of particles with the Hela cells representing a baseline measurement of the fluorescent emission, (b) is the fluorescent emission after 4 hours of incubation, and finally (c) is the fluorescent emission after adjusting the pH to 10 with KOH. As can be seen in the graph, after incubating the nanoparticles with the cells for four hours, only a small increase in fluorescence intensity was observed. The slight fluorescence intensity increase that was observed may due to cellular auto fluorescence. Therefore, if the particles did not get inside the cells, they must still be in the solution. After measuring the fluorescence intensity of the incubated particles with cells, we added drops of concentrated potassium hydroxide to adjust the pH from 7.4 to 10.0. Upon adjusting the pH, the fluorescence intensity increased significantly, which suggested that the nanoparticles did not efficiently penetrate into the cells. The same experiment was performed using the MCF 7 cells. The results were very similar to the ones with Hela cells, but after 4 hours incubation, the fluorescence increase was even smaller than was what observed with Hela cells. Hela cells were used for the rest of the experiments because Hela cells are generally exhibiting higher permeability.

The next step taken was to use a microplate reader to quantitate the penetrating efficiency of the sensors into the cells. The microplate reader is very similar to a fluorometer. However, this is the only system that can provide dual-mode measurement for a cuvette port and a 6-384 microplate reading setup. In the microplate reader setup for a 96 well microplate reading, the conditions to incubate the particles with cells were the

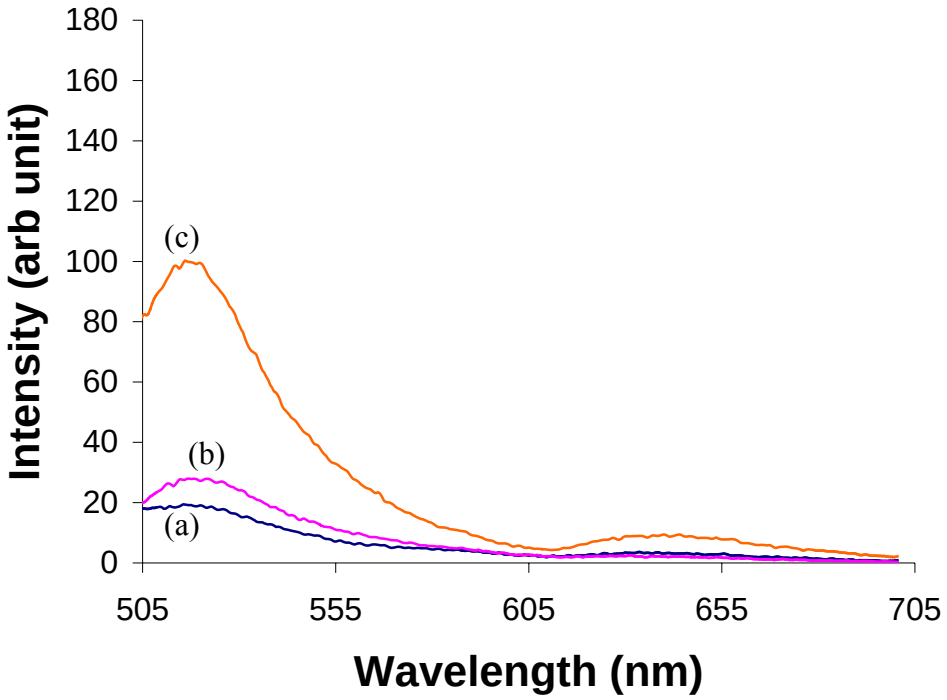

Figure 5.5. Plot of the emission spectra comparing the particles in a suspension of Hela cells where (a) is the mixture of particles with the Hela cells representing a baseline measurement of the fluorescent emission, (b) is the fluorescent emission after 4 hours of incubation with cells, and (c) is the fluorescent emission after adjusting the pH to 10 with KOH.

same as the ones used for the incubation experiments measured by digital fluorescence microscopy reported above. The incubation experiments included cells with cell growth medium, free fluibda, particles covalently bound with flubida, and particles covalently bound with either flubida or the Tat peptide separately. Figure 5.6 shows the microplate reader results with cells treated with (a) 20 μL Dulbecco's buffer, (b) 20 μL Tat peptide, (c) 20 μL particles with cells, (d) 20 μl flubida covalently bound particles incubated with

the cells for four hours, and (e) flubida and Tat peptide covalently bound particles incubated with the cells for 4 hours.

In Figure 5.6(a), only an initial increase in fluorescence intensity was observed with the buffer additive indicating cellular autofluorescence. The fluorescence intensity in Fig. 5.6(b) is also probably due to cellular autofluorescence. The fluorescence reading for Fig. 5.6(c) was very similar to (b), which means that the Tat peptide and particles were not fluorescent. In Fig. 5.6(d) there was observed a two-fold increase in the fluorescence intensity for the flubida covalently bound particles incubated with the cells. In Fig. 5.6(e) the fluorescence intensity increased less than two-fold. This result was not expected because it was assumed that the Tat peptide would facilitate particle penetration into the cells.

The next experiment was performed to determine whether the problem was from the cell medium. Using the microplate reader, the fluorescence intensity was measured for free flubida in (a) blank well, (b) 20 uL cell medium, (c) 20 μL Dulbecco's buffer, (d) 20 uL serum free medium, (e) 20 uL flubida biotin in cell growth medium, (f) 20 uL flubida biotin in Dulbecco's buffer, and (g) 20 uL flubida biotin in serum free medium. Figure 5.7 shows the graphical results of the timed fluorescence intensity studies for free flubida in Dulbecco's PBS buffer, cell growth medium and serum-free medium. Both Fig.s 5.7(a) and (c) show very low levels of fluorescence

which means the measured signal is primarily from background fluorescence. Fig.s 5.7(b) and (d) illustrate that the cell growth medium was emitting fluorescence due to the aromatic amino acid composition of the medium. Fig. 5.7(e) demonstrates that the flubida biotin complex was converted to the fluorescein biotin complex when in cell growth medium with increasing incubation time. Fig. 5.7(f) illustrates that the flubida biotin complex was not affected by Dulbecco's buffer. Fig. 5.7(g) demonstrates that less of the flubida biotin complex was converted to the fluorescein biotin complex in the serum free medium than what was observed to be converted in the cell growth medium. From the graphs, it can be concluded that the flubida biotin complex fluoresces in cell media including both the cell growth medium and the serum free medium. However, in serum free medium, the flubida biotin complex emits less fluorescence than that in the cell growth medium. Finally, it was observed that flubida does not convert to fluorescein in Dulbecco's PBS buffer.

(a)

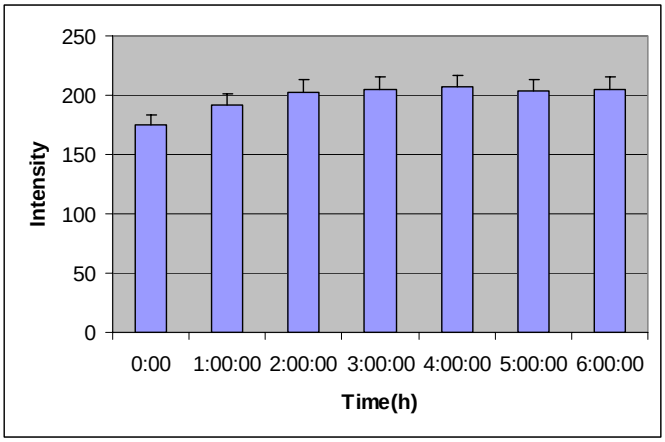
250
200
150
100
50
0
Intensity
0:00
1:00:00
2:00:00
3:00:00
4:00:00
5:00:00
6:00:00
Time(h)

(b)

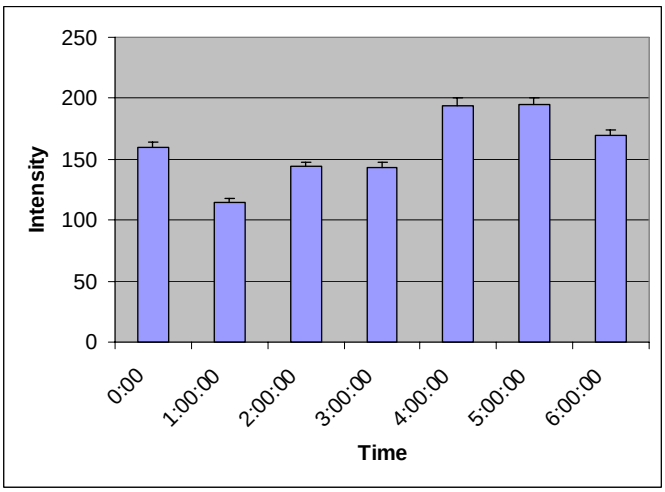
250
200
150
100
50
0
Intensity
0:00
1:00:00
2:00:00
3:00:00
4:00:00
5:00:00
6:00:00
Time

(c)

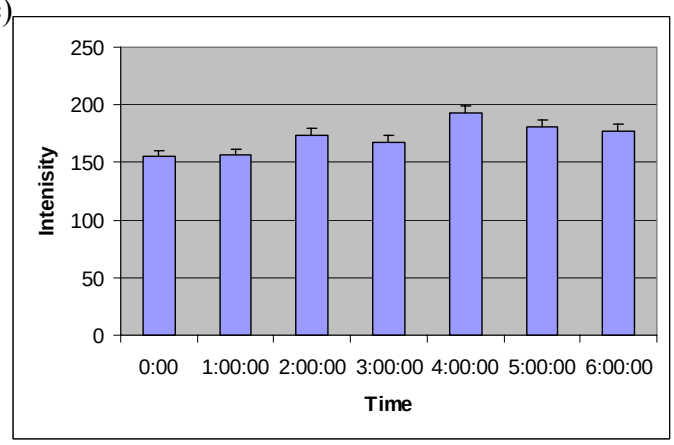
250
200
150
100
50
0
Intenisity
0:00
1:00:00
2:00:00
3:00:00
4:00:00
5:00:00
6:00:00
Time

(d)

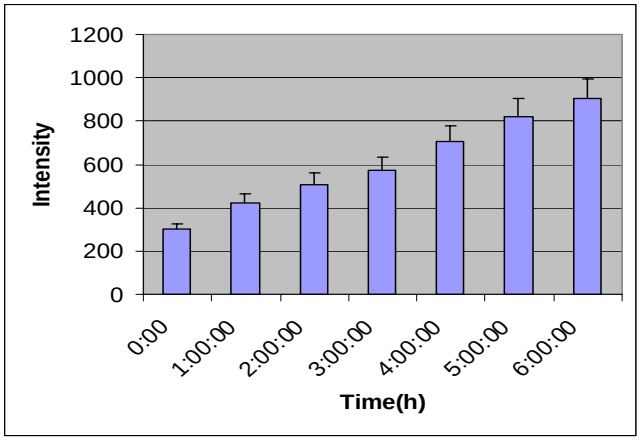

(e)

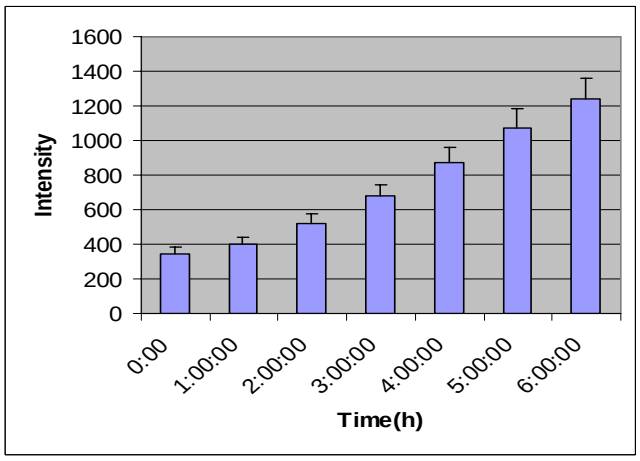

Figure 5.6. Microplate reader results for cells treated with (a) 30 µL Dulbecco's buffer, (b) 30 µL Tat peptide, (c) 30 µL particles with cells, (d) 20 µL flubida covalently bound particles incubated with the cells for four hours, and (e) flubida and Tat peptide covalently bound particles incubated with the cells for 4 hours.

(a)

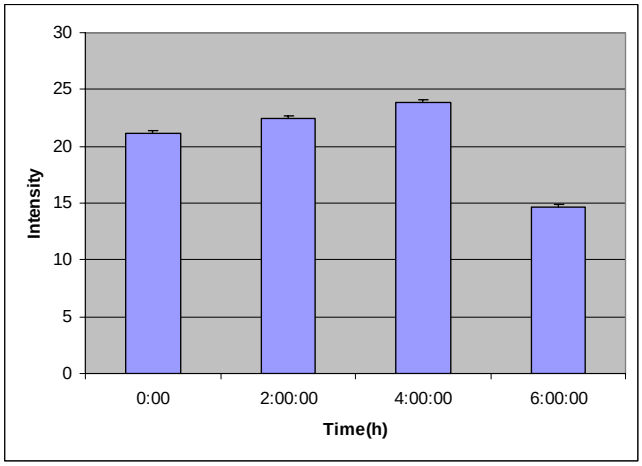
30
25
20
15
10
5
0
Intensity
0:00
2:00:00
4:00:00
6:00:00
Time(h)

(b)

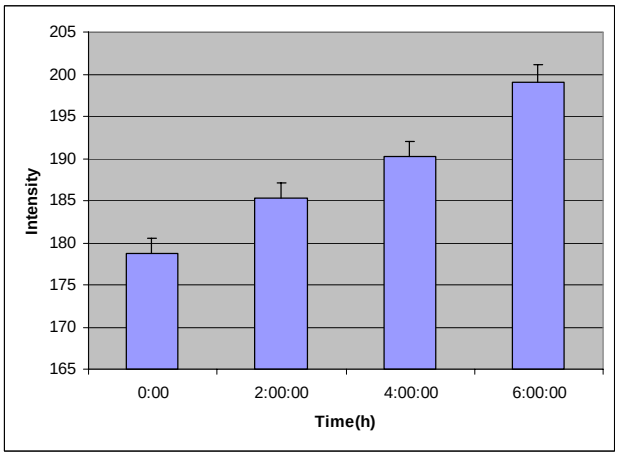
205
200
195
190
185
180
175
170
165
Intensity
0:00
2:00:00
4:00:00
6:00:00
Time(h)

(c)

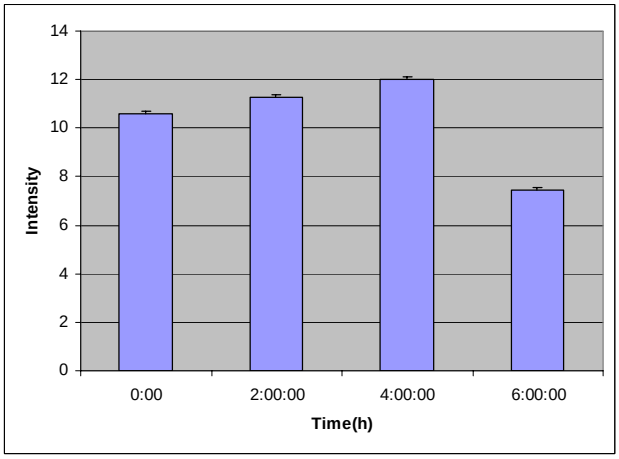
14
12
10
8
6
4
2
0
Intensity
0:00
2:00:00
4:00:00
6:00:00
Time(h)

(d)

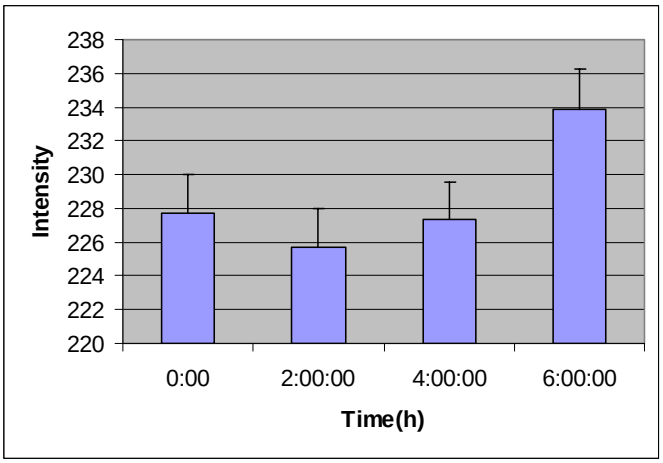
238
236
234
232
230
228
226
224
222
220
Intensity
0:00
2:00:00
4:00:00
6:00:00
Time(h)

(e)

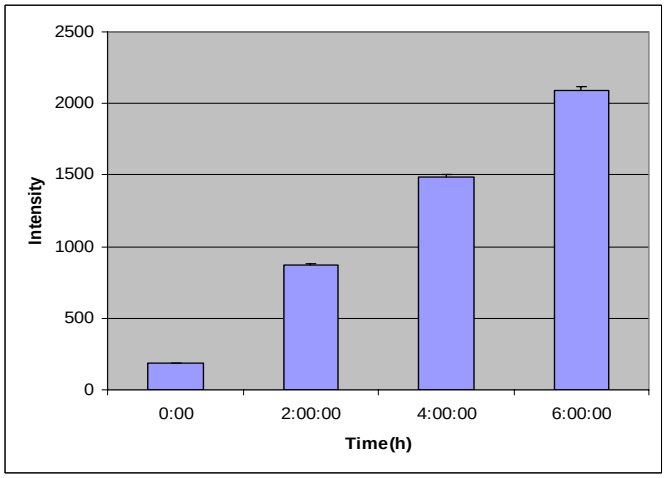
2500
2000
1500
1000
500
0
Intensity
0:00
2:00:00
4:00:00
6:00:00
Time(h)

(f)

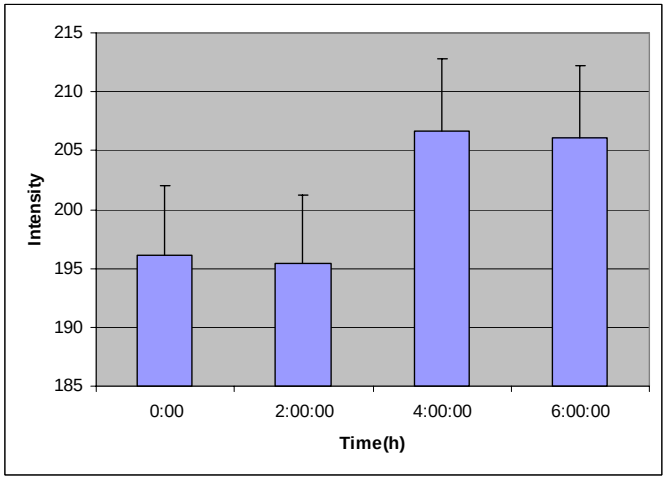
215
210
205
200
195
190
185
Intensity
0:00
2:00:00
4:00:00
6:00:00
Time(h)

(g)

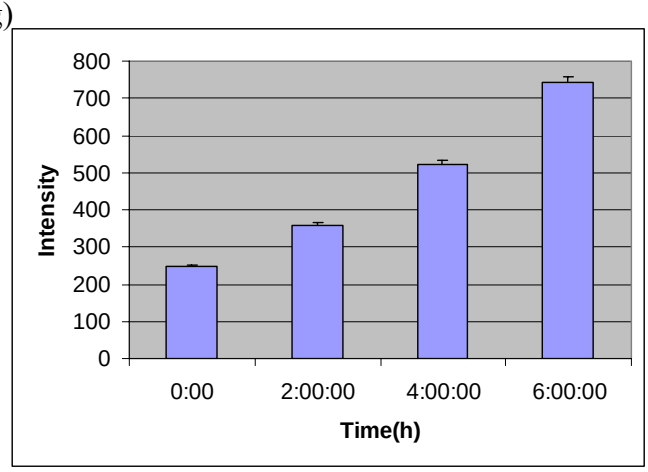

Figure 5.7. Fluorescence intensity versus time for free flubida in (a) blank well, (b) 30 uL cell medium, (c) 30 µL Dulbecco's buffer, (d) 30 uL serum free medium, (e) 20 uL flubida biotin in cell growth medium, (f) 20 uL flubida biotin in Dulbecco's buffer, and (g) 20 uL flubida biotin in serum free medium.

A 24-hour cell viability study of incubating the cells in cell growth medium, serum free medium, serum free medium (PBS, v/v, 1/1), and Dulbecco's PBS buffer was performed. The results of the study are shown in Table 5.1. From the tabulated results it can be seen that the cells were alive in all four different media up to six hours. After six hours, the cells incubated in PBS buffer started to die. If the particles can penetrate into the cells, they should have penetrated within 6 hours. To avoid the use of the different media which may pose an interference problem (i.e., GM, SFM, and SFM: PBS) the viability study demonstrates that Dulbecco's buffer can be used as the medium for incubating the particles with the cells.

Time (h)	Growth Medium (%)	Serum Free Medium (%)	Serum Free Medium: PBS (v/v, 1/1) (%)	PBS (%)
2	99 ± 4.8	98.4 ± 6.8	95 ± 3.8	90.4 ± 5.0
4	96.3 ±5.0	92.4 ± 5.9	92.5 ± 7.8	88.8 ± 4.6
6	94.5 ± 3	91.7 ± 7.5	90 ± 8.6	89.3 ± 7.8
8	85.3 ± 5	90.9 ± 9.1	85.2 ± 4.6	77.2 ± 5.3
12	89.6 ± 4.6	80.9 ± 9.0	81.4 ± 7.2	73.7 ± 15.0
24	85.9 ± 8.9	85.8 ± 14.0	78.2 ± 17.0	55.9± 20.0

Table 5.1. 24 hour cell viability study.

From Fig. 5.7 it was summarized that serum free medium did induce flubida to emit fluorescence. But in serum free medium, flubida emitted less fluorescence than that in cell growth medium. It is assumed that if the serum free medium was diluted with Dulbecco's PBS buffer, less fluorescence would be emitted from flubida so that the fluorescence could be ignored. A comparison was made for particles incubated with cells in serum free medium, in Dulbecco's PBS buffer (v/v, 1/1), and particles incubated in serum free medium-PBS buffer. Figure 5.8 shows the comparison of the results. Fig.s 5.8(a) and 5.8(b) represent the background signal from control blanks. Figures 5.8(c), (d), (e), and (f) demonstrate that the particles had similar increases in fluorescence intensity with and without cells, which appears to prove that the serum free cell medium did convert the flubida into fluorescein, and the particles did not penetrate inside the cells after the conversion. At the same time, we observed that the Tat peptide did not facilitate the penetration of the nanoparticles into the cells. There are two possibilities why the Tat peptide did not work. The first possibility is that the Tat peptide was stored too long thereby greatly reducing its efficiency; the other possibility is that our experimental design was not correct, and needs to be adjusted. Torchilin, V. P. et al. (34) demonstrated that the Tat peptide works most efficiently after adding a spacer between the particles and the Tat peptide. Based on this idea, we can modify our 120 nm particles with polyethylene glycol (PEG) as a spacer, and then the Tat peptide can covalently bind to the PEG terminus-reactive amine group.

(a)

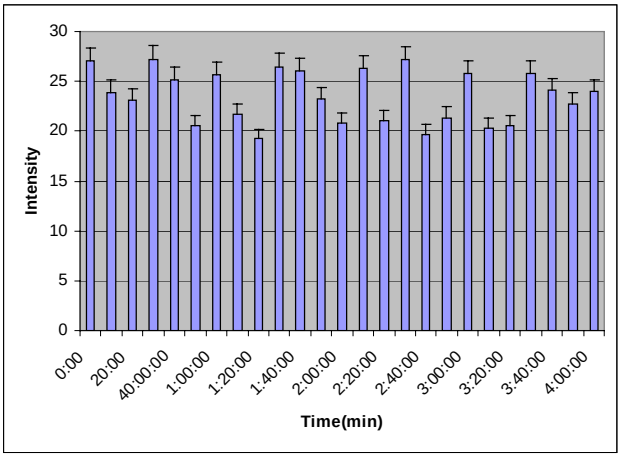
Intensity
30
25
20
15
10
5
0
0:00
20:00
40:00:00
1:00:00
1:20:00
1:40:00
2:00:00
2:20:00
2:40:00
3:00:00
3:20:00
3:40:00
4:00:00
Time(min)

(b)

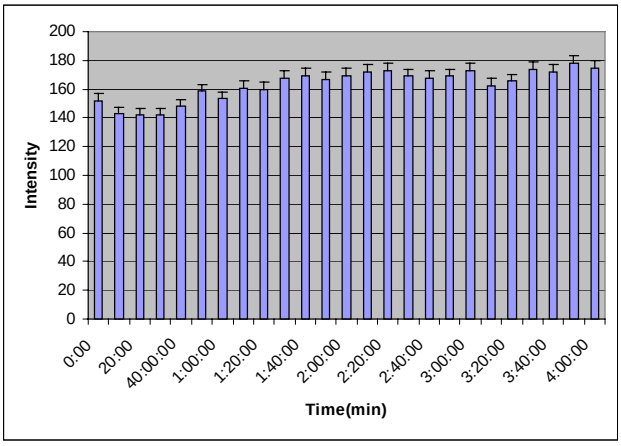
Intensity
200
180
160
140
120
100
80
60
40
20
0
0:00
20:00
40:00:00
1:00:00
1:20:00
1:40:00
2:00:00
2:20:00
2:40:00
3:00:00
3:20:00
3:40:00
4:00:00
Time(min)

(c)

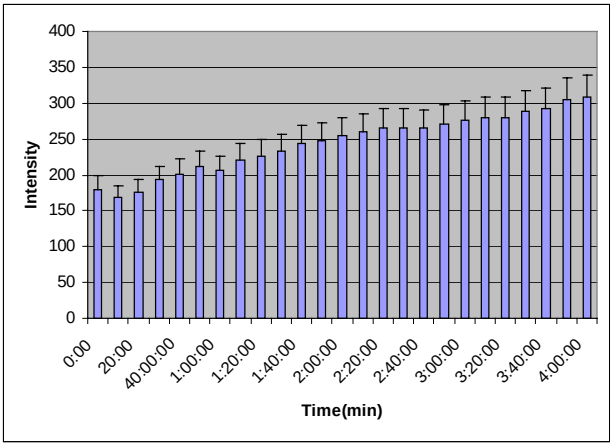
Intensity
400
350
300
250
200
150
100
50
0
0:00
20:00
40:00:00
1:00:00
1:20:00
1:40:00
2:00:00
2:20:00
2:40:00
3:00:00
3:20:00
3:40:00
4:00:00
Time(min)

(d)

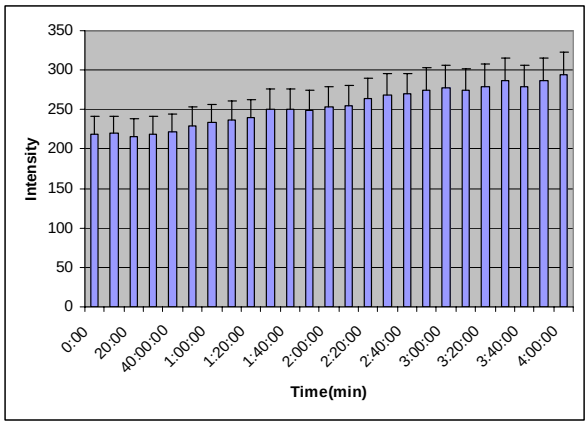

(e)

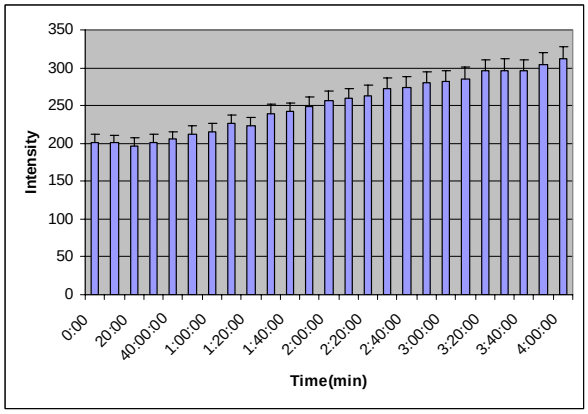

(f)

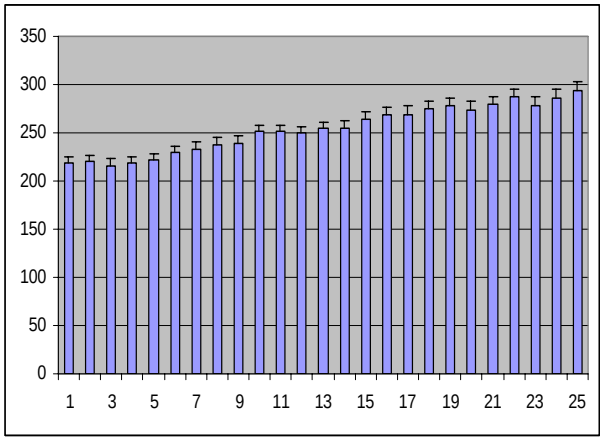

Figure 5.8. Comparison of nanoparticles incubated with cells in (a) control blank, (b) serum free medium- buffer (v/v, 1/1)(SFMB), (c) 20 µL particle-flubida incubated in cell with SFMB, (d) 20 µL particle-flubida-Tat incubated in cell with SFMB, (e) 20 µL particle-flubida incubated in SFMB, (f) 20 µL particle-flubida-Tat incubated in SFMB.

5.4 Conclusions

We have studied the use of cell penetrating peptides to facilitate the permeation of nanoparticles averaging 120 nm in diameter into cells. We have successfully attached the Tat peptide and the fluorophore flubida-2 to streptavidin coated particles using streptavidin biotin interactions. The immobilization of Tat and flubida did not affect their free solution properties. Initial microscopy observations suggested that the particles permeated into cells. It was unclear whether the particles were only attached to the membrane or indeed penetrated through the cell membrane into the cell cytoplasm. A more detailed study revealed that flubida-2 is unstable in cell growth medium and even in serum free medium. It was therefore possible that the acetate groups would be cleaved off the fluorescein skeleton of the molecule extracellularly. This led to fluorescein intensity increase of the particles without actual permeation into the cells. This negative result was also confirmed using averaged fluorescence measurements of cells in a well plate reader format. In these experiments the fluorescence enhancement observed when Tat and flubida coated particles were incubated with both MCF-7 and Hela cells under various incubation conditions was neglible. Future experiments will focus on the use of phosphate buffer solutions rather than growth medium as an incubation media. The incubation time will be shortened to ensure cell viability. If this step would prove unsuccessful we prove to increase the length of the linker that connects between the Tat peptide and the particles. Recent studies showed that increasing the linking length increases the penetration efficiency of cargo carried by cell penetrating peptides into cells.

Future studies will also focus on the use of these particles as intracellular pH sensors. However, to realize this goal the particles must be first internalized effectively by the cells of interest.

5.5 References

1. Tai-Kin Wong and Eberhard Neumann, Biochem Biophys Res Commun 1982, 107, 584-587.
2. Jaiswall, J.K., Goldman, E.R., Mattoussi, H. & Simon, S.M., Nature Methods, 2004, 1(1), 1-6.
3. E.F. Fynan, R.G. Webster, D.H. Fuller, J. R. Haynes, J.C. Santoro and H.L. Robinson, Proc. Natl. Acad. Sci. U.S.A., 1993, 90, 11,748-11,782.
4. McNeil, P.L., Murry, R.F., Lanni, F., and Taylor, D.L., J Cell Biol 1984, 98, 1556.
5. X.-H. N. Xu, J. Chen, R. B. Jeffers and S. Kyriacou, *Nano Lett.*, 2002, **2**, 175–182.
6. S. Prabha, W.-Z. Zhou, J. Panyam and V. Labhasetwar, *Int. J. Pharm.*, 2002, **244**, 105–115.
7. Fechheimer, M., Denny, C., Murphy, R.F., Taylor, D.L. Eur J Cell Biol, 1986, 40, 242.
8. Voura, E.B., Jaiswal, J.K., Mattoussi, H. & Simmon, S.M., Nat. Med. 2004, 10, 993-998.
9. Kneuer, C., Sameti, M., Bakowsky, U., Schiestel, T., Schirra, H., Schmidt, H. and Lehr, C.-M., Bioconjugate Chem., 2000, 11, 926-932.
10. Sandhu, K.K., McIntosh, C.M., Simard, J.M., Smith, S.W. and Rotello, V.M., Bioconjugate Chem, 2002, 13, 3-6.
11. Zhao, Y., Sadtler, B., Lin, m., Hockerman, G.H. and Wei. A., Chem. Commun. 2004, 784-785.
12. Sandhu, K.K., McIntosh, C.M., Simard, J.M., Smith, S.W. and Rotello, V.M., Bioconjugate Chem, 2002, 13, 3-6.
13. Richard, J.P., Melikov, K., Vives, E., Ramos, C., Verbeure, B., Gait, M.J., Chernomordik, L.V., Lebleu, B. *J. Biol. Chem.* **2003**, 278, 585-590.
14. Wunderbaldinger, P., Josephson, L., Weissleder, R. *Bioconjugate Chem.* **2002**, 13, 264-268.
15. Violini, S., Sharma, V., Prior, J.L., Dyszlewski, M., Piwnica-Worms, D. *Biochemistry* **2002**, 41, 12652-12661.
16. Futaki, S., Suzuki, T., Ohashi, W., Yagami, T., Tanaka, S., Ueda, K., Sugiura, Y. *J. Biol. Chem.* **2001**, 276, 5836-5840.
17. Gammon, S.T., Villalobos, V.M., Prior, J.L., Sharma, V., Piwnica-Worms, D. *Bioconjugate Chem.* **2003**, 14, 368-376.
18. Torchilin, V.P., Rammohan, R., Weissig, V., Levchenko, T.S. *Proc. Natl. Acad. Sci. USA* **2001**, 98, 8786-8791.
19. Lewin, M., Carlesso, N., Tung, C.H., Tang, X.W., Cory, D., Scadden, D.T., Weissleder, R. *Nature Biotech,* **2000**, 18, 410-414.
20. Fawell, S., Seery, J., Daike, Y., Moore, C., Chen, L.L., Pepinsky, B., Barsoum, J. *Proc. Natl. Acad. Sci. USA* **1994**, 91, 664-668.
21. Avrameas, A., Ternyck, T., Gasmi, L., Buttin, G. *Bioconjugate Chem.* **1999**, 10, 87-93.
22. Niesner, U., Halin, C., Lozzi, L., Gunthert, M., Neri, P., Wunderli-Allenspach, H., Zardi, L., Neri, D. *Bioconjugate Chem.* **2002**, 13, 729-736.
23. Zhou, X., Chang, Y.C., Oyama, T., McGuire, M.J., Brown, K.C. *J. Am. Chem. Soc.* **2004**,
24. Lewin, M., Carlesso, N., Tung, C.H., Tang, X.W., Cory, D., Scadden, D.T., Weissleder, R. Nat. Biotechnol. 2000, 18, 410-414.
25. Wunderbaldinger, P., Josephson, L., Weissleder, R. Bioconjugate Chem. 2002, 13, 264-268.

26. Zhao, M., Kircher, M.F., Josephson, L., Weissleder, R. Bioconjugate Chem. 2002, 13, 840-844.
27. Koch, A.M., Reynolds, F., Kircher, M.F., Merkle, H.P., Weissleder, R., Josephson, L. Bioconjugate Chem. 2003, 14, 1115-1121.
28. Torchilin, V.P., Rammohan, R., Weissig, V., Levchenko, T.S. *Proc. Natl. Acad. Sci. USA* **2001**, 98, 8786-8791.
29. Lentz, B. R.; Carpenter, T. J.; and Alford, D. R. Biochemistry, **1987**, 26, 5389.
30. Ji, J.; Rosenzweig, N.; Griffin, C.; Rosenzweig, Z. Anal. Chem. **2000**, 72(15), 3497-3503.
31. Ji, J.; Rosenzweig, N.; Jones, I.; Rosenzweig, Z. Anal. Chem., **2001**, 73(15), 3521-3527.
32. Wu, M.M., Llopis, J., Adams, S., McCaffery, J.M., Kulomaa, M.S., Machen, T.E., Moore, H.P.H., Tsien, R.Y. *Chemistry & Biology*, **2000**, **7**, 197-209.
33. Buranda, T, Jones, G.J., Nolan, J.P., Keij, J., Lopez, G.P., and Sklar, L.A. J. Phys.Chem. B, **1999**, 103, 3399-3410.
34. Torchilin, V.P., Rammohan, R., Weissig, V., Levchenko, T.S. *Proc. Natl. Acad. Sci. USA* **2001**, 98, 8786-8791.

CHAPTER VI: SUMMARY AND CONCLUSIONS

Fluorescence techniques are regarded as very sensitive and informative tools for cellular analysis. Combining the methods of spectrofluorimetry, digital fluorescence microscopy, and microplate reader, we can quantify not only intracellular, but also extracellular analysis in cellular environments and in biological fluids. The design of our chemical and biochemical sensors are compatible with cellular analysis, much more reproducible than those previously developed. In my dissertation, it includes the development of lipobeads based sensors for chloride measurement, urea measurement and intracellular measurement by nanoparticles penetrating into cells.

In our lab, we have developed particle-based sensors called lipobeads that are made of polystyrene particles coated with a phospholipids membrane, and the fluorescent indicators are embedded inside or outside the phospholipids membrane. This type of sensor is biocompatible with intracellular and extracellular analysis, and has a relatively fast response time while displaying high sensitivity. However, we have always had problems with reducing the lipobeads sizes and minimizing the sensor aggregation to as little as possible. For the first time, chapter 3 demonstrates the capability of developing our unique reduced-sized submicrometric lipobeads to quantify chloride ion levels in aqueous samples and biological fluids. For the first time, an oil-in-water microemulsion method was used to prepare the lipobeads. This led to forming smaller size lipobeads while minimizing the lipobeads aggregation as compared to other submicrometric particle-based sensors. From this work, the first lipobead based anion sensor was developed. The chloride sensitive dye lucigenin is hydrophilic. To decrease its hydrophilicity and to have it become absorbed inside the phospholipids membrane, an ion pair between lucigenin and alkyl

hexadecanesulfonate was formed. This resulted in a greater partition rate of the lucigenin dye into the membrane of the lipobeads and decreased the leakage of lucigenin from the sensing particles. The modification of lucigenin did not affect its luminescence properties, but did allow more lucigenin to be absorbed into the phospholipids membrane. However, the lucigenin containing lipobeads were unresponsive to chloride without a chloride ion transport from the solution into the membrane. The chloride ionophore [9] mercuracarborand-3 (MC-3) was incorporated into the phospholipids membrane for the required chloride transportation. The sensor was highly selective to chloride due to the chloride sensitive indicator lucigenin and chloride selective ionophore MC-3. The response time of the sensor was fast at about 5 seconds. With these analytical properties this unique lipobeads sensor demonstrated an effective technique for chloride measurement in biological fluids.

Although the chloride lipobeads sensor was fast and selective to chloride sensing, the reproducibility of that sensor was still not good due to the physical absorption of the fluorescent indicator into phospholipids membrane of the lipobeads. There always is an improvement by covalently attaching phospholipids and fluorescent indicators to the microspheres, however, polystyrene microspheres are not an ideal polymer to use for covalent binding in organic solvent due to its poor dispersity. Silica particles have been recently used as drug carriers without noticeable side effects. Chapter 4 presents a lipobeads fabrication by covalently attaching phospholipids and a fluorescent indicator to the silica particles for urea measurement. For the first time, this chapter describes the use of submicrometric silica particles as the core of urea sensing lipobeads. Silica particles modified with carboxyl groups were coated with functionalized phospholipids to form the membrane-coated beads. The lipobeads membrane was covalently bound by the enzyme urease and the pH sensitive indicator fluorecein-5-

thiosemicarbazide. SEM and digital fluorescent images showed that the synthesized lipobeads were bright and evenly dispersed, and no apparent aggregation was observed. Immobilization of the fluorescent indicator to the lipobeads demonstrated that the response of the immobilized pH indicator did not change appreciably due to immobilization. The working range of the immobilized fluorescein-5-thiosemicarbazide indicator was between pH 6 and 8.5. Reversibility studies indicated that the lipobeads were highly reproducible. The dynamic range was determined to be from 0.1 mM to 4 mM. The Michaelis-Menten constant K_m for the lipobeads particles was 7.0 ± 1.8 mM, 3.7 fold higher than the K_m of free urease. This indicated that immobilization of urease to the lipobeads membrane decreased the rate of the hydrolase's conversion of urea into ammonia. This was expected due to a diffusion barrier in the lipobeads membrane. The comparison between this lipobeads sensor with previously reported particle-based sensors proves that the lipobead-based biosensor is useful in *in-vivo* experiments that particle endocytosis would be prevented for long term monitoring of urea in serum. The phospholipids coating of the particles was previously shown to be effective in lowering the endocytotic rate.

We observed a very similar dynamic range between the urea lipobeads sensor and a previously developed fiber optic sensor that was applied in vivo. The lipobeads sensor showed a potential to be used in vivo. Chapter 5 described the application of avidin-biotin modified nanoparticles into cells by using Tat peptide for pH measurement. The strongest noncovalent binding between avidin and biotin was used to modify the nanoparticles by attaching Tat peptide and flubida-biotin to the surface of the nanoparticles without modifying the peptide properties. Flubida is nonfluorescent before penetrating into cells, where it has no background fluorescence for pH measurement. There are several methods for nanomaterials penetrating into cells, the

most popular and challenging one is to use the Tat peptide. Some progress was made towards the application of Tat peptide to the new sensor. The results demonstrated that in PBS buffer, flubida did not fluoresce, however, in cell medium, either cell growth medium or serum free medium; flubida can be converted to fluorescein before penetrating into the cell membrane, and subsequently emitting fluorescence.

Future work can be done by checking the behavior of the nanoparticles incubated with Hela cells in Dulbecco's PBS buffer for less than 6 hours. Also by replacing the Tat peptide with a newly synthesized Tat peptide and by adding a spacer between the nanoparticles and the Tat peptide that will allow the Tat peptide to break the cell membrane and let the intruder penetrate into the cells.

Combining this research work with previous studies of lipobeads sensor, it has been demonstrated that lipobeads based sensors are noninvasive, biocompatible due to the phospholipids membrane, highly reproducible due to the covalent attachment, selective because of the sensitive fluorescent indicator and selective ionophore, fast response times which can go to subsecond, photostable, and remains stable for a couple of month. My research work expanded this lipobeads study, reduced the lipobeads size, minimized the lipobeads aggregation, enhanced the lipobeads stability, improved the reproducibility of lipobeads and introduced the silica microspheres to the lipobeads system.

There are some limitations and advantages for this research study. First of all is the instrument stability. There is always a ~5% fluctuation for the mercury lamp in the microscopy, which will limit the quantitative analysis with digital fluorescence microscopy. The slits of the PTI spectrofluorimeter always vary for every measurement because the slits have to be manually operated every time, which limits the repeatability. For the time being, the quantitative analysis

can be done by using the multifunction microplate reader, which will minimize the subject error. The new spectrofluorimeter being used (Perkin Elmer) can set up the slit by software and minimizes the instruments limitation.

Second is the variability of the cells' growth stages. The cells were incubated in slightly different environments for every batch. So every batch of the cells is slightly different and at each batch, the individual cells are at a different growth stage from young to dead cells. This greatly affects the nanoparticles penetrating into the cells and the penetrating efficiency varies from batch to batch. To minimize the cells variability, a check on the viability of cells for every batch used can help to minimize this error.

In the future, it is very important to apply the lipobeads based sensor or particle based sensor into cells. The particle based sensors have been developed for a couple of decades now, and the applications from this development are still limited. It is still a big challenge to deliver submicrometric particle based sensors to cells non-invasively. The development of DNA modified particles is a promising direction. The DNA outlayer can be interacted with the cell membrane and the cells can engulf the intruder.

VITA

The author was born in Weifang, Shandong, P.R.China. She obtained her B.S. in chemistry in 1997 from Liaocheng University. To pursue higher education, she directly went to graduate school in Applied Chemistry at the Universy of Science and Technology of China and received her M.S in 2000. In the fall of 2000, she came to the University of New Orleans and joined Professor Zeev Rosenzweig's group for Ph.D. candidate study.